

THE BIOLOGICAL ACTIVITY OF RHODIUM METALLOINSERTORS

Thesis by

Russell J. Ernst, Jr.

In Partial Fulfillment of the Requirements

For the Degree of

Doctor of Philosophy

California Institute of Technology

Pasadena, California

2011

(Defended May 16, 2011)

© 2011

Russell J. Ernst

All Rights Reserved

ACKNOWLEDGEMENTS

To my research advisor, Professor Jacqueline Barton, thank you for taking me into your care and making me a scientist. Your support and guidance made so many things not only possibilities, but realities. You have drawn together the most amazing and humbling collection of brilliant minds, provided them with everything necessary for success, and united them with a shared vision. Most of all, your passion continues to inspire me, and I will carry you as my role model wherever life takes me. Working for you has been the most challenging and fulfilling thing I have ever done; it has brought me satisfaction and joy that I long sought, but could not find elsewhere. I owe that joy to you, and I am grateful for it. I know that I cannot repay you, but I will try to do for others what you have done for me.

To the members of my thesis committee, Professors Harry Gray, Ray Deshaies, and Rob Phillips, it has been a privilege to know you and to talk about science with you. Thank you for taking the time to make me a better scientist. Committee meetings can be stressful, but I always found it fun to have that much brainpower in a small room.

To Pamela Bjorkman, you taught me to teach. Your candor always boosted my faith in humanity, and made me laugh to beat the band. I will miss working with you.

To Maureen Renta, thank you for always helping me, even when I made it difficult for you to do so.

To Shelley Diamond, thank you for sharing so many of my successes and failures. Thank you for helping me up when I was down. I look forward to seeing you at the final table of the main event some day.

To my classmates and friends in the BMB option: Phil Romero, Cambrian Liu, Fred Tan, John Ngo, Peera Jaru-Ampornpan, Kelly Dusinberre, and John Phillips, you were my first teachers at Caltech, and became my oldest friends. Thank you for the grace, generosity, and knowledge you shared with me when I had so little to offer in return.

To the men and women of the Barton lab, thank you for making my time so productive and enjoyable. I would especially like to thank several of my colleagues: Cindy Puckett, for balancing a bright personality with a delightfully dark sense of humor; Hang Song, for your excellent perspectives in science and in life; Curtis Schneider and Alexis Komor, for sharing your knowledge and helping me to do things that I could not do alone; and Mike Smeaton, for teaching me so much in so little time – I wish we had more of it.

I owe a special debt of gratitude to three people who have been both mentors and friends to me. Jon Hart, you taught me from the beginning how to do science the right way, but we still had a great time doing it. Brian Zeglis, you have been my teacher, colleague, teammate, and friend. You are so smart that it scares me a little, but mostly, it brings me glee. Ward Walkup, I turned to you so many times when I needed help, whether to work or to play, to celebrate or to commiserate. You were always there. Thank you.

To my brethren from 702 East Colfax, thank you for teaching me to believe in myself, and for other reasons I need not mention here.

Finally, this thesis is dedicated to my family: to my mother Mary and my father Russell; my brothers Andy and Jon; my grandparents, Herbert and Elizabeth, and Elmer and Jean; my uncles, aunts, and cousins. You are the source of everything good in my life, and the reason that I want to make the world better. And to my fiancée, Maritza, who has been by my side through the best and the worst. I could not have done this without you. This adventure is just beginning.

ABSTRACT

Mismatches in DNA occur naturally during replication and as a result of endogenous DNA damaging agents, but the mismatch repair (MMR) pathway acts to correct mismatches before subsequent rounds of replication. The loss of MMR carries dire consequences, including increased mutation rates, carcinogenesis, and resistance to a variety of clinical anti-cancer agents, such as cisplatin and DNA alkylators. Rhodium metalloinsertors previously developed in our laboratory bind to DNA mismatches with high affinity and specificity, and represent a promising strategy to target mismatches in cells. Thus, uncorrected mismatches can be exploited to provide a basis of discrimination between MMR-deficient, cancerous cells and MMR-proficient, healthy cells.

Here we describe the application of rhodium metalloinsertors to inhibit cellular proliferation selectively in MMR-deficient cells compared to those that are MMR-proficient. The colorectal carcinoma cell lines HCT116N and HCT116O serve as an isogenic model system for MMR deficiency. We show that the Δ -isomer of an octahedral rhodium complex containing a bulky chelate ligand for insertion into a DNA mismatch is active both in targeting base mismatches *in vitro* and in inhibiting DNA synthesis selectively in the HCT116O cell line.

A family of derivative complexes with varying ancillary ligands has also been synthesized, and both DNA mismatch binding affinities and anti-proliferative activities against the HCT116 cell lines have been determined. DNA photocleavage experiments reveal that all complexes bind to the mismatched sites with high specificities; DNA binding affinities to oligonucleotides containing single base CA and CC mismatches,

obtained through photocleavage titration or competition, vary from 10^4 to 10^8 M^{-1} for the series of complexes. Significantly, binding affinities are found to be inversely related to ancillary ligand size and directly related to differential inhibition of the HCT116 cell lines. The observed trend in binding affinity is consistent with the metalloinsertion mode where the complex binds from the minor groove with ejection of mismatched base pairs. The correlation between binding affinity and targeting of the MMR-deficient cell line suggests that rhodium metalloinsertors exert their selective biological effects on MMR-deficient cells through mismatch binding *in vivo*.

In particular, rhodium metalloinsertors bearing dipyridylamine ancillary ligands are shown to exhibit accelerated cellular uptake. This increased uptake allows us to observe additional cellular responses to these agents, including disruption of the cell cycle, monitored by flow cytometry assays, and induction of necrosis, monitored by dye exclusion and caspase inhibition assays, that also occur preferentially in the HCT116O cell line. Finally, these cellular responses provide insight into the mechanisms underlying the selective activity of this novel class of targeted anti-cancer agents, and are consistent with the idea that repair proteins are activated in response to DNA mismatch binding.

TABLE OF CONTENTS

Chapter 1: Introduction	1
1.1 Deoxyribonucleic acid	1
1.2 Mismatch repair	5
1.3 Mismatch recognition by rhodium metalloinsertors	9
1.4 References.....	15
Chapter 2: Anti-proliferative effects of [Rh(bpy)₂chrysi]³⁺ and [Rh(bpy)₂phzi]³⁺	19
2.1 Introduction.....	19
2.2 Experimental protocols	20
2.2.1 Materials	20
2.2.2 Synthesis of metal complexes.....	21
2.2.3 Cell lines, media and culture.....	21
2.2.4 Cell proliferation assays.....	21
2.2.5 Photocleavage of mismatched DNA with rhodium isomers.....	22
2.3 Results.....	25
2.3.1 Preferential inhibition of cellular proliferation	25
2.3.2 Correlations between biological effects and DNA mismatch targeting.....	30
2.4 Discussion.....	35
2.5 Conclusion	36
2.6 References.....	36

Chapter 3: DNA mismatch binding and anti-proliferative effects of rhodium metalloinsertors.....	38
3.1 Introduction.....	38
3.2 Experimental Protocols.....	40
3.2.1 Materials	40
3.2.2 Oligonucleotide synthesis	40
3.2.3 Synthesis and characterization of metal complexes.....	41
3.2.4 Photocleavage titrations.....	46
3.2.5 Binding constant determination	46
3.2.6 Cell culture.....	47
3.2.7 Cellular proliferation ELISA	47
3.3 Results.....	48
3.3.1 Binding affinities for metal complexes at single base mismatches	48
3.3.1 Inhibition of cellular proliferation by ELISA assay	52
3.4 Discussion.....	62
3.5 Conclusion	68
3.6 References.....	69

Chapter 4: Cytotoxic effects of Rhodium metalloinsertors with dipyridylamine ancillary ligands	73
4.1 Introduction.....	73
4.2 Experimental Protocols.....	74
4.2.1 Materials	74
4.2.2 Synthesis of MeDPA ligand	76
4.2.3 Synthesis of metal complexes.....	76
4.2.4 Inductively coupled plasma mass spectrometry (ICP-MS)	78
4.2.5 Cell culture.....	81
4.2.6 Preparation of whole cell lysate.....	81
4.2.7 Preparation of nuclei.....	81
4.2.8 Preparation of mitochondrial fraction.....	81
4.2.9 Cellular proliferation ELISA	82
4.2.10 MTT cytotoxicity assay	82
4.2.11 Cell cycle distribution flow cytometry assay.....	84
4.2.12 Cell death mode flow cytometry assay	84
4.3 Results.....	84
4.3.1 ICP-MS for cellular accumulation.....	84
4.3.2 MTT cytotoxicity assay	87
4.3.3 Effects on the cell cycle.....	92

4.3.4 Cell death pathway by flow cytometry	95
4.3.5 Caspase inhibitor cytotoxicity assays	103
4.3.6 PARP inhibitor cytotoxicity assays	107
4.4 Discussion	109
4.5 Conclusion	114
4.6 References	115
Chapter 5: Conclusion	120

LIST OF FIGURES AND TABLES

Figure 1.1 Deoxyribonucleic acid.....	2
Figure 1.2 DNA mismatches.....	4
Figure 1.3 The mismatch repair (MMR) pathway in <i>E. coli</i>	6
Figure 1.4 X-ray crystal structures of some DNA mismatch.....	8
Figure 1.5 Design of a mismatch recognition agent	10
Figure 1.6 Metalloinsertion is a novel binding mode	12
Figure 1.7 Modes of cellular uptake	14
Figure 2.1 Structures of $[\text{Rh}(\text{bpy})_2\text{chrysi}]^{3+}$ and $[\text{Rh}(\text{bpy})_2\text{phzi}]^{3+}$	23
Figure 2.2 Enzyme-linked immunosorbent assay (ELISA) for BrdU incorporation.....	24
Figure 2.3 Differential anti-proliferative effect of $[\text{Rh}(\text{bpy})_2\text{chrysi}]^{3+}$ and $[\text{Rh}(\text{bpy})_2\text{phzi}]^{3+}$	27
Figure 2.4 Anti-proliferative effect of $[\text{Rh}(\text{bpy})_2\text{phzi}]^{3+}$ on mouse fibroblasts	28
Figure 2.5 Effect of varying drug incubation time on cell proliferation.....	29
Figure 2.6 Effect of stereoisomers on photocleavage.....	32
Figure 2.7 Anti-proliferative effects of different stereoisomers of $[\text{Rh}(\text{bpy})_2\text{chrysi}]^{3+}$	33
Figure 2.8 Anti-proliferative effects of different stereoisomers of $[\text{Rh}(\text{bpy})_2\text{chrysi}]^{3+}$ with irradiation	34
Figure 3.1 $[\text{Rh}(\text{L})_2\text{chrysi}]^{3+}$ family of metalloinsertors	39
Figure 3.2 $[\text{Rh}(\text{L})_2\text{chrysi}]^{3+}$ synthetic route I.....	44

Figure 3.3 $[\text{Rh}(\text{L})_2\text{chrysi}]^{3+}$ synthetic route II	45
Figure 3.4 Binding affinities determined through DNA photocleavage.....	49
Table 3.1 Binding affinities of $[\text{Rh}(\text{L})_2\text{chrysi}]^{3+}$ complexes for CC and AC mismatches.....	49
Figure 3.5 Inhibitory effects of $[\text{Rh}(\text{DIP})_2\text{chrysi}]^{3+}$ as a function of incubation time on cellular proliferation.....	53
Figure 3.6 Inhibitory effects of $[\text{Rh}(\text{phen})_2\text{chrysi}]^{3+}$ as a function of incubation time on cellular proliferation.....	54
Figure 3.7 Inhibitory effects of $[\text{Rh}(\text{bpy})_2\text{chrysi}]^{3+}$ as a function of incubation time on cellular proliferation.....	55
Figure 3.8 Inhibitory effects of $[\text{Rh}(\text{HDPA})_2\text{chrysi}]^{3+}$ as a function of incubation time on cellular proliferation.....	56
Figure 3.9 Inhibitory effects of $[\text{Rh}(\text{NH}_3)_4\text{chrysi}]^{3+}$ as a function of incubation time on cellular proliferation.....	57
Figure 3.10 Inhibitory effects of rhodium metalloinsertors as a function of incubation time	59
Figure 3.12 Crystal and model structures of rhodium metalloinsertors bound to the mismatch site	64
Figure 3.13 Inhibitory effects of rhodium metalloinsertors correlate with binding affinity for DNA mismatches	66
Figure 4.1 Rhodium metalloinsertors bearing dipyridylamine ancillary ligands	75
Figure 4.2 Synthesis of $[\text{Rh}(\text{MeDPA})_2\text{chrysi}]^{3+}$	77

Figure 4.3 Cellular ICP-MS.....	79
Figure 4.4 ICP-MS calibration.....	80
Figure 4.5 MTT cytotoxicity assay.....	83
Figure 4.6 ICP-MS assay for rhodium accumulation.....	86
Figure 4.7 [Rh(HDPA) ₂ chrysi] ³⁺ is selectively toxic in MMR-deficient cells.....	88
Figure 4.8 [Rh(MeDPA) ₂ chrysi] ³⁺ selectively inhibits MMR-deficient cells in ELISA...	90
Figure 4.9 [Rh(MeDPA) ₂ chrysi] ³⁺ is selectively toxic in MMR-deficient cells.....	91
Figure 4.10 Cell cycle distribution assay.....	93
Figure 4.11 Cell cycle distribution assay.....	94
Figure 4.12 Cell death mode dye exclusion assay.....	96
Figure 4.13 [Rh(HDPA) ₂ chrysi] ³⁺ induces necrosis in HCT116O cells.....	97
Figure 4.14 [Rh(HDPA) ₂ chrysi] ³⁺ induced necrosis is concentration dependent.....	99
Figure 4.15 [Rh(HDPA) ₂ chrysi] ³⁺ induces necrosis increases over 24 to 72 hours.....	100
Figure 4.16 [Rh(HDPA) ₂ chrysi] ³⁺ induces necrosis in combination with methotrexate (MTX).....	102
Figure 4.17 Z-VAD-fmk caspase inhibitor.....	104
Figure 4.18 20 μM caspase inhibition assay.....	105
Figure 4.19 40 μM caspase inhibition assay.....	106
Figure 4.20 PARP inhibition assay.....	108
Figure 4.21 Model of the cellular response to rhodium metalloinsertors.....	115

INTRODUCTION

1.1 Deoxyribonucleic acid (DNA)

DNA is the stuff of life. The anti-parallel double helix comprises two strands of the bases adenine (A), thymine (T), cytosine (C), and guanine (G) connected by the sugar-phosphate backbones (figure 1.1).¹ The sequence of these bases encodes the genetic information of the cell, and the pairings of bases between the strands follow simple rules for complementarity revealed by Watson, Crick, and Franklin over 60 years ago: A pairs with T, and C pairs with G. The pairings between the bases are mediated by hydrogen bonds, with AT pairs forming two bonds while CG pairs form three bonds. The double helix is further stabilized by π -stacking interactions between adjacent pairs of the aromatic bases.

Just three years later, Kornberg identified DNA polymerase I as the enzyme responsible for the template-directed synthesis of DNA in *E. coli*.² Meselson and Stahl showed that DNA replication occurs through a semi-conservative mechanism wherein the double helix separates, and each old strand serves as the template for a new strand, yielding two duplexes that each contain one strand from the parent molecule.³ As a consequence of this mechanism, errors on either strand are converted to permanent mutations when the strands are copied. Thus, DNA polymerase δ and DNA polymerase ϵ , the main human replicative polymerases, must replicate the genome with the greatest possible fidelity.⁴

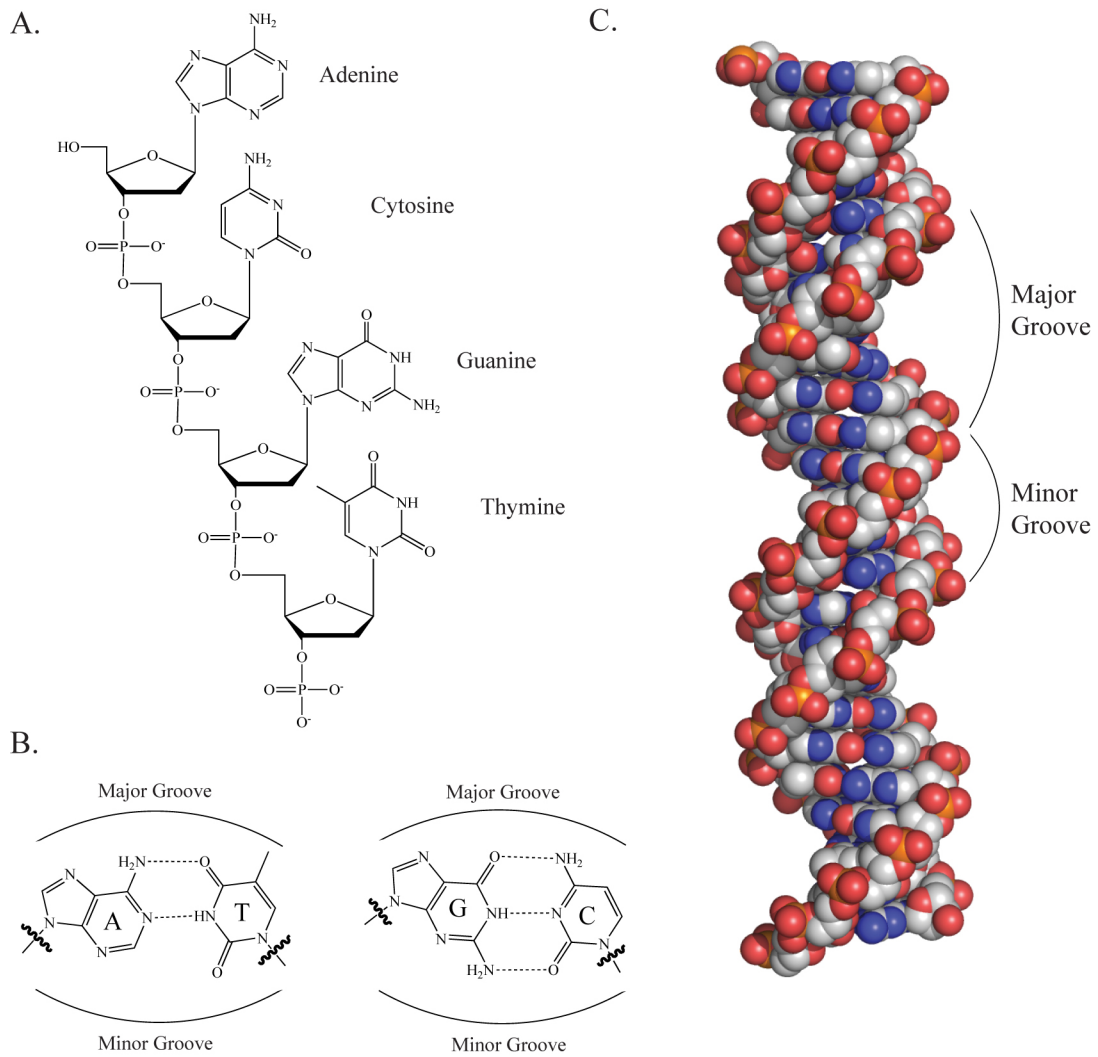


Figure 1.1 Deoxyribonucleic acid (DNA).

Three factors contribute to accuracy of replication.⁵ The hydrogen bonding complementarity between the template and the next deoxyribonucleotide triphosphate (dNTP) to be added to the newly growing DNA provides an error rate of 1 in 10^4 bases, which is clearly insufficient. The proofreading domain of DNA polymerase has evolved to check the newly incorporated base immediately, lowering the error rate to 1 in 10^7 - 10^8 bases, an impressive level of accuracy. However, the human genome contains over 3×10^9 base pairs; thus, on the order of 10^2 - 10^3 errors are made during each cycle of DNA replication that result in incorrectly paired bases, termed DNA mismatches (figure 1.2). These mismatches are corrected by a different set of enzymes termed the mismatch repair pathway (MMR, figure 1.3). MMR further reduces the error rate of DNA replication to 1 in 10^9 - 10^{10} bases, affording essentially error-free duplication of the human genome under normal circumstances.⁶

In addition to replication errors, DNA mismatches can arise naturally from other cellular processes. Translesion synthesis occurs when error-prone polymerases, such as DNA polymerase ζ or DNA polymerase η , are utilized to replicate chemically damaged DNA, which is not an acceptable template for the high fidelity polymerases.⁷ Genetic recombination is an essential process in which homologous DNA sequences are exchanged between two DNA molecules, but the process generates mismatches when the sequences exchanged are not identical.⁸ Spontaneous deamination converts cytosine to uracil, resulting in GU mismatches that must be corrected before replication.⁹ Finally, B lymphocytes undergo somatic hypermutation, generating mismatches that increase the diversity of antibodies.¹⁰ With the exception of somatic hypermutation, mismatches arising from all of these processes are detected and repaired by MMR.

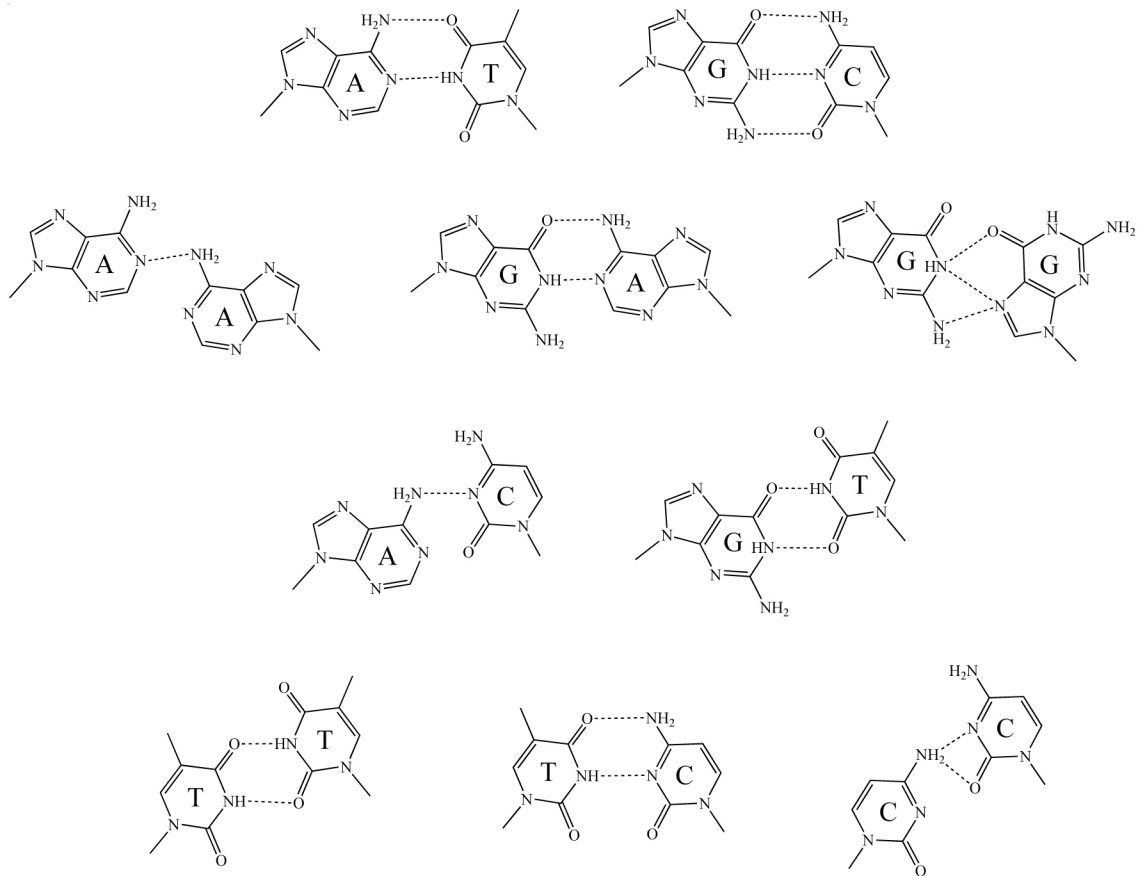


Figure 1.2. DNA mismatches. In well-matched DNA, bases pair according to Watson-Crick hydrogen bonding rules: A pairs with T and C pairs with G (top row). Alternative base pairings are termed DNA mismatches (AA, GA, GG, AC, GT, TT, TC, CC).

1.2 Mismatch repair

The mismatch repair (MMR) pathway corrects DNA mismatches, as well as insertion/deletion loops that arise during DNA synthesis, increasing the fidelity of DNA replication by a factor of 50-1000.¹¹ The pathway is best characterized in *E. coli* and is shown schematically in figure 1.3. Mismatches are first recognized by the *MutS* dimer, which then recruits the *MutL* dimer. The *MutS-MutL* complex in turn activates *MutH*, an endonuclease specific for the sequence GATC. Newly synthesized DNA strands in *E. coli* are unmethylated at these sites, and thus hemimethylation of the duplex provides the strand discrimination signal to direct the nicking activity of *MutH*. After scission a long patch, between 1,000–2,000 bases, is removed by the combined action of DNA helicase II and any one of several exonucleases. DNA polymerase fills the gap left by the excised strand, and the nicks surrounding the newly synthesized DNA are closed by DNA ligase. Several homologues of the MMR proteins exist in eukaryotes. Six homologues of *MutS* (*MSH1-6*) and four homologues of *MutL* (*MLH1*, *MLH3*, *PMS1*, and *PMS2*) have been identified; of these, *MSH2* and *MLH1* have been shown to be essential for MMR in humans.¹²

Not surprisingly, as uncorrected mismatches are converted to mutations in subsequent cycles of DNA replication, cells with MMR deficiencies exhibit elevated mutation rates.¹³⁻¹⁵ Germline mutations in *MLH1* or *MSH2* dramatically increase the risk of developing hereditary nonpolyposis colon cancer (HNPCC), the most common type of inherited colon cancer.^{16,17} HNPCC is marked by early onset and the presence of cancers in several other tissue types.¹⁷ Roughly 15% of sporadic colorectal cancer cases have also been linked to MMR deficiency.¹⁸ Epigenetic silencing of the MMR genes has been identified as the cause of MMR deficiency in these cases.¹⁹

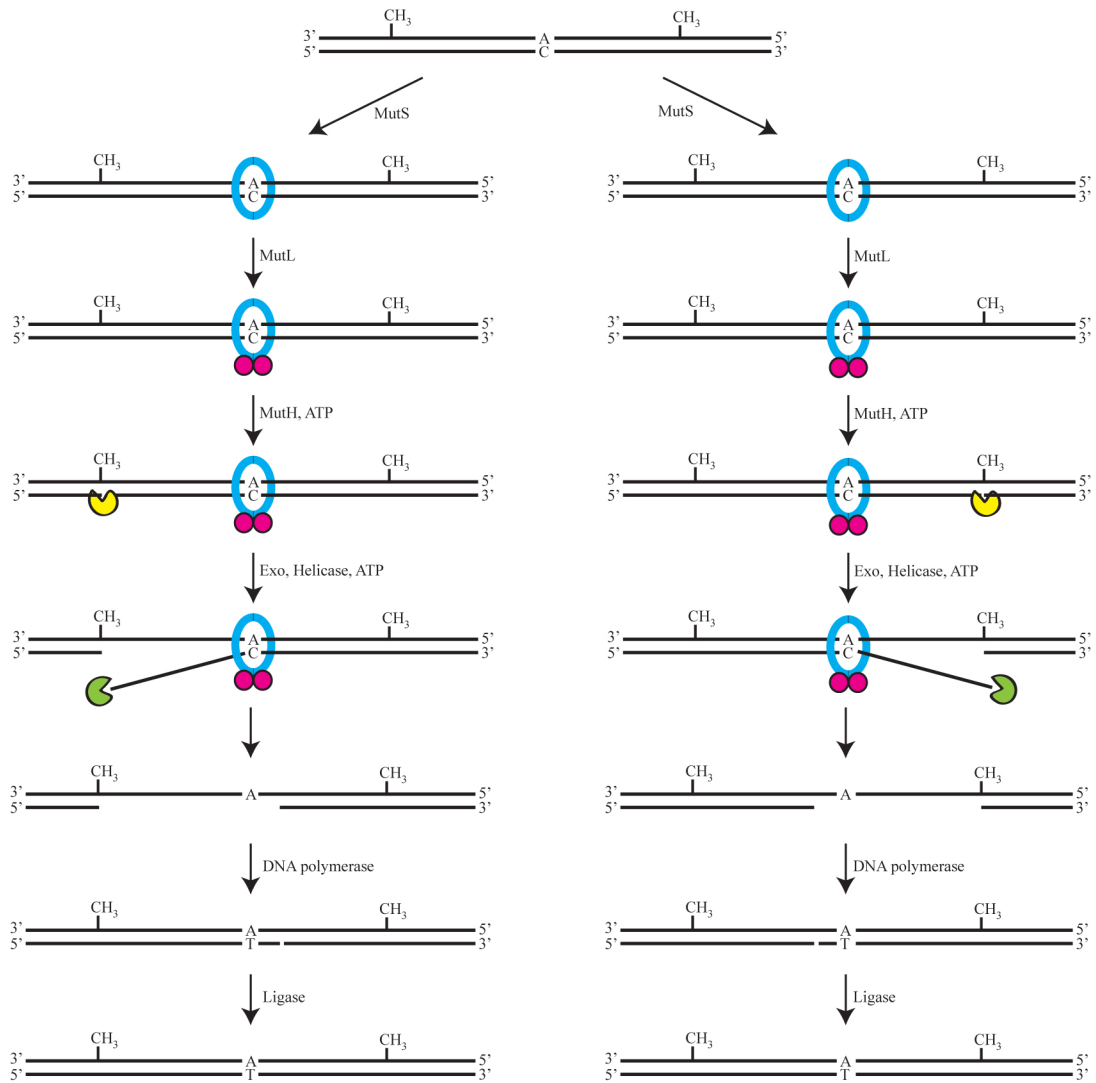


Figure 1.3. The mismatch repair (MMR) pathway in *E. coli*.

In addition to colorectal cancer, mismatch repair deficiencies have been found in approximately 16% of solid tumors of all tissue types.^{14,20}

Importantly, MMR deficiency confers resistance or tolerance to many of the anti-cancer agents currently in clinical use.^{21,22} Alkylation by the commonly used chemotherapeutic agents N-methyl-N-nitrosourea (MNU) and N-methyl-N'-nitro-N-nitrosoguanidine (MNNG) at the O6 position of guanine nucleotides triggers an apoptotic response after recognition of O6-meG:C and O6-meG:T base pairs by the MMR pathway, while MMR-deficient cells tolerate this DNA methylation.²¹⁻²³ Failure to recognize DNA adducts is also involved in the resistance of MMR-deficient cells to the platinum compounds cisplatin and carboplatin.²¹⁻²⁴ The incorporation of anti-metabolites such as 5-fluorouracil and 6-thioguanine into DNA triggers cell cycle arrest and apoptosis through the MMR pathway, and consequently MMR-deficient cells are resistant to these agents as well.^{25,26} Other studies have shown low-level resistance to the type I topoisomerase poisons camptothecin and topotecan in *MLH1* deficient lines and to the type II topoisomerase poisons doxorubicin, epirubicin, and mitoxantrone in *MLH1* or *MSH2* deficient lines.²⁷ It has been hypothesized that treatment regimens with agents such as cisplatin might enrich tumors for MMR-deficient cells²⁸ and has been shown that roughly half of secondary, or therapy-related, leukemias show signs of MMR deficiency.^{28,29} Collectively, these results show the broad involvement of MMR in mediating drug response to DNA-targeted agents, the effects of MMR deficiency on this response, and the need to develop therapeutic agents that specifically target MMR-deficient cells.

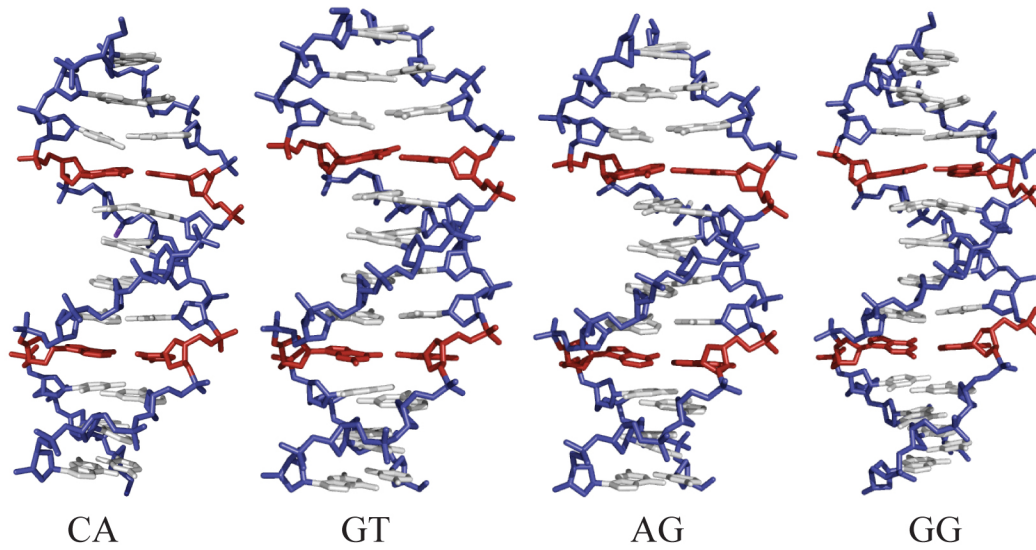


Figure 1.4. X-ray crystal structures of some DNA mismatches. The mismatched base pairs (red) do not significantly perturb the structure of the DNA duplex or differ noticeably from the well-matched base pairs (white).³⁶⁻⁴⁰

1.3 Mismatch Recognition by Rhodium Metalloinsertors

Previous work in our laboratory focused on tris(chelate) rhodium complexes that intercalated in well-matched DNA, such as $[\text{Rh}(\text{bpy})_2\text{phi}]^{3+}$ (bpy = 2,2'-bipyridine; phi = 9,10-phenanthrenequinonediimine).³⁰ These mononuclear, d^6 octahedral complexes are coordinately saturated and inert to substitution, making them resistant to decomposition under physiologically relevant conditions. While the phi ligand is responsible for DNA binding, judicious introduction of functional groups on the ancillary ligands confers sequence specificity on the complexes, such as $\Delta\text{-}\alpha\text{-}[\text{Rh}\{(\text{R,R})\text{-Me}_2\text{trien}\}(\text{phi})]^{3+}$, which recognizes 5'-TGCA-3'.³¹

These complexes have since been adapted to target DNA mismatches *in vitro*.³²⁻³⁴ Because DNA mismatches fail to obey Watson-Crick rules for hydrogen bonding, they are destabilized relative to well-matched DNA. The relative stability of mismatches has been studied extensively by UV-Vis and NMR, and it is widely accepted that base pair stability follows the sequence $\text{CG} > \text{AT} >> \text{GG} \sim \text{GT} \sim \text{AG} >> \text{TT} \sim \text{AA} > \text{CT} \sim \text{AC} > \text{CC}$.³⁵ It is this thermodynamic destabilization that our laboratory seeks to exploit as a means of targeting mismatches, since mismatches do not significantly perturb the structure of the B-form DNA duplex (figure 1.4).³⁶⁻⁴⁰ By expanding the aromatic system of the phi ligand to make the tetracyclic chrysi ligand (chrysi = chrysene-5,6-quinonediimine, figure 1.5), the width of the DNA binding ligand increases from 9.2 Å to 11.3 Å, thus exceeding the width of well-matched base pairs, 10.8 Å for both AT and CG. As a result, complexes bearing the chrysi ligand can only be accommodated by DNA at thermodynamically destabilized mismatch sites.

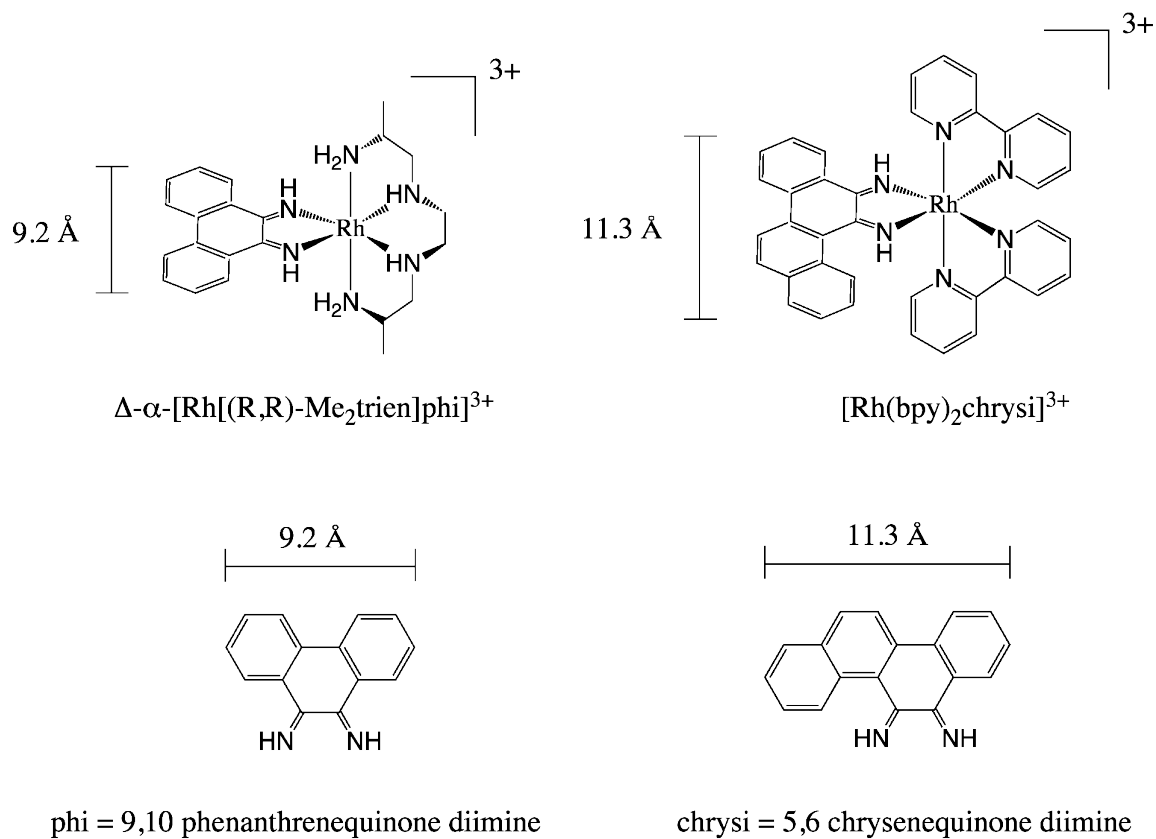


Figure 1.5 Design of a mismatch recognition agent. Extension of the aromatic system of the phi ligand to the bulkier chrysi ligand increases the width of the complex beyond the width of well-matched DNA, 10.8 Å for either base pair, and restricts binding to thermodynamically destabilized mismatched sites within the DNA duplex.

In addition to their DNA binding capabilities, these complexes also promote single-stranded cleavage of the DNA backbone upon photoactivation. This provides a useful tool to probe DNA binding. Photocleavage titration experiments revealed that the first generation compound, $[\text{Rh}(\text{bpy})_2\text{chrysi}]^{3+}$, binds 80% of DNA mismatches with typical binding constants of 10^6 M^{-1} and remarkable specificity for mismatched DNA; similar experiments also showed specific targeting of the mismatch in a 2.7 kb DNA fragment.^{32,33} Subsequent work led to the incorporation of nitrogen atoms into the intercalating ligand and a 50-fold increase in binding affinity for the second compound, $[\text{Rh}(\text{bpy})_2\text{phzi}]^{3+}$ (phzi = benzo[*a*] phenazine-5,6-quinonediimine).³⁴

A high resolution crystal structure of $[\text{Rh}(\text{bpy})_2\text{chrysi}]^{3+}$ bound to single base mismatches within a DNA oligonucleotide duplex reveals a distinctive binding mode at the mismatched site.⁴¹ We had previously demonstrated that rhodium intercalators bearing the phi ligand bind to well-matched DNA by partial intercalation of the planar phi ligand from the major groove side into the base pair stack.³¹ However, binding to the mismatched site involves instead insertion of the more expansive chrysi ligand into the DNA duplex from the minor groove side at the mismatched site with ejection of the mismatched bases out of the DNA stack; the inserted ligand stacks fully with adjacent base pairs (figure 1.6, left). NMR studies confirm this metalloinsertion mode for the complex at mismatched sites in solution.⁴² Further crystallographic studies revealed the generality of the metalloinsertion binding mode; in independent views of metalloinsertion at four different mismatch sites, the ejected bases superimpose identically (figure 1.6, right).⁴³

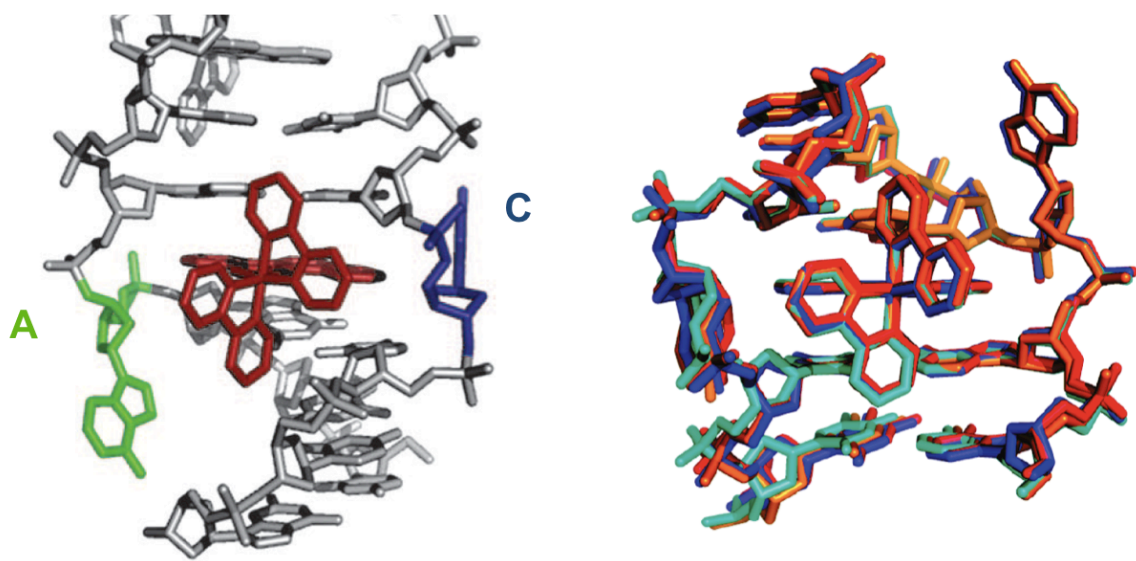


Figure 1.6 Metalloinsertion is a novel binding mode. *Left:* The metal complex approaches the duplex from the minor groove, ejecting the mismatched bases (A, C) from the helix and replacing them with the chrysi ligand, which stacks fully with the adjacent base pairs.⁴¹ *Right:* Superposition of four independent crystallographic views reveals the generality of the metalloinsertion binding mode.⁴³

Target binding alone is insufficient to ensure biological activity in a cellular context; cellular accumulation is also a prerequisite, and several possible avenues exist for metalloinsertors to gain entry to the cell.⁴⁴ Uptake can occur by energy-dependent processes, such as active transport or endocytosis, by facilitated diffusion through ion channels, or by passive diffusion across the plasma membrane (figure 1.7). Confocal microscopy and flow cytometry studies have been performed to determine the method of uptake for tris(chelate) luminescent ruthenium complexes.^{45,46} Metabolic inhibition either by incubation at low temperature or by treatment with deoxyglucose and oligomycin had no effect on ruthenium accumulation within HeLa cells. This result clearly eliminated any active mode of uptake from consideration. Similarly, fluorescence levels were not affected by pre-incubation with a panel of organic cation transporter (OCT) inhibitors. Although other ion channels may not have been targeted by the inhibitors, these data argue against facilitated diffusion. Ultimately, uptake was shown to depend on membrane potential; hyperpolarization with valinomycin increased mean cellular fluorescence while depolarization with high potassium buffer decreased cellular fluorescence. As a whole, these data provide strong evidence that passive diffusion driven by the membrane potential is the most likely route of cellular uptake for these cationic complexes. In addition, variations in the ancillary ligands have dramatic effects on cellular uptake, with increased lipophilicity facilitating uptake; this is consistent with diffusion across the lipid bilayer of the plasma membrane. By analogy, it is likely that rhodium metalloinsertors also accumulate within cells via passive diffusion. For both rhodium and ruthenium complexes, it has also been shown that uptake can be increased through functionalization with a nuclear localizing peptide.^{47,48}

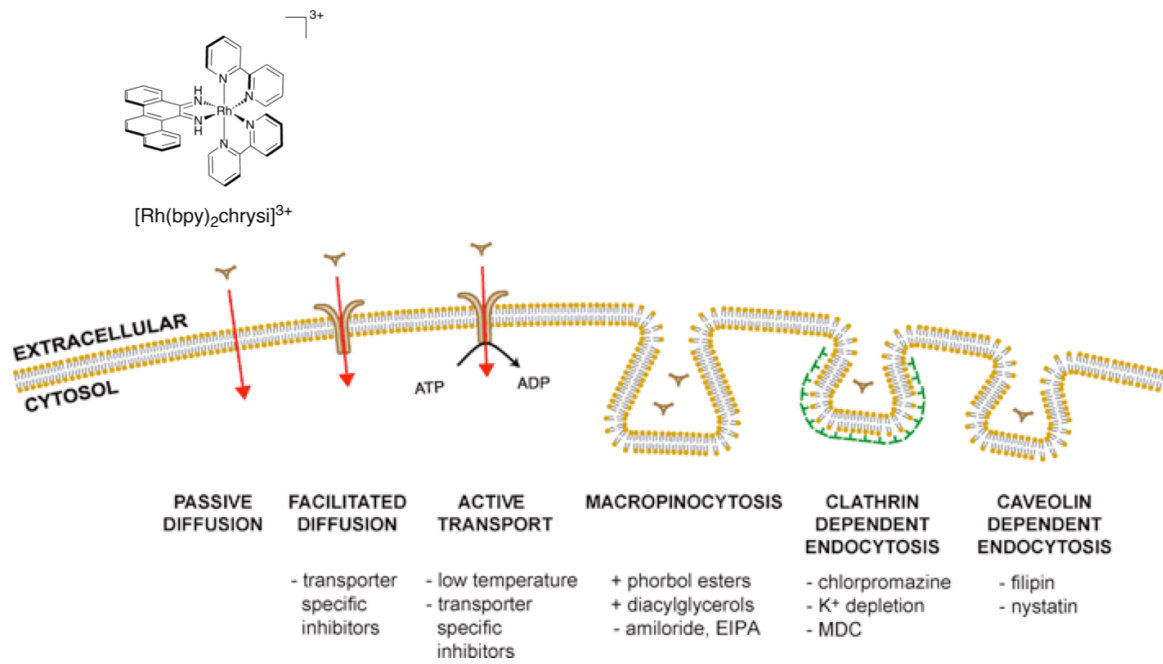


Figure 1.7 Modes of cellular uptake.⁴⁴

Taken together, the observations that (i) rhodium metalloinsertors are capable of recognizing mismatches with high selectivity and (ii) analogous ruthenium complexes accumulate within cells and nuclei form a sound basis for the hypothesis that rhodium metalloinsertors recognize mismatched DNA within cells. Furthermore, the unique geometry of the metalloinsertion binding mode, where the mismatched bases are ejected by the metal complex into extrahelical space, suggests that recognition would likely trigger a cellular response. Finally, the approximately 1,000-fold greater number of mismatches within MMR-deficient cells affords a means of discrimination as a function of MMR status, affording rhodium metalloinsertors the opportunity to act as targeted therapeutic agents. The studies described herein constitute the first steps in translating the development of these complexes from *in vitro*, molecular models of mismatch recognition to *in cellulo* models of mismatch targeting in MMR-deficient human carcinoma cell cultures.

1.4 References

1. J.D. Watson and F.H. Crick. *Nature* **1953** 171, 737-738.
2. A. Kornberg, I.R. Lehman, M.J. Bessman, and E.S. Simms. *Biochim. Biophys. Acta* **1956** 21, 197-198.
3. M. Meselson and W.F. Stahl. *Proc. Natl. Acad. Sci. USA.* **1958** 44, 671-682.
4. T.A. Kunkel. *J. Biol. Chem.* **2004** 279, 16895-16898.
5. R.M. Schaaper. *J. Biol. Chem.* **1993** 268, 23762-23765.
6. T.A. Kunkel and D.A. Erie. *Annu. Rev. Biochem.* **2005** 74, 681-710.
7. A.R. Lehmann. *FEBS Lett.* **2005** 579, 873-876.
8. J.L. Gerton and R.S. Hawley. *Nat. Rev. Genet.* **2005** 6, 477-487.

9. M. Samaranayake, J.M. Bujnicki, M. Carpenter, and A.S. Bhagwat. *Chem. Rev.* **2006** *106*, 700-719.
10. M. Seki, P.J. Gearhart, and R.D. Wood. *EMBO Rep.* **2005** *6*, 1143-1148.
11. R.R. Iyer, A. Pluciennik, V. Burdett, and P.L. Modrich. *Chem. Rev.* **2006** *106*, 302-323.
12. R.D. Kolodner and G.T. Marsischky. *Curr. Opin. Genet. Dev.* **1999** *9*, 89-96.
13. L.A. Loeb. *Cancer Res.* **2001** *61*, 3230-3239.
14. N.P. Bhattacharya, A. Skandalis, A. Ganesh, J. Groden, and M. Meuth. *Proc. Natl. Acad. Sci. USA.* **1994** *91*, 6319-6323.
15. B.S. Strauss. *Mutation Res.* **1999** *437*, 195-203.
16. N. Papadopoulos and A. Lindblom. *Human Mutation.* **1997** *10*, 89-99.
17. P. Peltomaki. *Human Mol. Gen.* **2001** *10*, 735-740.
18. D.A. Lawes, S. SenGupta, and P.B. Boulos. *European J. of Surgical Oncology.* **2003** *29*, 201-212.
19. J.G. Herman, A. Umar, K. Polyak, J.R. Graff, N. Ahuja, J.J. Issa, S. Markowitz, J.K.V. Willson, S.R. Hamilton, K.W. Kinzler, M.F. Kane, R.D. Kolodner, B. Vogelstein, T.A. Kunkel, and S.B. Baylin. *Proc. Natl. Acad. Sci. USA.* **1998** *95*, 6870-6875.
20. I.I. Arzimanoglou, F. Gilbert, and H.R.K. Barber. *Cancer.* **1998** *82*, 1808-1820.
21. K. Pors and L.H. Patterson. *Current Topics in Medicinal Chemistry.* **2005** *5*, 1133-1149.
22. A.M. Valentini, M. Armentano, M. Pirrelli, and M.L. Caruso. *Cancer Treatment Reviews.* **2006** *32*, 607-618.

23. J.M. Carethers, M.T. Hawn, D.P. Chauhan, M.C. Luce, G. Marra, M. Koi, and C.R. Boland. *J. of Clinical Investigation*. **1996** *98*, 199-206.
24. D. Fink, S. Nebel, S. Aebi, H. Zheng, B. Cenni, A. Nehme, R.D. Christen, and S.B. Howell. *Cancer Res*. **1996** *56*, 4881-4886.
25. J.M. Carethers, D.P. Chauhan, D. Fink, S. Nebel, R.S. Bresalier, S.B. Howell, and C.R. Boland. *Gastroenterology*. **1999** *117*, 123-31.
26. S. Aebi, D. Fink, R. Gordon, H.K. Kim, H. Zheng, J.L. Fink, and S.B. Howell. *Clinical Cancer Res*. **1997** *3*, 1763-1767.
27. A. Fedier, V.A. Schwarz, H. Walt, R.D. Carpini, U. Haller, and D. Fink. *International J. of Cancer*. **2001** *93*, 571-576.
28. D. Fink, S. Aebi, and S.B. Howell. *Clinical Cancer Res*. **1998** *4*, 1-6.
29. P. Karran, J. Offman, and M. Bignami. *Biochimie*. **2003** *85*, 1149-1160.
30. B.M. Zeglis, V.C. Pierre, and J.K. Barton. *Chemical Communications* **2007** *44*, 4565-79.
31. C.L. Kielkopf, K.E. Erkkila, B.P. Hudson, J.K. Barton, and D.C. Rees. *Nature Structural Biology* **2000** *7*, 117-121.
32. B.A. Jackson and J.K. Barton. *J. Am. Chem. Soc.* **1997** *119*, 12986-12987.
33. B.A. Jackson and J.K. Barton. *Biochemistry*. **2000** *39*, 6176-6182.
34. H. Junicke, J.R. Hart, J. Kisko, O. Glebov, I. Kirsch, and J.K. Barton. *Proc. Natl. Acad. Sci. USA*. **2003** *100*, 3737-3742.
35. N. Peyret, P.A. Seneviratne, H.T. Allawi, and J. SantaLucia. *Biochemistry* **1999** *38*, 3468-3477.

36. T. Brown, W.N. Hunter, G. Kneale, and O. Kennard. *Proc. Natl. Acad. Sci. USA*. **1996** *83*, 2402-2406.
37. W.N. Hunter, T. Brown, and O. Kennard. *Nucleic Acids Research* **1987** *15*, 6589-6606.
38. W.N. Hunter, T. Brown, G. Kneale, N.N. Anand, D. Rabinovich, and O. Kennard. *J. of Biological Chemistry* **1987** *262*, 9962-9970.
39. J.V. Skelly, K.J. Edwards, T.C. Jenkins, and S. Neidle. *Proc. Natl. Acad. Sci. USA*. **1993** *90*, 804-808.
40. H.R. Drew, R.M. Wing, R. Takano, C. Broa, S. Tanaka, K. Itakura, and R.E. Dickerson. *Proc. Natl. Acad. Sci. USA*. **1981** *78*, 2179-2183.
41. V.C. Pierre, J.T. Kaiser, and J.K. Barton. *Proc. Natl. Acad. Sci. USA*. **2007** *104*, 429-434.
42. C. Cordier, V.C. Pierre, and J.K. Barton. *J. Am. Chem. Soc.* **2007** *129*, 12287-12295.
43. B.M. Zeglis, V.C. Pierre, J.T. Kaiser, and J.K. Barton. *Biochemistry* **2009** *20*, 4247-4253.
44. C.A. Puckett, R.J. Ernst, and J.K. Barton. *Dalton Transactions* **2010** *39*, 1159-70.
45. C.A. Puckett and J.K. Barton. *J. Am. Chem. Soc.* **2007** *129*, 46-47.
46. C.A. Puckett and J.K. Barton. *Biochemistry* **2008** *47*, 11711-11716.
47. J. Brunner and J.K. Barton. *Biochemistry* **2006** *45*, 12295-12302.
48. C.A. Puckett and J.K. Barton. *Bioorganic & Medicinal Chemistry* **2010** *18*, 3564-3569.

CHAPTER 2: ANTI-PROLIFERATIVE EFFECTS OF [RH(BPY)₂CHRYSI]³⁺ AND [RH(BPY)₂PHZI]³⁺

Note: This chapter was adapted from “DNA mismatch-specific targeting and hypersensitivity of mismatch-repair-deficient cells to bulky rhodium(III) intercalators.” J.R. Hart, O. Glebov, R.J. Ernst, I.R. Kirsch, and J.K. Barton. *J. Am. Chem. Soc.* **2006**, *103*, 15359-15363

2.1. Introduction

We have developed bulky rhodium metalloinsertors (figure 2.1) that bind single base mismatches in DNA selectively and irrespective of sequence context.¹⁻⁴ These compounds bind the mismatch by intercalation and, upon photoexcitation, promote strand breaks at the mismatched site. [Bis(2,2'-bipyridine)(chrysene-5,6-quinonediimine)Rh(III)], [Rh(bpy)₂(chrysi)]³⁺, binds mismatches with moderate affinity and high specificity. The site-specificity depends upon the thermodynamic instability associated with a base pair mismatch; the bulky intercalator cannot stack easily within well-matched DNA but can more easily insert neighboring a destabilized mismatched site. The high specificity of [Rh(bpy)₂chrysi]³⁺ is well demonstrated in its ability to cleave a single mismatched site in a 2700 base pair duplex.² This specificity has been used advantageously in a site-specific assay for single nucleotide polymorphisms in pooled genomic DNA.⁵ Our second generation complex [bis(2,2'-

Acknowledgements: J.R.H. performed the syntheses of *rac*-[Rh(bpy)₂chrysi]³⁺ and *rac*-[Rh(bpy)₂phzi]³⁺, the photocleavage and capillary electrophoresis, and assisted with some ELISA assays. O.G. performed the ELISA for the mouse fibroblast cell lines.

bpipyridine)(benzo[a]phenazine-5,6,-quinonediimine)Rh(III)], $[\text{Rh}(\text{bpy})_2(\text{phzi})]^{3+}$, utilizes heterocyclic nitrogens within the bulky intercalating ligand to boost the affinity of the complex for mismatched sites.⁴ $[\text{Rh}(\text{bpy})_2\text{phzi}]^{3+}$ is capable of binding mismatched sites with 100 nM affinity and similar specificity to $[\text{Rh}(\text{bpy})_2\text{chrysi}]^{3+}$.

Importantly, both of these complexes have been applied in probing whether MMR-deficient cells accumulate mismatches.⁴ In photocleavage assays of genomic DNA from a series of cell lines, some proficient in mismatch repair and others wholly or partially deficient in repair, a clear correlation between photocleavage by $[\text{Rh}(\text{bpy})_2\text{chrysi}]^{3+}$ and $[\text{Rh}(\text{bpy})_2\text{phzi}]^{3+}$ and MMR deficiency was evident.

Here we explore the efficacy of these rhodium complexes in inhibiting the growth of MMR-deficient versus MMR-proficient cell lines in the presence and absence of photoactivation. The biological effects are assessed in two cell lines, both of which are derivatives of HCT116. These cell lines have had an extra copy of either chromosome 2, HCT116O, or 3, HCT116N, inserted in the cell; placing a copy of chromosome 3 within this cell line corrects the mismatch repair deficiency by introducing a functional copy of the MLH1 gene with a normal promoter.⁶ Additionally, mouse fibroblast cells derived from litter mates which are *Msh2*⁻ or *Msh2*⁺ were also studied. These cells and cell lines provide a convenient method for testing whether a particular compound will differentially target MMR-deficient cells, because these cells are essentially identical genetically, except with regard to mismatch repair.

2.2. Experimental Protocols

2.2.1 Materials

Media and supplements were purchased from Invitrogen (Carlsbad, CA). 5-

bromodeoxyuridine (BrdU), antibodies, buffers and peroxidase substrate were purchased

in kit format from Roche Molecular Biochemicals (Mannheim, Germany). Irradiations were performed with an Oriol (Darmstadt, Germany) 1,000 W Hg/Xe solar simulator using a UVB/C blocking filter.

2.2.2 Synthesis of Metal Complexes

Rac-[Rh(bpy)₂(chrysi)]Cl₃ and *rac*-[Rh(bpy)₂(phzi)]Cl₃ were synthesized using established procedures.^{1,4} *Rac*-[Rh(bpy)₂(chrysi)]Cl₃ was resolved into Δ and Λ isomers using potassium antimonyl tartrate as previously described.⁷ Salts were exchanged to chloride before use using Sephadex QAE ion exchange resin.

2.2.3 Cell lines, Media, and Culture

The HCT116N and HCT116O cell lines were obtained from Bert Vogelstein (The Johns Hopkins University, Baltimore, MD) and were originally derived from the laboratory of C.R. Boland (University of California at San Diego, La Jolla, CA).⁶ Cells were grown in RPMI-1640 media supplemented with 10% fetal bovine serum, 2 mM L-glutamine, 0.1 mM non-essential amino acids, 1 mM sodium pyruvate, 100 U/ml penicillin, 100 ug/ml streptomycin, 400 ug/ml geneticin (G418). Cells were grown in tissue culture flasks and dishes (Corning Costar, Acton, MA) at 37 °C under 5% CO₂ atmosphere. Mouse fibroblasts were obtained as previously reported and established for heterozygous and homozygous littermates and used at passages 5 and 6.⁸ Cells were grown in DMEM with media as for HCT116 cells.

2.2.4 Cell proliferation assays

Cell proliferation was measured using the 5-bromouracil incorporation assay (figure 2.2).⁹ Cells were plated in 96 well plates at 2000 cells/well and grown for 24 hours. At this point, variable concentrations of rhodium complexes were added. The cell cultures

were then allowed to grow for 48 hours or 6-96 hours as indicated. Cells were then either irradiated or not followed by the addition of 5-bromodeoxyuridine, BrdU. Irradiations of cells were performed using a solar simulator adapted for irradiation from the bottom of the well plates. The cells were grown for an additional 24 hours. The BrdU incorporation was assayed by antibody assay using established procedures.⁹

2.2.5 Photocleavage of mismatched DNA with rhodium isomers

Photocleavage experiments were conducted on the 436-mer PCR product as described in detail earlier⁵ but using 500 nM of the purified isomers, Δ - or Λ -[Rh(bpy)₂chrysi]³⁺.

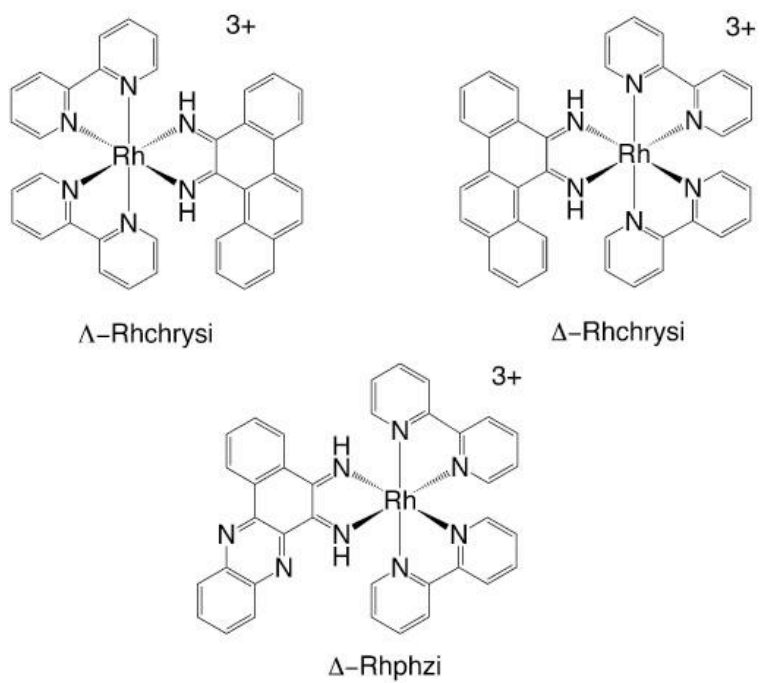
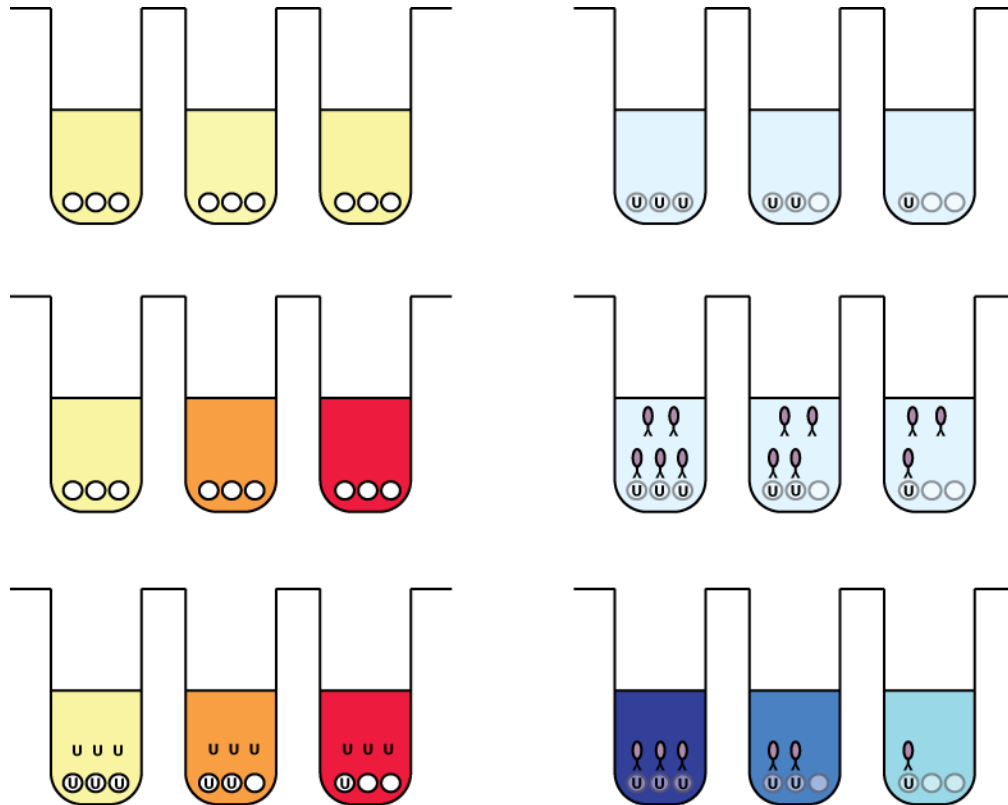


Figure 2.1. Structures of (top) Λ - (left) and Δ - (right) $[\text{Rh}(\text{bpy})_2\text{chrysi}]^{3+}$ and (bottom) Δ - $[\text{Rh}(\text{bpy})_2\text{phzi}]^{3+}$.



Adapted from: Gratzner, H. G. (1982). *Science* 218, 474-475.

Figure 2.2. Enzyme-linked immunosorbent assay for BrdU incorporation

(ELISA).⁹ Cells are plated at a density of 2×10^3 cells/well and treated with varying concentrations of rhodium complex. Before analysis, cells are labeled with BrdU for 24 hours. The amount of BrdU incorporated during DNA synthesis can then be quantified with an enzyme-conjugated antibody and a chromogenic substrate.

2.3. Results

2.3.1 Preferential inhibition of cellular proliferation

The HCT116 derived cells were treated with either $[\text{Rh}(\text{bpy})_2\text{chrysi}]^{3+}$ or $[\text{Rh}(\text{bpy})_2\text{phzi}]^{3+}$ for 96 hours at varying concentrations in the absence of irradiation. As is evident for both complexes (figure 2.3), we see a significant inhibition of cell proliferation. Importantly, for both complexes we also see a preferential inhibition in the MMR-deficient strain. This selectivity seen with the rhodium complexes for the MMR-deficient HCT116O contrasts the action, also shown, of *N*-methyl, *N'*-nitro-nitrosoguanidine (MNNG), a common DNA-methylating agent, that is found to be more toxic to the MMR-proficient cell line, HCT116N.⁶ MNNG is typical of most chemotherapeutics that target genomic DNA.

Experiments using mouse fibroblasts that are deficient for MMR, *Msh2*⁻, or proficient for MMR, *Msh2*⁺, were also performed. These experiments complement those conducted with HCT116, because the cells also are genetically identical except for the *Msh2* gene. Experiments probing these fibroblast cells, which are not cancerous, therefore provide a rigorous test that targets MMR-deficiency. The data given in figure 2.4 show that the MMR-defective mouse embryo fibroblasts that are *Msh2*⁻ yield decreased DNA synthesis and are therefore more sensitive to $[\text{Rh}(\text{bpy})_2\text{phzi}]^{3+}$ compared with the control littermate cells that are *Msh2*⁺. These results parallel those obtained with the HCT116 model system. These results furthermore provide strong support for the idea that the inhibition of cell proliferation is related to the MMR-deficiency of the cell, regardless of which mismatch repair gene is absent.

The effect of incubation time was also investigated, and the results are shown in figure 2.5. Cells were exposed to variable concentrations of $[\text{Rh}(\text{bpy})_2\text{chrysi}]^{3+}$ for

varying amounts of time from 6 hour to 96 hours, before testing the effects on DNA synthesis. In this series, it is clear that the maximum effect is obtained after 48 hours of incubation. Based upon studies with analogous ruthenium complexes^{10,11}, we believe cellular uptake to be rate-limiting; indeed, with more hydrophobic chrysi analogues, we find differential biological effects with much shorter incubation times (Chapter 3).

Significantly, the results seen here with the bulky rhodium complexes are distinctive, in contrast with common therapeutics and MNNG. MMR-deficient cell lines are generally resistant to the majority of alkylating drugs, platinum compounds, and metabolic analogues, because the antiproliferative effects these therapeutic agents have on cancerous cells are due in part to recognition of the drug-induced genomic DNA damage by the MMR system.^{12,13} In contrast, we find with the rhodium complexes the preferential inhibition of cellular proliferation in cells that depends strictly on their deficiency in MMR.

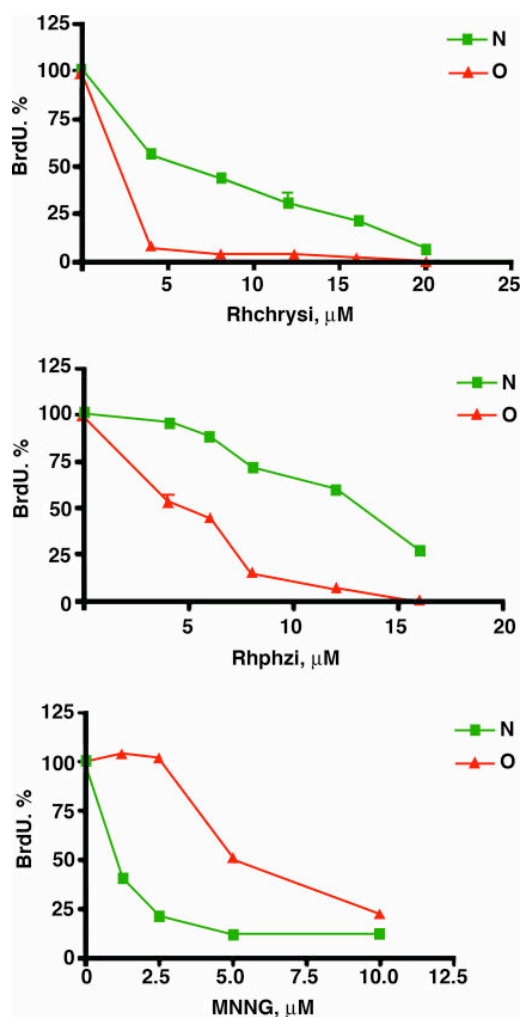


Figure 2.3. Differential antiproliferative effect of *rac*-[Rh(bpy)₂chrysi]³⁺, *rac*-[Rh(bpy)₂phzi]³⁺, and MNNG on MMR-deficient (red) and MMR-proficient (green) cell lines. Cell lines derived from the HCT116 cell line were treated with the methylating agent MNNG, [Rh(bpy)₂chrysi]³⁺, or [Rh(bpy)₂phzi]³⁺ as described in Experimental Protocols. Note that the MMR-deficient population HCT116O is resistant to the action of MNNG but is sensitive preferentially to [Rh(bpy)₂chrysi]³⁺ and [Rh(bpy)₂phzi]³⁺.

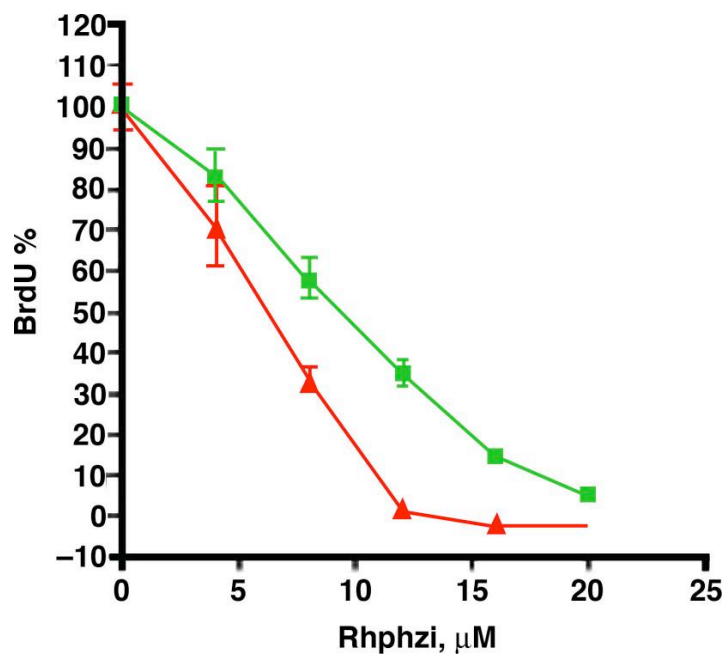


Figure 2.4. Antiproliferative effect of $\text{rac-}[\text{Rh}(\text{bpy})_2\text{phzi}]^{3+}$ on MMR-deficient ($Msh2^-$, red) and MMR-proficient ($Msh2^+$, green) mouse embryonic fibroblasts. The preferential inhibition of DNA synthesis parallels the effects seen with the HCT116 cell lines.

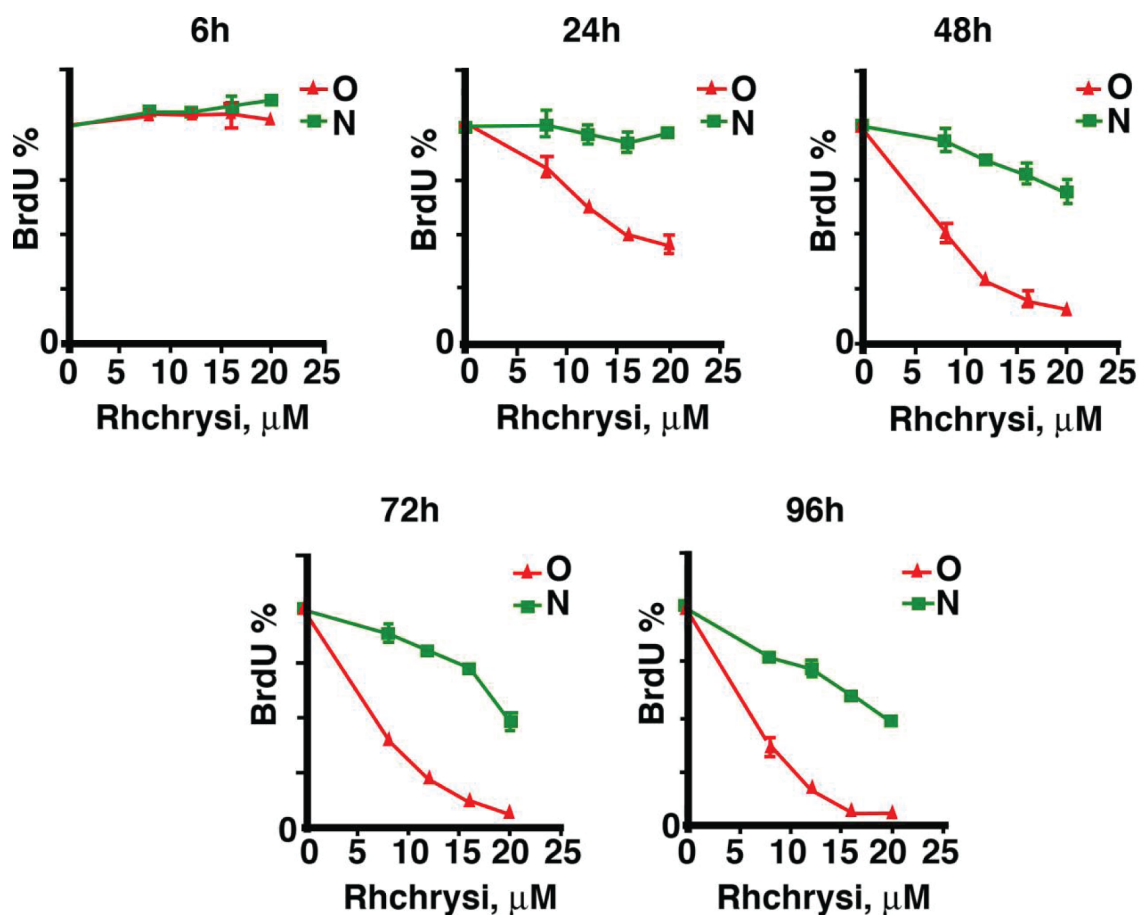


Figure 2.5. Effect of varying drug incubation time on cell proliferation. HCT116O cells that are MMR-deficient (red) and HCT116N cells that are MMR-proficient (green) were exposed to varying concentrations of $rac\text{-}[\text{Rh}(\text{bpy})_2\text{chrysi}]^{3+}$ for different incubation times as shown. Antiproliferative effects increase with longer incubation times up to 48 hours.

2.3.2 Correlations between biological effects and DNA mismatch targeting

In an effort to correlate the biological effects we observed by using these bulky metalloinsertors with their DNA binding characteristics, experiments were conducted also using enantiomers of $[\text{Rh}(\text{bpy})_2\text{chrysi}]^{3+}$. Only the Δ -isomer of $[\text{Rh}(\text{bpy})_2\text{chrysi}]^{3+}$ binds and cleaves, with photoactivation, a neighboring mismatched DNA site.¹ Shown in figure 2.6 is an illustration of the enantiospecific reaction of $[\text{Rh}(\text{bpy})_2\text{chrysi}]^{3+}$ at a single CC mismatch on a 436-mer DNA duplex PCR product containing a single CC mismatch. As illustrated in the capillary gel electrophoresis results, upon photolysis of the complex bound to DNA, the bulky Δ -isomer cleaves the DNA neighboring the destabilized mismatch. No cleavage is seen without metal complex (light control) or after photolysis using the Λ -isomer. In general, surveying different mismatched sites in a variety of sequence contexts, we have found the recognition to be enantioselective; it is Δ - $[\text{Rh}(\text{bpy})_2\text{chrysi}]^{3+}$ that binds and cleaves mismatched DNA preferentially.³

We therefore also compared the antiproliferative effects of the two isomers (Figure 2.7). Consistent with DNA targeting studies, it is Δ - $[\text{Rh}(\text{bpy})_2\text{chrysi}]^{3+}$ that shows selective inhibition of cellular proliferation in the MMR-deficient HCT116O cell line. At 5 μM rhodium, incubation with Λ - $[\text{Rh}(\text{bpy})_2\text{chrysi}]^{3+}$ shows no effect on DNA synthesis in either HCT116O or HCT116N cells, whereas the Δ -isomer selectively inhibits DNA synthesis in the MMR-deficient HCT116O cells. Although these rhodium complexes are coordinatively saturated and generally inert to substitution, we had considered the possibility that the biological activity of the complexes might be associated with complex decomposition and ligand release. The finding of high enantioselectivity associated with the biological effect argues against complex

decomposition as being responsible for the inhibition of cellular proliferation, since a similar decomposition would be likely for both isomers.

Because the complexes bind mismatched DNA only non-covalently in the absence of light, but with photolysis, promote DNA strand breaks, we also explored cell proliferation assays after exposing the cells to compound and light, conditions under which the rhodium complex might be expected to be more potent. We therefore irradiated cells for 10, 15, or 20 minutes after 48 h incubation with the rhodium complex. These results are shown in figure 2.8. Here it should be noted that longer periods of irradiation even without metal complex lead to some inhibitory effects in both MMR-deficient and MMR-proficient cell lines; evaporation of the medium is also somewhat of a problem. Nonetheless, light activation over short periods does indeed lead to greater inhibition of cell proliferation and only for Δ -[Rh(bpy)₂chrysi]³⁺ in the mismatch repair deficient HCT116O cells. Again, parallel experiments with Δ -[Rh(bpy)₂chrysi]³⁺ provide a useful control. Under the conditions utilized, light activation appears to enhance the inhibition of DNA synthesis preferentially by Δ -[Rh(bpy)₂chrysi]³⁺ and only in the MMR-deficient HCT116O cells. These data are consistent with DNA serving as the target for the rhodium complex inside the cell. Certainly these results demonstrate a clear correlation between mismatch targeting by rhodium photocleavage and biological potency in a cell-selective manner.

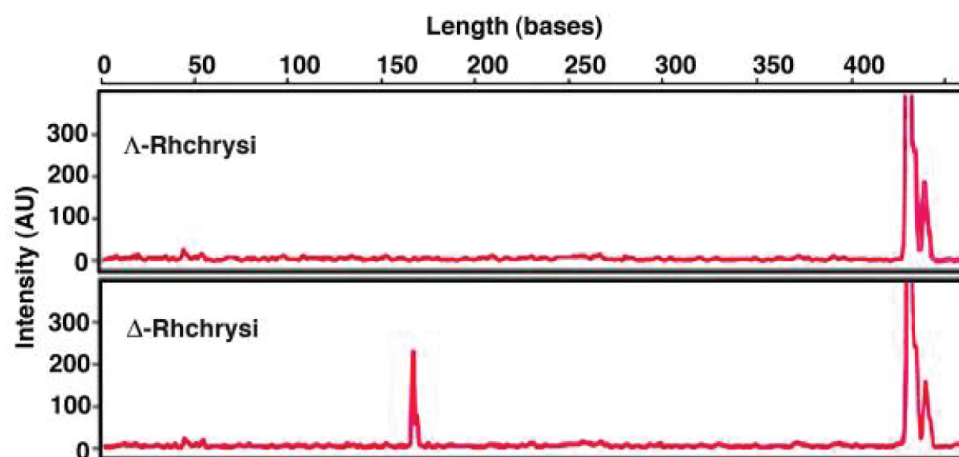


Figure 2.6. Effect of stereoisomers on photocleavage. Shown are capillary electropherograms after photolysis of 436-mer PCR products containing a single CC mismatch with 500 nM Λ -(middle) or Δ -(bottom) $[\text{Rh}(\text{bpy})_2\text{chrysi}]^{3+}$, as described earlier.³ Mismatch-specific photocleavage to produce a 170 base fragment is evident only with the Δ -isomer.

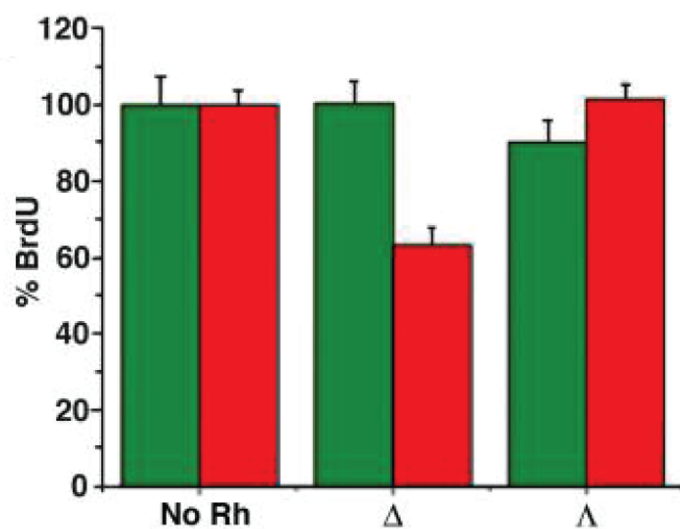


Figure 2.7. Antiproliferative effects of different stereoisomers of $\text{Rh}(\text{bpy})_2\text{chrysi}^{3+}$.

Shown are the effects on BrdU incorporation in HCT116O (red) and HCT116N (green) cells after 48 h incubation without with $5\mu\text{M}$ Λ - or Δ - $[\text{Rh}(\text{bpy})_2\text{chrysi}]^{3+}$. The selective inhibition of the mismatch repair deficient HCT116O cell line is seen only with the Δ -isomer.

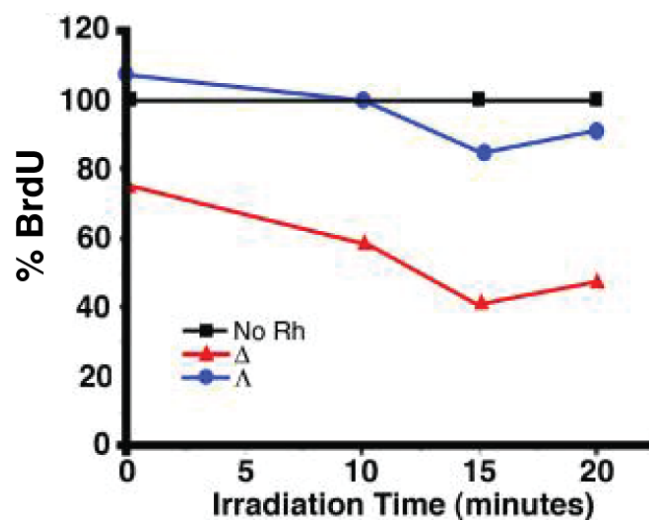


Figure 2.8. Antiproliferative effect of different stereoisomers of $\text{Rh}(\text{bpy})_2\text{chrysi}^{3+}$ with irradiation. Shown are the effects of varying amounts of irradiation of HCT1160 cells in the absence of $[\text{Rh}(\text{bpy})_2\text{chrysi}]^{3+}$ (black), in the presence of $5\mu\text{M}$ Δ - $[\text{Rh}(\text{bpy})_2\text{chrysi}]^{3+}$ (red) or Λ - $[\text{Rh}(\text{bpy})_2\text{chrysi}]^{3+}$ (blue) after 48 h incubation.

2.4. Discussion

The results reported here establish that the bulky rhodium metalloinsertors serve as inhibitors of cellular proliferation and, significantly, that the complexes do so with cellular selectivity. Biological effects are seen preferentially in MMR-deficient cells. These results do not establish DNA mismatch targeting as the basis for the cell selectivity. However, these data are consistent with mismatched DNA being the target of these complexes, and hence the basis of the preferential reaction in MMR-deficient cell lines, in which mismatches are more abundant.

It is noteworthy that in the absence of light, the complexes bind DNA mismatches non-covalently, albeit with high affinity and specificity. Because a covalent adduct is not formed and, in the absence of light, no DNA damage is directly generated, any biological effect would be expected to be more modest; irradiation, which does cause DNA strand breaks, should enhance the effect, as we observe. Likely, then, without light the metal-mismatch complex provides a secondary signal for protein binding or activation. It should also be noted that light activation of the metal complex generates only a short lived ligand radical; thus, intimate association of the rhodium complex with its target is needed for a light dependent reaction.¹⁴

Significantly, the biological effects we observe in MMR-deficient cells also are enantiospecific, just as binding of the bulky rhodium metalloinsertors at mismatched DNA sites is enantiospecific. It is the Δ -isomer of $[\text{Rh}(\text{bpy})_2\text{chrysi}]^{3+}$ that binds and selectively cleaves a neighboring base pair mismatch, and it is the Δ -isomer that shows the biological effect preferentially in MMR-deficient cells.

2.5. Conclusions

There is a clear correlation if not an established causality between DNA mismatch targeting by the rhodium complexes and the observed inhibition of cellular proliferation in MMR-deficient cells. These results therefore highlight a new class of compounds for possible application in cancer therapeutics. The work furthermore underscores a cell-selective strategy in chemotherapeutic design by chemically and site-specifically targeting DNA mismatches.

2.6. References

1. B.A. Jackson and J.K. Barton. *J. Am. Chem. Soc.* **1997** *119*, 12986-12987.
2. B.A. Jackson, V.Y. Alekseyev, and J.K. Barton. *Biochemistry* **1999** *38*, 4655-4662.
3. B.A. Jackson and J.K. Barton. *Biochemistry* **2000** *39*, 6176-6182.
4. H. Junicke, J.R. Hart, J. Kisko, O. Glebov, I.R. Kirsch, and J.K. Barton. *Proc. Natl. Acad. Sci. U.S.A.* **2003** *100*, 3737-3742.
5. J.R. Hart, M.D. Johnson, and J.K. Barton. *Proc. Natl. Acad. Sci. U.S.A.* **2004**, *126*, 14040-14044.
6. M. Koi, A. Umar, D.P. Chauhan, S.P. Cherian, J.M. Carethers, T.A. Kunkel, and C.R. Boland. *Cancer Res.* **1994** *54*, 4308-4312.
7. H. Murner, B.A. Jackson, and J.K. Barton. *Inorg. Chem.* **1998** *37*, 3007-3012.
8. Reitmar, H. Armin, R. Risley, R.G. Bristow, T. Wilson, A. Ganesh, A. Jang, J. Peacock, S. Benchimol, and R.P. Hill, *et al.* *Cancer Res.* **1997** *57*, 3765-3771.
9. H.G. Gratzner. *Science* **1982** *218*, 474-475.
10. C.A. Puckett and J.K. Barton. *J. Am. Chem. Soc.* **2007**, *129*, 46-47.
11. C.A. Puckett and J.K. Barton. *Biochemistry* **2008**, *47*, 11711-11716.

12. D. Fink, S. Aebi, and S.B. Howell. *Clinical Cancer Research* **1998** 4, 1-6.
13. V. O'Brien and R. Brown. *Carcinogenesis* **2006** 27, 682-692.
14. A. Sitlani, A.M. Pyle, and J.K. Barton. *J. Am. Chem. Soc.* **1992** 114, 2303-2312.

CHAPTER 3: DNA MISMATCH BINDING AND ANTI-PROLIFERATIVE EFFECTS OF RHODIUM METALLOINSERTORS

Note: This chapter was adapted from “DNA mismatch binding and anti-proliferative effects of rhodium metalloinsertors.” R.J. Ernst, H.G. Song, and J.K. Barton. *J. Am. Chem. Soc.* **2009**, *131*, 2359-2366.

3.1. Introduction

Recent work within our laboratory on luminescent ruthenium dppz complexes has shown that these tris(chelate) complexes are taken up inside cells through passive diffusion facilitated by the membrane potential.^{28,29} Variations in ancillary ligands of these ruthenium complexes have dramatic effects on cellular uptake, with increased lipophilicity facilitating uptake. Here we examine the effects of ancillary ligand variation in the $\text{Rh(L)}_2\text{chrysi}^{3+}$ family (figure 3.1) on the ability of these complexes to target DNA mismatches *in vitro* and *in vivo*. Rhodium metalloinsertors bearing ammine, 2,2-bipyridine (bpy), 9,10-phenanthroline (phen), 1,4-diphenylphenanthroline (DIP), and 2,2-dipyridylamine (HDPA) ancillary ligands were synthesized. Their mismatch targeting capabilities were determined by photocleavage titration and cellular proliferation assays. Importantly we establish that the differential inhibition of cellular proliferation in MMR-deficient cells is correlated with mismatch binding affinity.

Acknowledgements: Hang Song performed all photocleavage assays, the initial synthesis of $[\text{Rh}(\text{HDPA})_2\text{chrysi}]^{3+}$, and the structural modeling of $[\text{Rh}(\text{DIP})_2\text{chrysi}]^{3+}$ bound to mismatched DNA. Jon Hart performed the initial synthesis of $[\text{Rh}(\text{NH}_3)_4\text{chrysi}]^{3+}$.

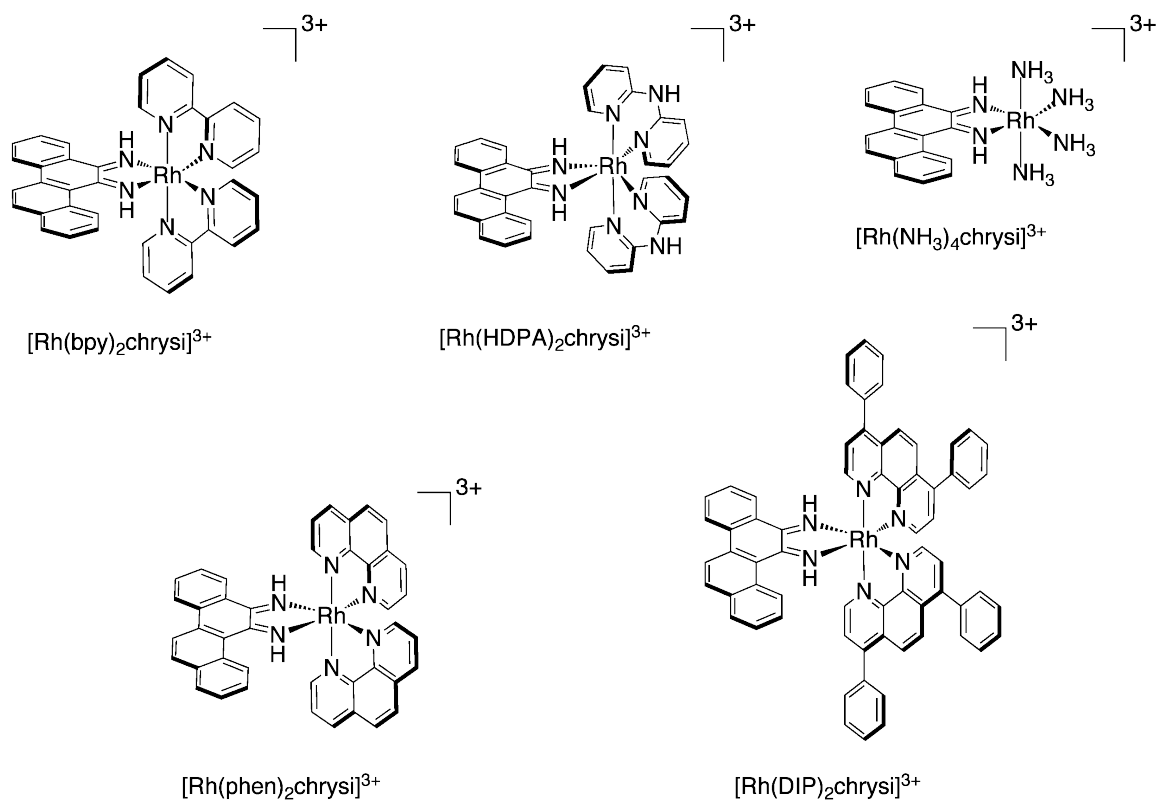


Figure 3.1. Rh(L)₂chrysi³⁺ family of metalloinsertors.

3.2. Experimental Protocols

3.2.1 Materials

RhCl₃ was purchased from Pressure Chemical, Inc. (Pittsburgh, PA). [Rh(NH₃)₅Cl]Cl₂ was obtained from Strem Chemical, Inc. (Newburyport, MA). 2,2'-dipyridylamine (HDPA), 4,7-diphenyl-1,10-phenanthroline (DIP), and Sephadex ion exchange resin were obtained from Sigma-Aldrich (St. Louis, MO). Sep-Pak C₁₈ solid phase extraction cartridges were purchased from Waters Chemical Co. (Milford, MA). Phosphoramidites were purchased from Glen Research (Sterling, VA). Media and supplements were purchased from Invitrogen (Carlsbad, CA). BrdU, antibodies, buffers, and peroxidase substrate were purchased in kit format from Roche Molecular Biochemicals (Mannheim, Germany). All commercial materials were used as received.

3.2.2 Oligonucleotide Synthesis

Oligonucleotides were synthesized on an Applied Biosystems 3400 DNA synthesizer using standard phosphoramidite chemistry. DNA was synthesized with a 5'-dimethoxy trityl (DMT) protecting group. The oligonucleotides were cleaved from the beads by reaction with concentrated ammonium hydroxide at 60°C overnight. The resulting free oligonucleotides were purified by HPLC using a C₁₈ reverse-phase column (Varian, Inc.) on a Hewlett-Packard 1100 HPLC. The DMT group was removed by reaction with 80% acetic acid for 15 min at room temperature. The DMT-free oligonucleotides were precipitated with absolute ethanol and purified again by HPLC. Positive identification of the oligonucleotides and their purity were confirmed by MALDI-TOF mass spectrometry. Quantification was performed on a Beckman DU 7400 spectrophotometer using the extinction coefficients at 260 nm (ϵ_{260}) estimated for single stranded DNA.

3.2.3 Synthesis and Characterization of Metal Complexes

Chrysene-5,6-dione, $[\text{Rh}(\text{bpy})_2\text{chrysi}]\text{Cl}_3$ and $[\text{Rh}(\text{phen})_2\text{chrysi}]\text{Cl}_3$ were prepared according to previously reported procedures.^{19,20,31} Rhodium complexes were prepared by one of two synthetic routes; the first is shown in figure 3.2. Two equivalents of ancillary ligand are added to RhCl_3 . The remaining two chlorides are then exchanged for ammine ligands through a triflate intermediate as described by Sargeson and coworkers.^{32,33} Lastly, the chrysi ligand is installed by condensing the quinone onto the amines. This is the standard approach for the bpy, phen, and DIP complexes. Alternatively, the route shown in figure 3.3 may be taken. Here, the commercially available chloropentammine complex is converted to the hexaammine complex, again as described by Sargeson.^{32,33} The chrysi ligand is then installed by the condensation reaction as before, and finally the chelating ancillary ligands are substituted for the remaining four ammine ligands. This pathway is taken for the tetraammine and HDPA complexes.

[Rh(NH₃)₄chrysi]OTf₃: $[\text{Rh}(\text{NH}_3)_6]\text{OTf}_3$ was prepared as described by Sargeson.^{32,33} $[\text{Rh}(\text{NH}_3)_6]\text{OTf}_3$ was reacted with a limiting amount of chrysene quinone in a 3:1 acetonitrile:water mixture with excess sodium hydroxide as a catalyst to form $[\text{Rh}(\text{NH}_3)_4\text{chrysi}]\text{OTf}_3$. Acetonitrile was removed *in vacuo*, followed by filtration to remove unreacted chrysi quinone. The product was separated from unreacted $[\text{Rh}(\text{NH}_3)_6]\text{OTf}_3$ by solid phase extraction on a C₁₈ cartridge and eluted with 1:1:0.001 acetonitrile:water:TFA. ¹H NMR (d₆-DMSO, 50°C, 300 MHz): δ 13.30 (s), 12.32 (s), 8.876 (t, 1H, 7.7Hz), 8.787 (d, 1H, 7.9Hz), 8.57-8.51 (m, 2H), 8.358 (dd, 1H, 8.9Hz, 4.6Hz), 8.145 (d, 1H, 7.7Hz), 7.85-7.70 (m, 4H), 4.73-4.54 (broad m, 6H), 3.862 (s, 3H) ppm. UV/vis (H₂O, pH 5): 263 nm, (60,900 M⁻¹cm⁻¹), 283 nm (38,100 M⁻¹cm⁻¹), 326 nm

(12,600 $M^{-1}cm^{-1}$), 413 nm (12,000 $M^{-1}cm^{-1}$). MALDI-MS (cation) 425 m/z ($M-2H^+$) obs., 427 m/z calc.

[Rh(HDPA)₂(chrysi)]OTf₃: $[Rh(NH_3)_4(chrysi)]OTf_3$ (15 mg, 0.02 mmol) was reacted with HDPA (20 mg, 0.12 mmol, excess) in 20 mL ethanol and 20 mL water. The dark red solution was heated under reflux for 16 h. The reaction mixture turned reddish brown upon heating. Ethanol was removed under vacuum and the resulting solution filtered to remove any residue. The filtrate was concentrated on a Sep-Pak C₁₈ cartridge eluting with 1:1:0.1% acetonitrile:water:TFA, lyophilized, and purified on an alumina column eluting with 2% methanol in dichloromethane. The fractions were collected and dried under vacuum to give an orange-brown solid (8 mg, 39%). ¹H-NMR (*d*₆-DMSO, 300 MHz): δ 12.84 (s, 1H), 12.34 (s, 1H), 11.78 (s, 1H), 10.32 (d, 1H, 8.7Hz), 8.63 (d, 1H, 6.9Hz), 8.40 (d, 1H, 8.4Hz), 8.31 (d, 1H, 9.3Hz), 8.14 (m, 2H), 8.07 (d, 1H, 8.7Hz), 8.04 (d, 1H, 5.4Hz), 7.94 (m, 4H), 7.77 (m, 5H), 7.58 (m, 2H), 7.48 (d, 1H, 8.1Hz), 7.41 (d, 1H, 8.4Hz), 7.32 (s, 1H), 7.14 (m, 2H), 7.04 (t, 1H, 6.8Hz), 6.98 (t, 1H, 6.9Hz), 6.81 (t, 1H, 6.5Hz) ppm. UV/vis (H₂O, pH 5): 287 nm (42,200 $M^{-1}cm^{-1}$), 321 nm (23,000 $M^{-1}cm^{-1}$), 442 nm (8,800 $M^{-1}cm^{-1}$). ESI-MS (cation): 699.2 m/z ($M-2H^+$), 350.1 m/z ($M-H^+$) obs., 699.2 m/z ($M-2H^+$) calc.

[Rh(DIP)₂(NH₃)₂]OTf₃: $RhCl_3$ and 2 equivalents of DIP were combined in 1:1 ethanol:water and refluxed overnight. The solvent was removed *in vacuo* and the product was recrystallized by dissolving in acetonitrile at 60°C and cooling to -20°C. The precipitate was collected by filtration, washed in diethyl ether, and dissolved in neat triflic acid. The solution was again cooled and added dropwise to NH_4OH at -20°C. The

pale white precipitate was collected by filtration and washed with a small amount of water to give $[\text{Rh}(\text{DIP})_2(\text{NH}_3)_2]\text{OTf}_3$.

[Rh(DIP)₂chrysi]Cl₃: $[\text{Rh}(\text{DIP})_2(\text{NH}_3)_2]\text{OTf}_3$ was combined with a 10% excess of 5,6-chrysenquinone and a catalytic amount of NaOH in acetonitrile and stirred at room temperature overnight. The condensation was terminated by addition of a stoichiometric amount of HCl. The solvent was removed *in vacuo* and the product was purified by alumina column chromatography. Unbound chrysi ligand eluted first with ethyl acetate, and the purified product then eluted with acetonitrile. Finally, the compound was dissolved in 3:2 MeCN:H₂O and the triflate counterion was exchanged for chloride ion with Sephadex QAE-125 ion exchange resin. UV/vis (H₂O, pH 5): 290 nm (104,000 M⁻¹cm⁻¹); 335 nm (43,900 M⁻¹cm⁻¹); 373 nm (22,300 M⁻¹cm⁻¹). ESI-MS (cation): 1020.9 m/z (M-2H⁺), 511.0 m/z (M-H²⁺) obs., 1023 calc.

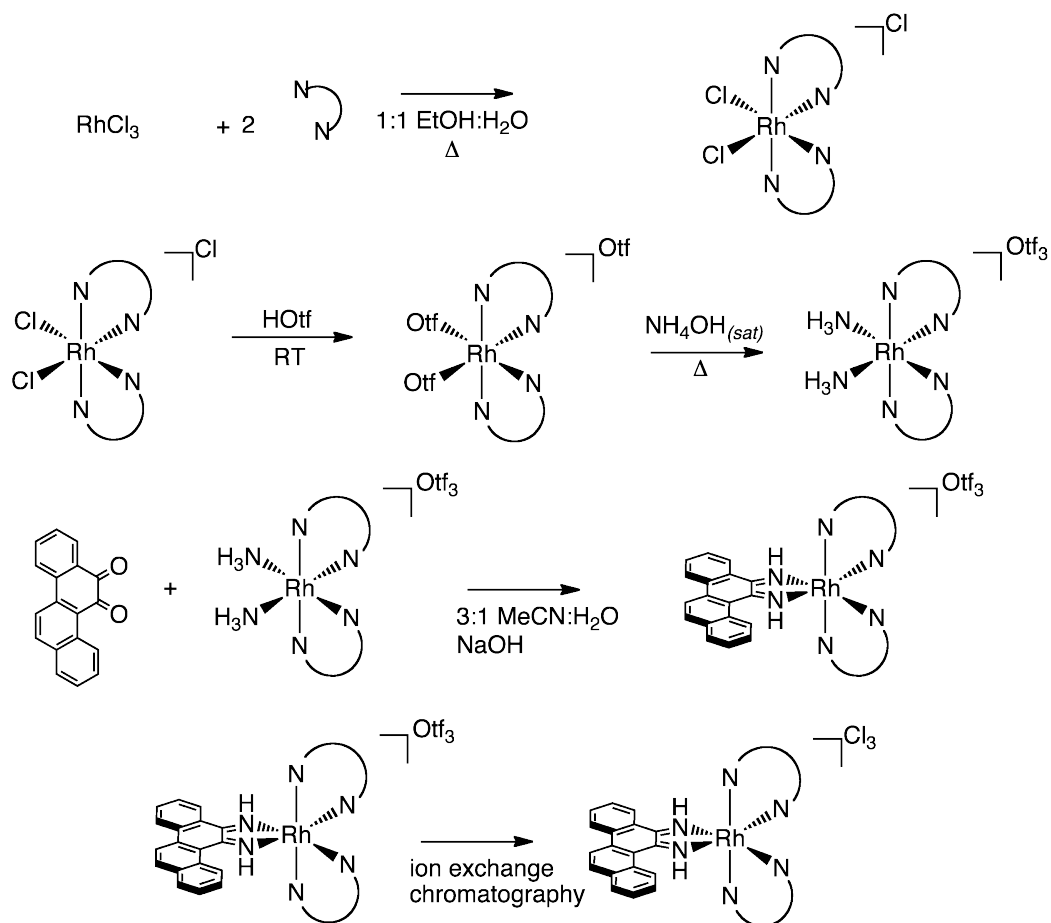


Figure 3.2. $\text{Rh(L)}_2\text{chrysi}^{3+}$ synthetic route I.

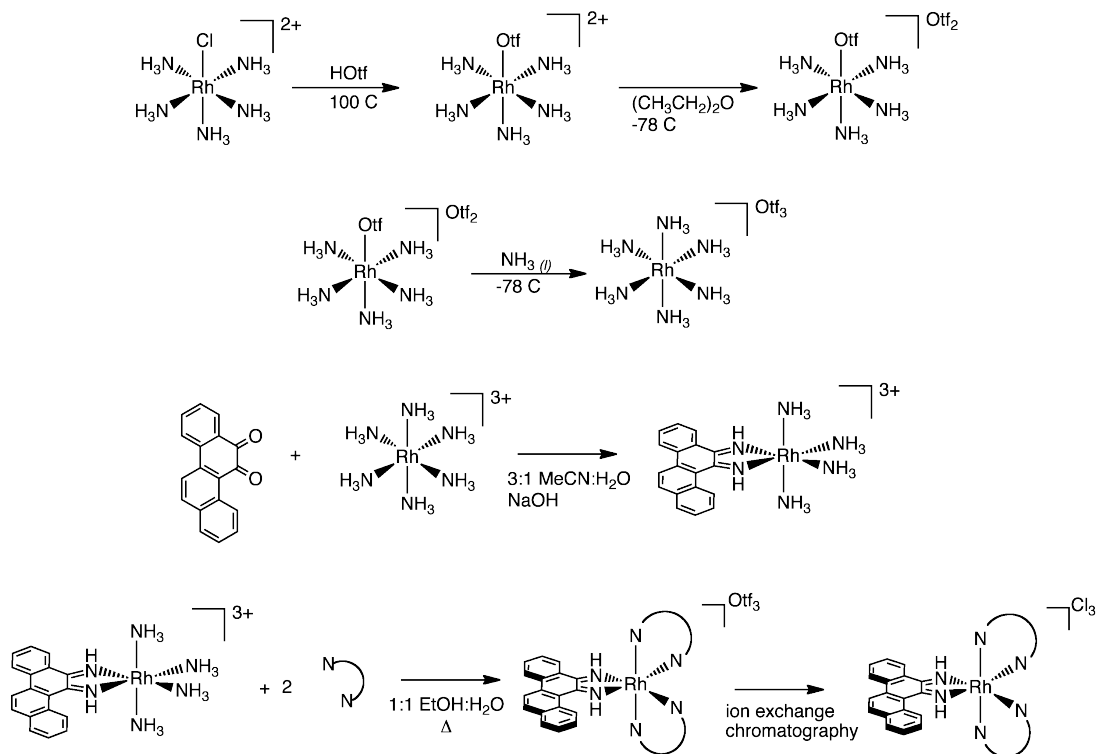


Figure 3.3. Rh(L)₂chrysi³⁺ synthetic route II.

3.2.4 Photocleavage Titrations

The oligonucleotide was ^{32}P -labeled at the 5'-end by incubating DNA with ^{32}P -ATP and polynucleotide kinase (PNK) at 37°C for 2 h, followed by purification using gel electrophoresis. A small amount of the labeled DNA (less than 1% of the total amount of DNA) was added to $2\ \mu\text{M}$ DNA in $100\ \text{mM NaCl}$, $20\ \text{mM NaP}_i$, pH 7.1 buffer. The DNA hairpin was annealed by heating at 90°C for 10 min and cooling slowly to room temperature over a period of 2 h. Racemic rhodium complex solutions ranging from nanomolar to micromolar concentration were made in Milli-Q water. Annealed $2\ \mu\text{M}$ DNA ($10\ \mu\text{L}$) and $10\ \mu\text{L}$ of Rh solution at each concentration were mixed in a microcentrifuge tube and incubated at 37°C for 10 min. A light control (LC), in which the DNA was mixed with $10\ \mu\text{L}$ of water and irradiated, and a dark control (DC), in which the DNA was mixed with the highest concentration of rhodium complex without irradiation, were also prepared. The samples were left in the heat block and irradiated on an Oriel (Darmstadt, Germany) 1000 W Hg/Xe solar simulator (320–440 nm) for 5 min. The irradiated samples were dried and electrophoresed in a 20% denaturing polyacrylamide gel. The gel was then exposed to a phosphor screen, and the relative amounts of DNA in each band were quantitated by phosphorimagery (ImageQuant).

3.2.5 Binding Constant Determination

The fraction of DNA cleaved in each lane on the gel was normalized and plotted against the log of the concentration of rhodium complex. At least three photocleavage titrations were carried out for each metal complex. The pooled data were fit to a sigmoidal curve using OriginPro 6.1. The resulting midpoint value (i.e., the log of [rhodium complex] at the inflection point of the curve) was converted to units of concentration ($[\text{Rh}_{50\%}]$). The

dissociation constant was calculated according to $K_d = [Rh_{50\%}] - 0.5[DNA]$, and the binding constant was defined as $K_B = 1/K_d$. The errors were derived from the errors associated with the midpoint values. For complexes that did not photocleave DNA, a binding competition titration was carried out with a constant amount (1 μ M) of $Rh(bpy)_2(chrysi)^{3+}$ added to each sample. The binding and dissociation constants of the non-photocleaving complex were calculated by solving simultaneous equilibria involving DNA, $Rh(bpy)_2(chrysi)^{3+}$ and the complex in question in Mathematica 6.0.

3.2.6 Cell Culture

HCT116N and HCT116O cells were grown in RPMI medium 1640 supplemented with: 10% FBS; 2 mM L-glutamine; 0.1 mM non-essential amino acids; 1 mM sodium pyruvate; 100 units/mL penicillin; 100 μ g/mL streptomycin; and 400 μ g/mL geneticin (G418). Cells were grown in tissue culture flasks and dishes (Corning Costar, Acton, MA) at 37°C under 5% CO₂ atmosphere.

3.2.7 Cellular Proliferation ELISA

HCT116N and HCT116O cells were plated in 96-well plates at 2,000 cells/well and allowed 24 hours to adhere. The cells were then incubated with rhodium complexes for the durations specified. For incubation less than 72 hours, the Rh-containing media was replaced with fresh media, and the cells were grown for the remainder of the 72 hour period. Cells were labeled with BrdU 24 hours before analysis. The BrdU incorporation was quantified by antibody assay according to established procedures.^{34,35} Cellular proliferation was expressed as the ratio of the amount of BrdU incorporated by the treated cells to that of the untreated cells.

3.3. Results

3.3.1 Binding Affinities for Metal Complexes at Single Base Mismatches

The binding constants of the family of $\text{Rh}(\text{L}_2)\text{chrysi}^{3+}$ complexes at a CC and AC mismatch in a 29-mer DNA hairpin with the sequence:



($\underline{\text{X}}$ = C or A, underline denotes the mismatch) were measured. The hairpin sequence allows cleavage site determination on both strands around the DNA mismatch. By irradiating samples of DNA titrated with varying concentrations of a rhodium complex, a photocleavage titration curve is obtained from which the binding constant of the rhodium complex is determined. A typical autoradiogram, taken after electrophoresis through a denaturing gel, of samples in a photocleavage titration with *rac*- $\text{Rh}(\text{bpy})_2\text{chrysi}^{3+}$ at a CC mismatch is shown in figure 3.4 (A). The position of the photocleavage bands indicates that $\text{Rh}(\text{bpy})_2\text{chrysi}^{3+}$ cleaves one base neighboring the mismatch site near the 3'-end. This cleavage pattern is found both for *rac*- $\text{Rh}(\text{phen})_2\text{chrysi}^{3+}$ and *rac*- $\text{Rh}(\text{DIP})_2\text{chrysi}^{3+}$ and holds for the AC mismatch for *rac*- $\text{Rh}(\text{bpy})_2\text{chrysi}^{3+}$ and *rac*- $\text{Rh}(\text{phen})_2\text{chrysi}^{3+}$. No other photocleavage bands are observed, demonstrating the high specificity of $\text{Rh}(\text{L}_2)\text{chrysi}^{3+}$ complexes binding to the mismatch. The photocleavage titration curve is generated from the autoradiogram by quantifying the amount of photocleavage relative to the total amount of DNA at each Rh concentration. Pooled data from at least three repeats were fitted to a sigmoidal curve (Figure 3.4, B) for determination of the midpoint ($[\text{Rh}_{50\%}]$) and the dissociation constant (K_d). The K_d value for *rac*- $\text{Rh}(\text{bpy})_2\text{chrysi}^{3+}$ at a CC mismatch is found to be 30 nM. For *rac*- $\text{Rh}(\text{phen})_2\text{chrysi}^{3+}$ and *rac*- $\text{Rh}(\text{DIP})_2\text{chrysi}^{3+}$ at a CC mismatch, K_d values of 320 nM and 11 μM are found, respectively (Table 3.1).

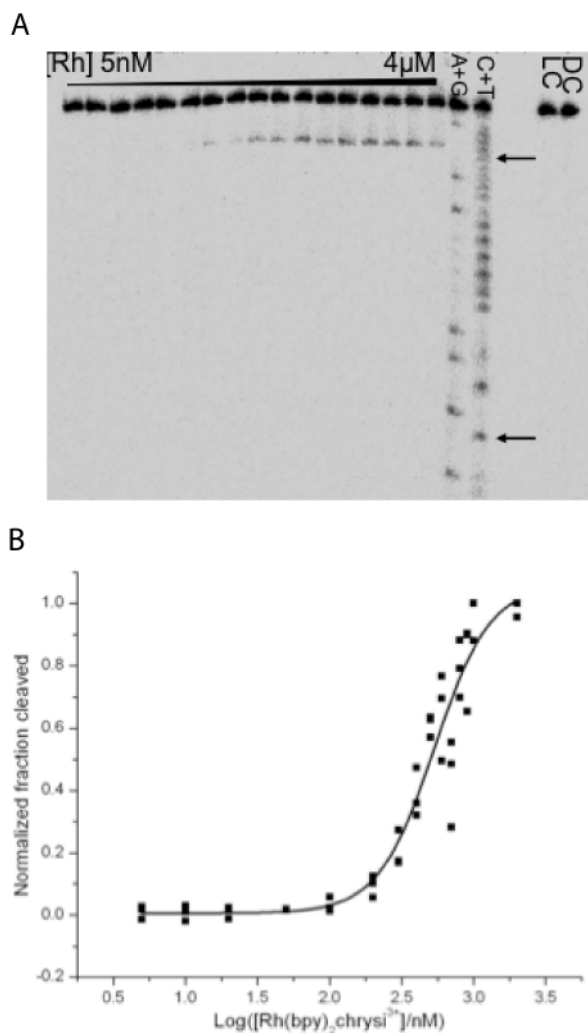


Figure 3.4. Binding affinities determined through DNA photocleavage. The DNA hairpin sequence is 5'-GGCAGGXATGGCTTTTTGCCATCCCTGCC-3' (X = C or A, underline denotes the mismatch). Samples were irradiated and electrophoresed through a 20% denaturing PAGE gel. A light control (LC, without rhodium) and dark control (DC, without irradiation) were included. A representative autoradiogram of a photocleavage titration with Rh(bpy)₂chrysi³⁺ (A, arrows indicate positions of mismatched bases) and a representative sigmoidal curve fit of pooled data from photocleavage titrations for binding constant determination (B) are shown.

For the AC mismatch with both *rac*-Rh(bpy)₂chrysi³⁺ and *rac*-Rh(phen)₂chrysi³⁺, K_d values are somewhat higher, as we expect given the greater thermodynamic stability of an AC mismatch versus a CC mismatch. *Rac*-Rh(DIP)₂chrysi³⁺ does not yield any photocleavage up to 100 μM; thus, its K_d value is estimated to be greater than that.

As with phenanthrenequinone diimine rhodium complexes containing saturated amine ligands, Rh(NH₃)₄ chrysi³⁺ and *rac*-Rh(HDPA)₂chrysi³⁺ promote relatively little DNA cleavage upon irradiation.³⁶ As a result, their binding affinities were determined through binding competition titrations with 1 μM *rac*-Rh(bpy)₂chrysi³⁺. Based on the binding constant of Rh(bpy)₂chrysi³⁺, the binding constant of Rh(NH₃)₄chrysi³⁺ is calculated by solving simultaneous equilibria at the inflection point of the photocleavage titration curve. Through this competitive titration, the binding constant of Rh(NH₃)₄chrysi³⁺ at a CC mismatch is found to be $1.0 \times 10^8 \text{ M}^{-1}$. At an AC mismatch, K_B of Rh(NH₃)₄chrysi³⁺ is $3.4 \times 10^6 \text{ M}^{-1}$. From similar binding competition titrations, the binding constant of *rac*-Rh(HDPA)₂chrysi³⁺ is found to be $2.0 \times 10^7 \text{ M}^{-1}$ at a CC mismatch and $2.6 \times 10^6 \text{ M}^{-1}$ at an AC mismatch. It is apparent that the binding affinity correlates inversely with complex size; the smallest complex, Rh(NH₃)₄chrysi³⁺, shows the highest affinities for mismatched sites. The binding constants for the entire series of Rh(L₂)chrysi³⁺ complexes are summarized in table 3.1.

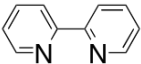
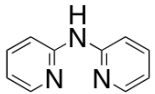
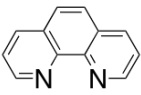
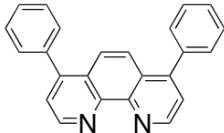
Complex	Ancillary ligand	K_B (CC)/M ⁻¹	K_B (AC)/M ⁻¹
Rh(NH) ₃ chrysi ³⁺	NH ₃	1.0×10^8	3.4×10^6
Rh(bpy) ₂ chrysi ³⁺		3.4×10^7	2.2×10^6
Rh(HDPA) ₂ chrysi ³⁺		2.0×10^7	2.6×10^6
Rh(phen) ₂ chrysi ³⁺		3.2×10^6	1.4×10^6
Rh(DIP) ₂ chrysi ³⁺		9.1×10^4	$< 10^4$

Table 3.1. Binding Affinities of Rh(L)₂chrysi³⁺ complexes^c for CC and AC

Mismatches. Binding constants are determined from photocleavage or binding competition titrations using a DNA hairpin with the sequence:



X = C or A, underline denotes the mismatch. Samples were irradiated with a solar simulator (320–440 nm) at 37°C in 50 mM NaCl, 10 mM NaP_i, pH 7.1 as described in the Experimental section. For the polypyridyl complexes, values are given for racemic mixtures. Uncertainties are estimated to be 10%.

3.3.2 Inhibition of Cellular Proliferation by ELISA Assay

An ELISA assay for DNA synthesis was used to quantify the effects of the metalloinsertors on the proliferation of HCT116N cells (MMR-proficient) and HCT116O cells (MMR-deficient).²⁶ Both cell lines were incubated with 0–25 μM of each member of the $\text{Rh(L)}_2\text{chrysi}^{3+}$ family except $\text{Rh(DIP)}_2\text{chrysi}^{3+}$, which was administered at 0–5 μM concentrations due to its unique uptake characteristics. Incubations were performed for 12, 24, 48 or 72 hours. After the 12, 24, and 48 hour incubations, the media containing Rh was replaced with fresh media, and the cells were grown for the remainder of the 72 hour period. The extent of cellular proliferation is expressed as the ratio of BrdU incorporated by the rhodium treated cells as compared to untreated controls. Figures 3.5–3.9 show representative data for each member of the $\text{Rh(L)}_2\text{chrysi}^{3+}$ family at various incubation times. No significant preferential inhibition of the HCT116O cell line is seen at incubation times less than 24 hours, consistent with previous results for $\text{Rh(bpy)}_2\text{chrysi}^{3+}$, with the exception of $\text{Rh(DIP)}_2\text{chrysi}^{3+}$, which displays a small differential effect at 12 hours.²⁶ With longer incubation times, however, $\text{Rh(NH}_3)_4\text{chrysi}^{3+}$ in particular (figure 3.9) displays a strong differential effect with preferential inhibition of the MMR-deficient HCT116O cell line over the MMR-proficient HCT116N cell line. In particular, 48 hour treatment with 10 μM $\text{Rh(NH}_3)_4\text{chrysi}^{3+}$ inhibits the proliferation of the HCT116O line by $82\pm 2\%$ while exerting little to no effect on the HCT116N line ($7\pm 6\%$ inhibition).

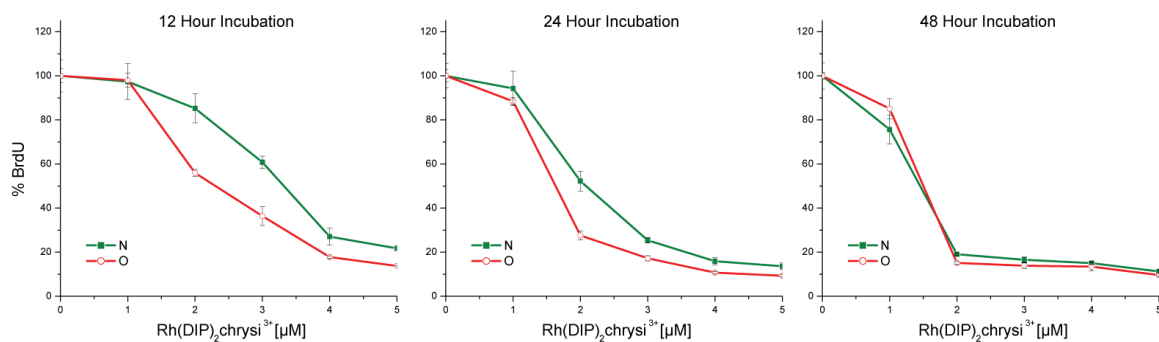


Figure 3.5. Inhibitory effects of Rh(DIP)₂chrysi³⁺ as a function of incubation time on cellular proliferation. Shown are plots of BrdU incorporation normalized to the BrdU incorporation of untreated cells as a function of rhodium concentration. Standard error bars for 5 trials are shown. MMR-proficient HCT116N cells (green) and MMR-deficient HCT116O cells (red) were plated and allowed 24 hours to adhere before incubation with 0–5 μM Rh(DIP)₂chrysi³⁺ for 12, 24, or 48 hours. At the end of the incubation, the media containing Rh was replaced with fresh media and cells were grown for an additional 60 hours before ELISA analysis. BrdU was added to the media 24 hours prior to analysis.

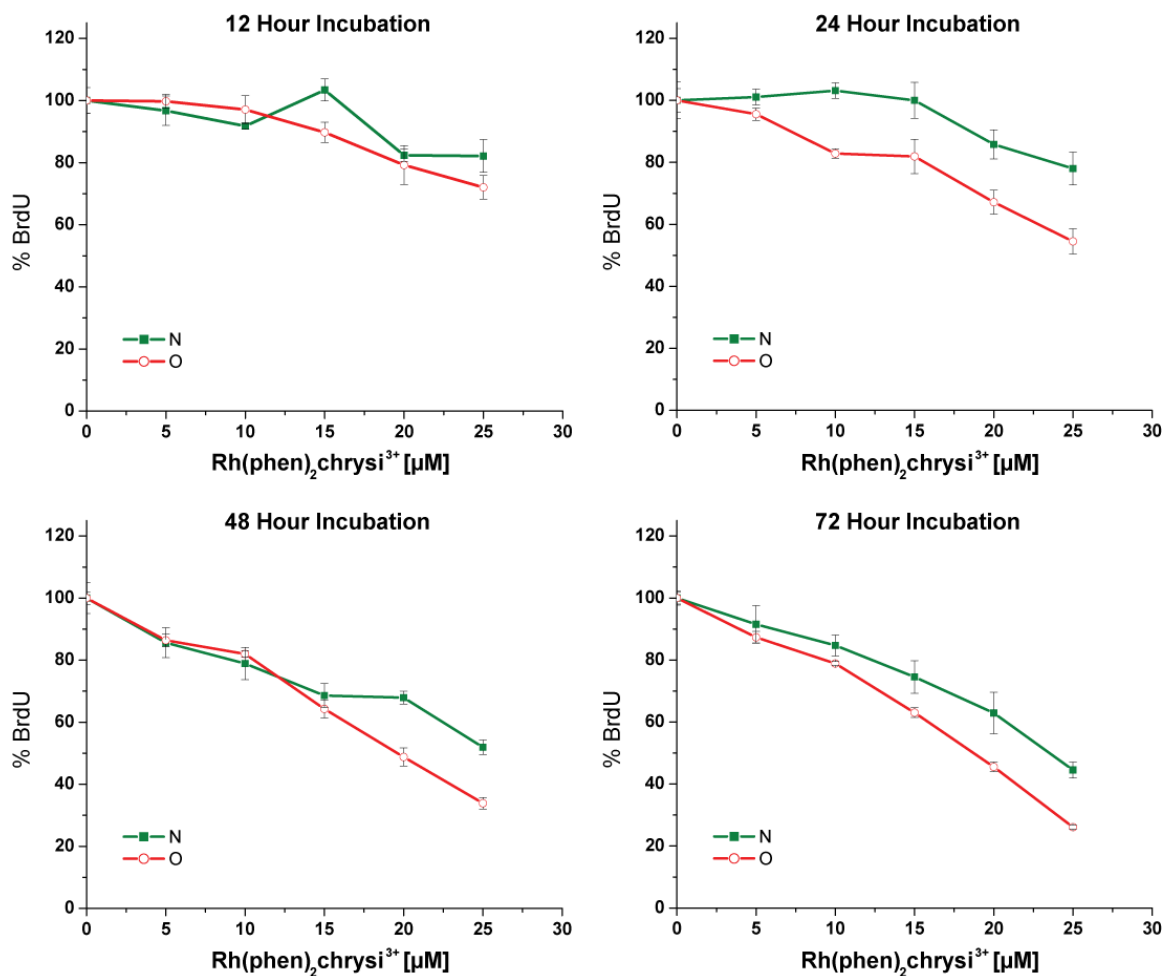


Figure 3.6. Inhibitory effects of Rh(phen)₂chrysi³⁺ as a function of incubation time on cellular proliferation. Shown are plots of BrdU incorporation (a measure of DNA synthesis and therefore cellular proliferation) normalized to the BrdU incorporation of untreated cells as a function of rhodium concentration. Standard error bars for 5 trials are shown. MMR-proficient HCT116N cells (green) and MMR-deficient HCT116O cells (red) were plated and allowed 24 hours to adhere before incubation with 0–25 μM Rh(phen)₂chrysi³⁺ for 12, 24, 48, or 72 hours. At the end of the 12, 24, and 48 hour incubations, the media containing Rh was replaced with fresh media for the remainder of the 72 hours, followed by ELISA analysis. BrdU was added to the media 24 hours prior to analysis.

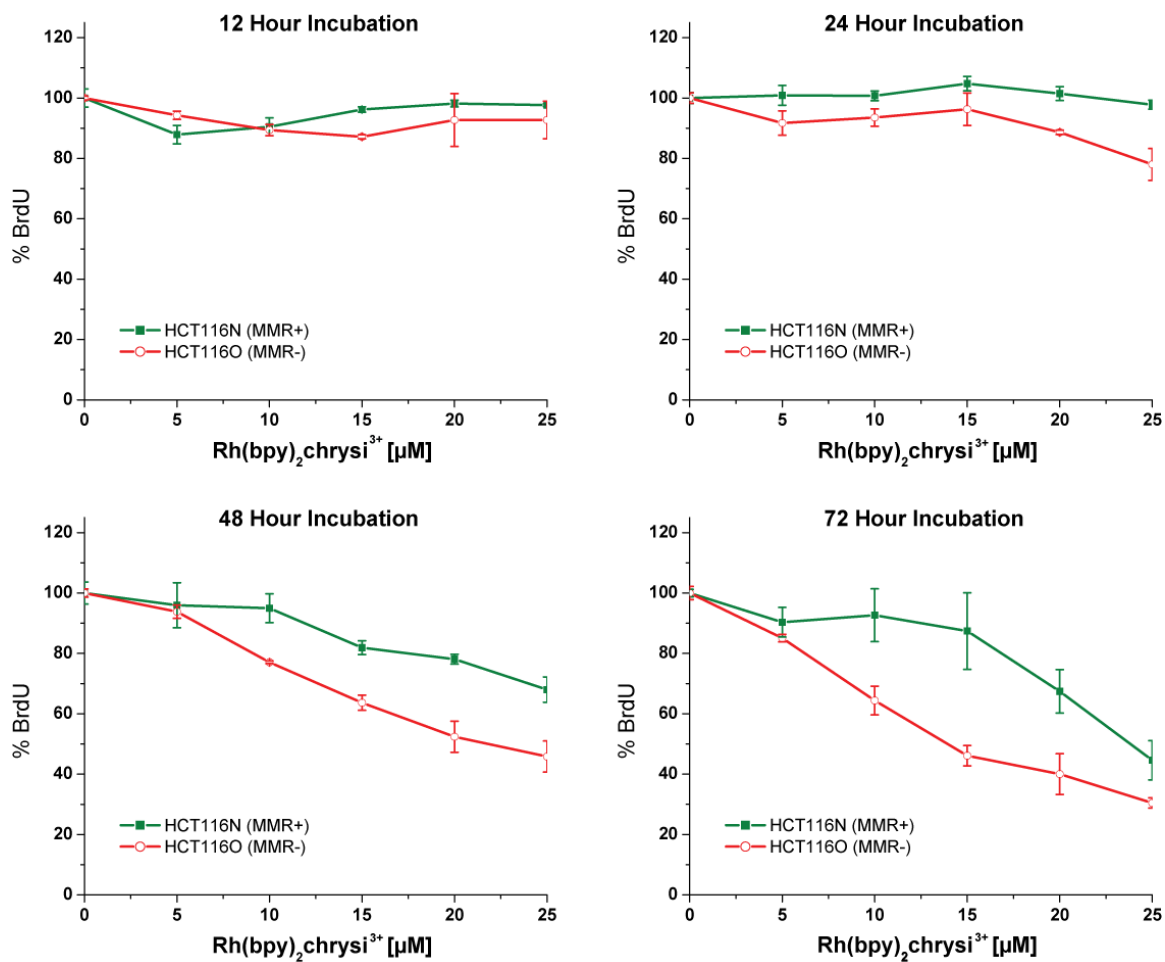


Figure 3.7. Inhibitory effects of Rh(bpy)₂chrysi³⁺ as a function of incubation time on cellular proliferation. Shown are plots of BrdU incorporation (a measure of DNA synthesis and therefore cellular proliferation) normalized to the BrdU incorporation of untreated cells as a function of rhodium concentration. Standard error bars for 5 trials are shown. MMR-proficient HCT116N cells (green) and MMR-deficient HCT116O cells (red) were plated and allowed 24 hours to adhere before incubation with 0–25 μM Rh(bpy)₂chrysi³⁺ for 12, 24, 48, or 72 hours. At the end of the 12, 24, and 48 hour incubations, the media containing Rh was replaced with fresh media for the remainder of the 72 hours, followed by ELISA analysis. BrdU was added to the media 24 hours prior to analysis.

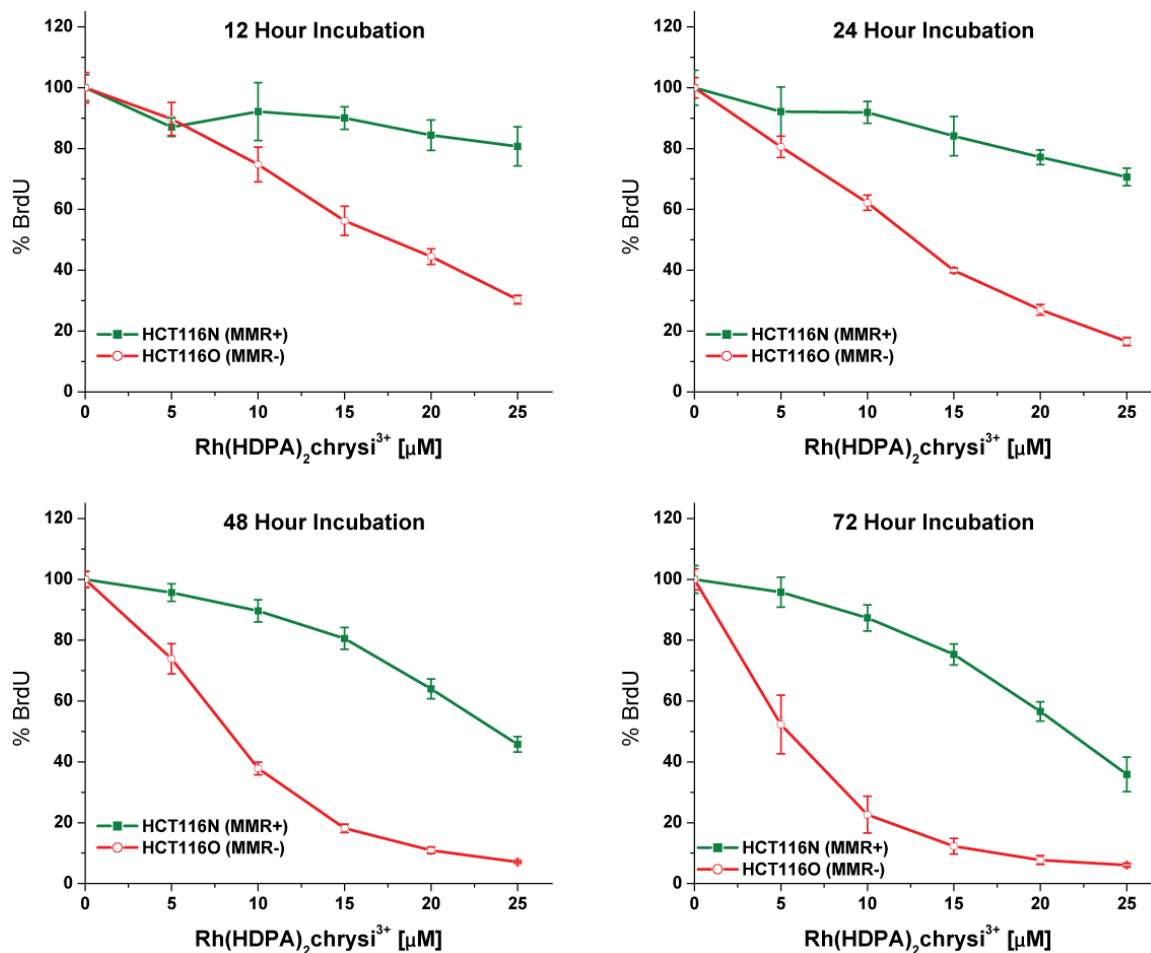


Figure 3.8. Inhibitory effects of Rh(HDPA)₂chrysi³⁺ as a function of incubation time on cellular proliferation. Shown are plots of BrdU incorporation (a measure of DNA synthesis and therefore cellular proliferation) normalized to the BrdU incorporation of untreated cells as a function of rhodium concentration. Standard error bars for 5 trials are shown. MMR-proficient HCT116N cells (green) and MMR-deficient HCT116O cells (red) were plated and allowed 24 hours to adhere before incubation with 0–25 μM Rh(HDPA)₂chrysi³⁺ for 12, 24, 48, or 72 hours. At the end of the 12, 24, and 48 hour incubations, the media containing Rh was replaced with fresh media for the remainder of the 72 hours, followed by ELISA analysis. BrdU was added to the media 24 hours prior to analysis.

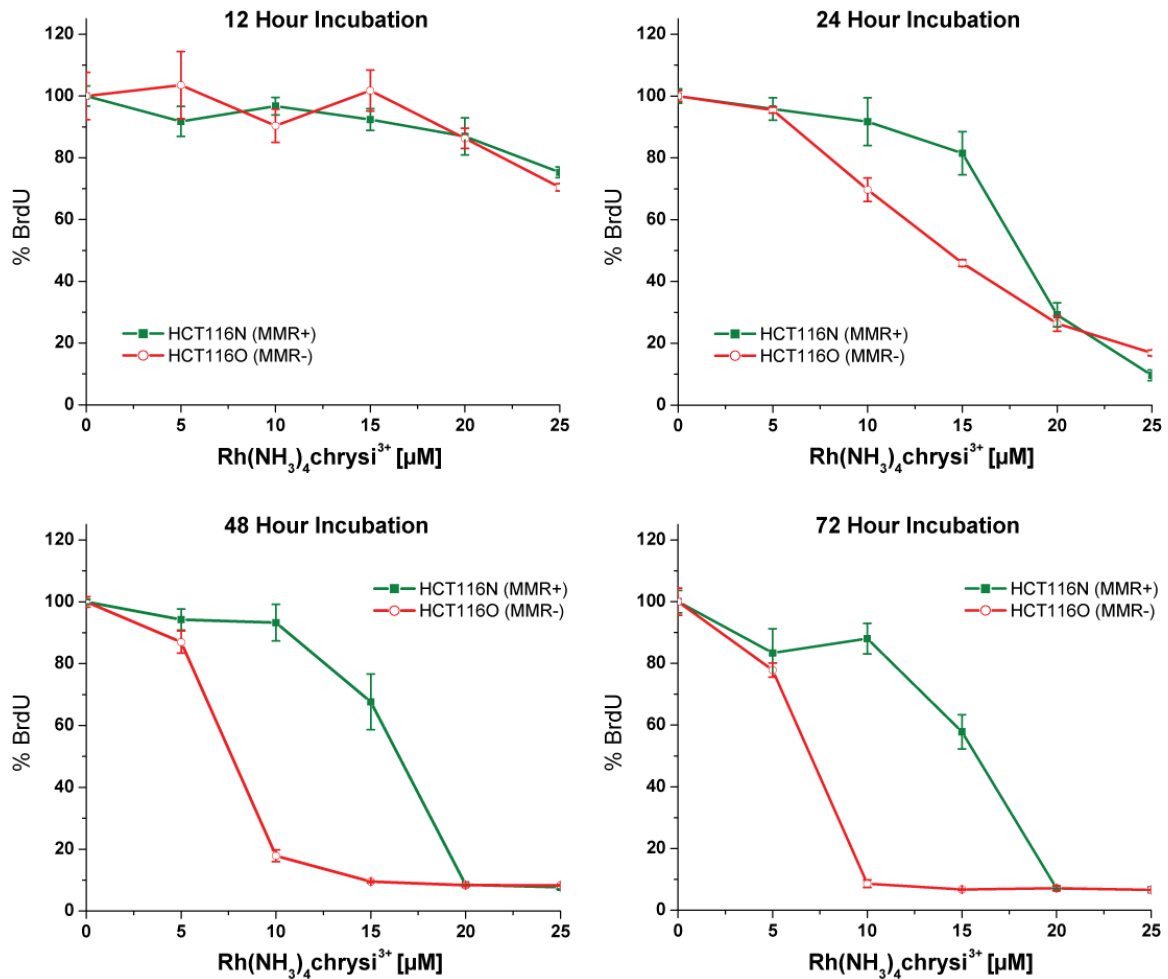


Figure 3.9. Inhibitory effects of Rh(NH₃)₄chrysi³⁺ as a function of incubation time on cellular proliferation. Shown are plots of BrdU incorporation (a measure of DNA synthesis and therefore cellular proliferation) normalized to the BrdU incorporation of untreated cells as a function of rhodium concentration. Standard error bars for 5 trials are shown. MMR-proficient HCT116N cells (green) and MMR-deficient HCT116O cells (red) were plated and allowed 24 hours to adhere before incubation with 0–25 μM Rh(NH₃)₄chrysi³⁺ for 12, 24, 48, or 72 hours. At the end of the 12, 24, and 48 hour incubations, the media containing Rh was replaced with fresh media for the remainder of the 72 hours, followed by ELISA analysis. BrdU was added to the media 24 hours prior to analysis.

Figure 3.10 shows the ELISA results for members of the metalloinsertor family as a function of incubation time. We have shown previously that the Λ -enantiomer of $\text{Rh}(\text{bpy})_2\text{chrysi}^{3+}$ is biologically inactive²⁶ and that structurally binding to a mismatch site is enantiospecific for the Δ -isomer.²³ For this reason, treatment with the 10 μM achiral tetraammine complex was compared to treatment with 20 μM racemic mixtures of the $\text{Rh}(\text{L})_2\text{chrysi}^{3+}$ complexes ($\text{L} = \text{HDPA}, \text{bpy}, \text{or phen}$). The differential effect of rhodium treatment between the cells lines was quantified by subtracting the normalized percentages of cellular proliferation for each cell line. Notably, the optimal incubation time for each compound is inversely related to the hydrophobicity of the ancillary ligands, with *rac*- $\text{Rh}(\text{phen})_2\text{chrysi}^{3+}$ exhibiting an optimal incubation time of 24 hours. This trend also continues with *rac*- $\text{Rh}(\text{DIP})_2\text{chrysi}^{3+}$, which exhibits differential effects in as little as 12 hours at concentrations as low as 2 μM (Figure 3.5). Based on the early effect at 12 hours, the HDPA complex may have different uptake characteristics (see Chapter 4). With the exception of the HDPA complex, this variation in activity with incubation time for the family of complexes parallels closely results seen earlier for uptake in HeLa cells by $\text{Ru}(\text{bpy})_2\text{dppz}^{2+}$, $\text{Ru}(\text{phen})_2\text{dppz}^{2+}$, and $\text{Ru}(\text{DIP})_2\text{dppz}^{2+}$ where the most rapid uptake is apparent with the lipophilic DIP complex.^{28, 29}

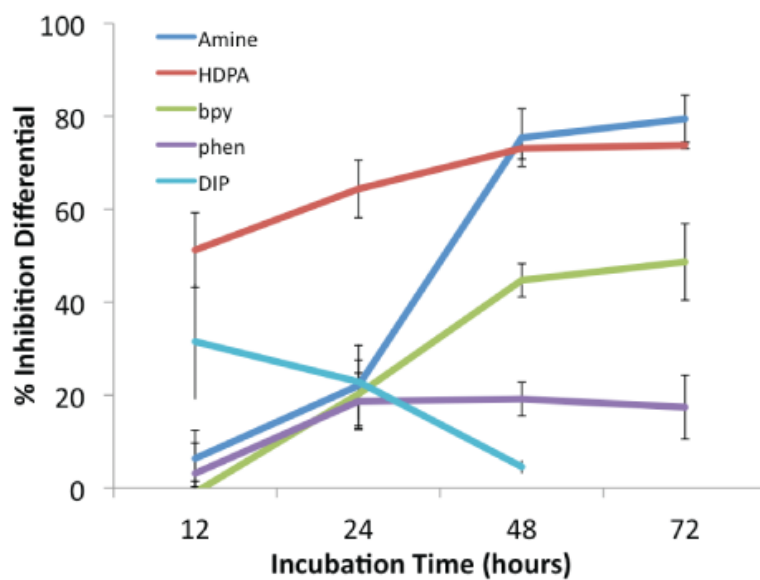


Figure 3.10. Inhibitory effects of rhodium metalloinsertors as a function of incubation time. Shown are plots of BrdU incorporation normalized to the BrdU incorporation of untreated cells as a function of rhodium concentration. The inhibition differential is the difference of the normalized percentages of cellular proliferation for each cell line, with standard error bars ($S_{N-O} = \sqrt{(S_N^2 + S_O^2)}$). Cells were incubated with no rhodium, 2 μM $\text{Rh}(\text{DIP})_2\text{chrysi}^{3+}$, 10 μM $\text{Rh}(\text{NH}_3)_4\text{chrysi}^{3+}$, or 20 μM $\text{Rh}(\text{L})_2\text{chrysi}^{3+}$ (L = HDPa, bpy, or phen).

Figure 3.11 summarizes the differential effects on cell proliferation and the incubation time for the family of complexes. Clear correlations are evident with the binding constants for these complexes (Table 3.1). Significantly, the differential effect in inhibiting cell proliferation in MMR-deficient cells is directly correlated to the binding affinity of the compound for DNA mismatches. $\text{Rh}(\text{NH}_3)_4\text{chrysi}^{3+}$ ($K_b = 1 \times 10^8 \text{ M}^{-1}$ at a CC mismatch), for example, shows the largest differential effect in inhibiting proliferation of MMR-deficient versus -proficient HCT116 cells after 72 hours ($79 \pm 5\%$), while $\text{Rh}(\text{phen})_2\text{chrysi}^{3+}$ ($K_b = 3.2 \times 10^6 \text{ M}^{-1}$ at a CC mismatch) shows a small differential effect ($17 \pm 7\%$). The DIP complex is rapidly taken up by the cells but also shows only a small differential inhibitory effect correlating with its poor specific binding at the mismatch site.

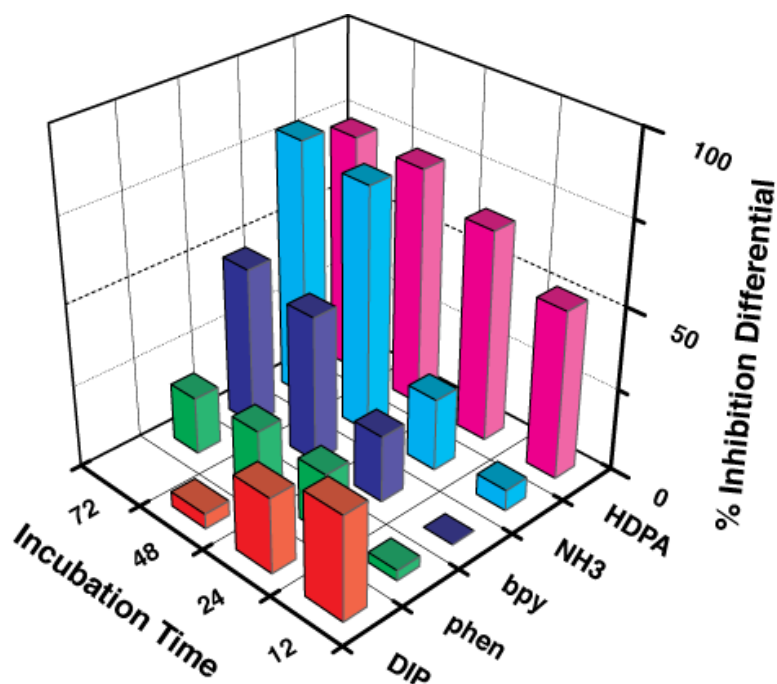


Figure 3.11. Inhibitory effects of rhodium metalloinsertors as a function of metal complex identity. Shown are bar graphs of BrdU incorporation normalized to the BrdU incorporation of untreated cells as a function of rhodium concentration. The inhibition differential is the difference of the normalized percentages of cellular proliferation for the two cell lines, HCT116O versus HCT116N. Cells were incubated with no rhodium, 2 μM $\text{Rh}(\text{DIP})_2\text{chrysi}^{3+}$, 10 μM $\text{Rh}(\text{NH}_3)_4\text{chrysi}^{3+}$, or 20 μM $\text{Rh}(\text{L})_2\text{chrysi}^{3+}$ (L = HDPA, bpy, or phen). A correlation between mismatch binding affinity and differential inhibition of MMR-deficient cells is evident.

3.4. Discussion

A clear trend emerges when comparing the binding constants of the series of rhodium complexes to mismatched sites: The DNA mismatch binding affinity increases as the size of the ancillary ligand decreases. This trend is consistent with what we have learned from the structural studies, specifically that mismatch binding by insertion via the minor groove is subject to stringent space constraints. With major groove intercalation, the base rise is increased and the major groove offers space to accommodate the ancillary ligands. In contrast, with insertion, there is no increase in base pair rise, the mismatched bases are instead ejected and replaced by the deeply inserted chrysi ligand. Moreover, the minor groove, small even for hydrophobic groove binding molecules, offers little space for the ancillary ligands. While little enantioselectivity is apparent for intercalation of bpy complexes into B-form DNA, Δ -Rh(bpy)₂chrysi³⁺ binds enantiospecifically to single base mismatches.^{23,37} Thus steric interactions of the ancillary ligands are seen as an extremely important factor governing the binding affinity of a metal complex at the mismatch site.

The other clear trend is that binding to the CC mismatch is tighter than binding to the AC mismatch. We understand this trend since AC is the thermodynamically more stable mismatch, and in this case is estimated to stabilize the hairpin duplex by ~0.5 kcal/mol relative to one containing a CC mismatch.³⁸ This stabilization is translated into a higher dissociation constant (smaller binding constant) for the entire series of rhodium complexes. This decrease in binding affinity depends upon the greater energy required to eject the mismatched bases from the base pair stack, as evident crystallographically.²³ Nonetheless, the inverse relationship between the size of the ancillary ligand and the binding affinity still holds, with the smallest complex Rh(NH₃)₄chrysi³⁺ showing the

highest affinity and that of the largest complex $\text{Rh}(\text{DIP})_2\text{chrysi}^{3+}$ more than two orders of magnitude lower.

Figure 3.12 compares the crystal structure of $\Delta\text{-Rh}(\text{bpy})_2\text{chrysi}^{3+}$ bound to the mismatch site²³ with models of $\Delta\text{-Rh}(\text{DIP})_2\text{chrysi}^{3+}$ and $\text{Rh}(\text{NH}_3)_4\text{chrysi}^{3+}$ similarly bound via the minor groove through metalloinsertion. Preserving the DNA conformation from the crystal structure, we see that $\Delta\text{-Rh}(\text{DIP})_2\text{chrysi}^{3+}$ runs into substantial steric hindrance as its axial phenyl rings extend up and down into the groove, directly clashing with the bases. However, its equatorial phenyl rings do not pose any steric problems as they point away from the DNA. These observations are supported by the small binding constant measured for $\text{Rh}(\text{DIP})_2\text{chrysi}^{3+}$. $\text{Rh}(\text{phen})_2\text{chrysi}^{3+}$, intermediate in size, shows binding affinities for the mismatches that are an order of magnitude lower than the bpy derivative but more than an order of magnitude higher than the DIP complex. $\text{Rh}(\text{HDPA})_2\text{chrysi}^{3+}$ is slightly larger in size than the bpy derivative, but the HDPA ligands are more flexible, and there is an opportunity for hydrogen bonding; as a result $\text{Rh}(\text{bpy})_2\text{chrysi}^{3+}$ and $\text{Rh}(\text{HDPA})_2\text{chrysi}^{3+}$ have comparable affinities for the mismatch. Analogously, the large binding constant of $\text{Rh}(\text{NH}_3)_4\text{chrysi}^{3+}$ can be mostly attributed to its small size. Here it is reasonable to suggest that the axial amines may also hydrogen bond with the neighboring base pairs to form additional stabilizing interactions.

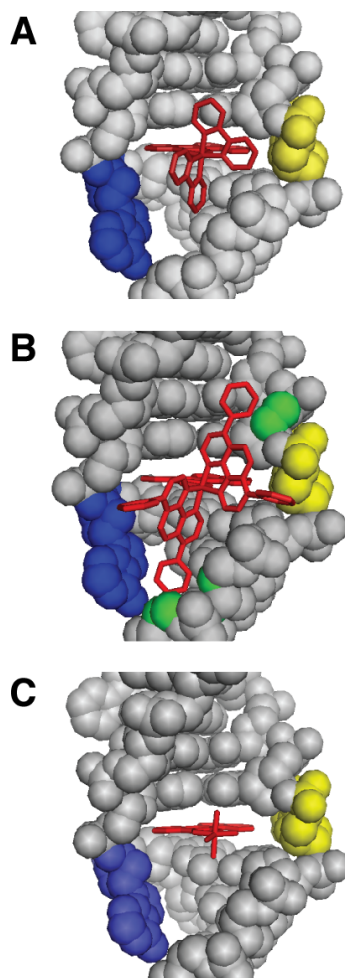


Figure 3.12. Crystal and model structures of rhodium metalloinsertors bound to the mismatch site. Rhodium insertors (red) are shown bound to the DNA (gray) from the minor groove, at the mismatch site with the bases (adenine in blue, cytosine in yellow) ejected and the chrysi ligand stacked fully with the adjacent base pairs. The crystal structure of $\text{Rh}(\text{bpy})_2\text{chrysi}^{3+}$ bound to the CA mismatch is shown in (A), along with structural models of $\text{Rh}(\text{DIP})_2\text{chrysi}^{3+}$ (B) and $\text{Rh}(\text{NH}_3)_4\text{chrysi}^{3+}$ (C) binding based on the crystal structure. Superposition of the DIP complex upon the rhodium center of the bpy complex leads to steric clashes with the sugar-phosphate backbone (possible atoms involved in green), whereas the tetraammine complex is easily accommodated.

Nonetheless, as evident in Figure 3.12, the small cone size of the tetraammine structure clearly facilitates deep insertion within the minor groove site. In fact, the clear inverse correlation of binding affinity with ancillary ligand size, and the finding that $\text{Rh}(\text{DIP})_2\text{chrysi}^{3+}$, despite its cumbersome size, is able to bind at all to a mismatch site with some specificity, corroborate our understanding of the driving force and the dynamics of mismatch recognition: The π -stacking between the inserted chrysi ligand and the adjacent bases provides the major stabilizing force for binding, and both the metal complex and DNA distort their conformations to accommodate each other in the bound state.

Importantly, the DNA mismatch binding affinities of the $\text{Rh}(\text{L})_2\text{chrysi}^{3+}$ family correlate well with the differential biological effects seen between the repair-proficient HCT116N and repair-deficient HCT116O cell lines (figure 3.13). This correlation supports the hypothesis that DNA mismatches are the target of rhodium metalloinsertors *in vivo*. Because of this correlation, we may attribute the preferential inhibitory effect on MMR-deficient cells to binding of the complexes to DNA mismatches. Since the MMR-deficient cells contain more mismatches, the tighter binding complexes would be expected to display a greater inhibitory effect. It should be noted that finding any inhibitory effect with these complexes was at first surprising, since they bind DNA non-covalently and might be expected to be readily displaced. Although the mechanism of inhibition is not yet fully understood, it is likely that protein recognition of the metal-mismatch complex, perhaps by RNA polymerase or topoisomerase, may generate a covalent protein/DNA lesion and contribute to the cellular response.

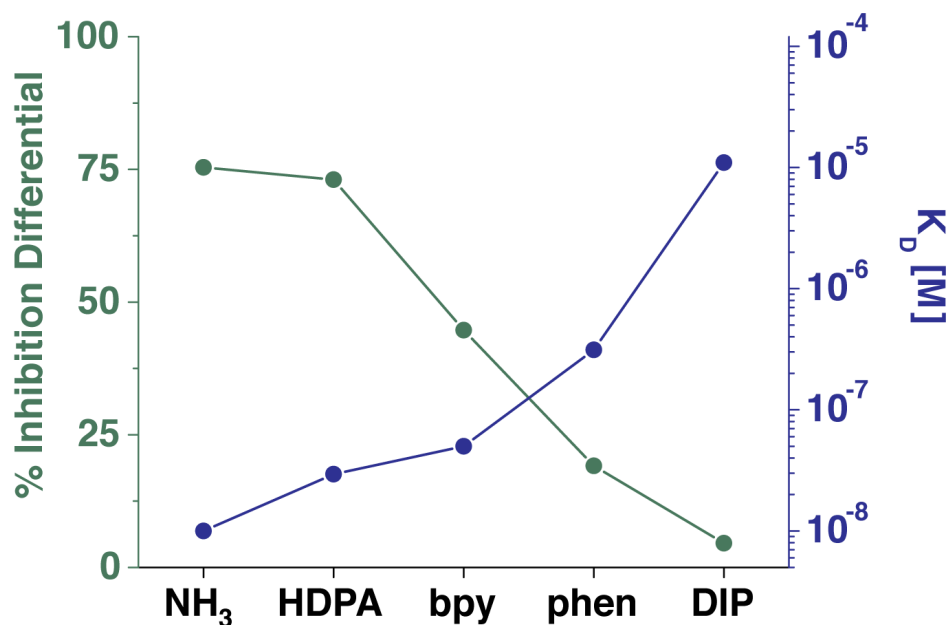


Figure 3.13. Inhibitory effects of rhodium metalloinsertors correlate with binding affinity for DNA mismatches. Shown are bar graphs of BrdU incorporation normalized to the BrdU incorporation of untreated cells as a function of rhodium concentration. The inhibition differential is the difference of the normalized percentages of cellular proliferation for the two cell lines, HCT116O versus HCT116N. Cells were incubated with no rhodium, 2 μM $\text{Rh}(\text{DIP})_2\text{chrysi}^{3+}$, 10 μM $\text{Rh}(\text{NH}_3)_4\text{chrysi}^{3+}$, or 20 μM $\text{Rh}(\text{L})_2\text{chrysi}^{3+}$ (L = HDPA, bpy, or phen). A correlation between mismatch binding affinity and differential inhibition of MMR-deficient cells is evident.

The differential inhibitory effect seen with $\text{Rh}(\text{HDPA})_2\text{chrysi}^{3+}$ cannot be understood simply on the basis of binding affinities. Despite having essentially the same mismatch binding affinity as $\text{Rh}(\text{bpy})_2\text{chrysi}^{3+}$, the HDPA complex preferentially inhibits the MMR-deficient cell line almost as well as $\text{Rh}(\text{NH}_3)_4\text{chrysi}^{3+}$ with long incubation times; with short times of incubation, the differential inhibitory effect by $\text{Rh}(\text{HDPA})_2\text{chrysi}^{3+}$ is greatest. Both the HDPA ligand and the primary amine group have the potential to form hydrogen bonds. This hydrogen bonding capability and flexibility of the ligands might serve to make them more effective inhibitors of any protein-DNA interactions. Indeed, ruthenium complexes bearing HDPA ligands have been shown to exhibit DNA binding and cytotoxicity.³⁹

Certainly, as with any pharmaceutical design, cellular uptake must also be considered. In the case of the HDPA complex, based upon the variations in inhibitory effect with incubation time, the amine ligands may facilitate nuclear uptake. Dppz analogues with the HDPA ligands have not yet been examined with respect to their uptake characteristics. For the bpy complexes, the 48 hour incubation time required for $\text{Rh}(\text{bpy})_2\text{chrysi}^{3+}$ to exert its anti-proliferative effect matches the 48 hour requirement observed for $\text{Ru}(\text{bpy})_2\text{dppz}^{2+}$ uptake in HeLa cells.^{25,27} The more lipophilic $\text{Rh}(\text{DIP})_2\text{chrysi}^{3+}$ here is found to exert anti-proliferative effects at much shorter incubation times and lower concentrations, which also matches the accelerated uptake observed for $\text{Ru}(\text{DIP})_2\text{dppz}^{2+}$. Cellular uptake is surely a rate-limiting factor in biological activity of the rhodium metalloinsertors. Yet cellular uptake is not the only challenge; proper subcellular localization must also be achieved in order for any drug to act upon its target. It has been well established that lipophilic cations preferentially target

the mitochondria, whereas hydrophilic cations do not.^{40,41} It may be that $\text{Rh}(\text{HDPa})_2\text{chrysi}^{3+}$ and $\text{Rh}(\text{NH}_3)_4\text{chrysi}^{3+}$ lack the lipophilicity required for mitochondrial accumulation, allowing a greater proportion of these compounds to reach the nucleus once inside the cell. This difference in intracellular partitioning could then account for the differential effects of $\text{Rh}(\text{HDPa})_2\text{chrysi}^{3+}$.

3.5. Conclusions

In the development of octahedral rhodium complexes as anti-cancer agents, the choice of ancillary ligand can be seen as a design tradeoff, with the binding affinity for a DNA mismatch greatly outweighing uptake properties as the critical factor in the successful targeting of repair-deficient cells. Beyond their effects on DNA binding and overall cellular uptake, it is highly likely that the ancillary ligands affect the cellular response in other ways, including the potential for hydrogen bonding and differences in uptake and intracellular distribution. Here we are confronted with a tradeoff that may seem inevitable: more hydrophobic ligands facilitate cellular uptake but impede mismatch binding. Perhaps this trade-off can be avoided by making conjugates arranged with functional moieties tethered with consideration of the structure of the DNA-bound complex associated snugly in the minor groove. Most importantly, these data support the contention that the cell-specific inhibitory effect we observe depends upon binding to the DNA mismatch inside the cell. This cell-specific strategy thus represents a promising direction in the development of small metal complexes that react preferentially in MMR-deficient cells, those susceptible to cancerous transformation.

3.6. References

1. R.R. Iyer, A. Pluciennik, V. Burdett, P.L. Modrich. *Chem. Rev.* **2006**, *106*, 302-323.
2. L.A. Loeb. *Cancer Res.* **2001**, *61*, 3230-3239.
3. N.P. Bhattacharya, A. Skandalis, A. Ganesh, J. Groden, and M. Meuth. *Proc. Natl. Acad. Sci. USA.* **1994**, *91*, 6319-6323.
4. B.S. Strauss. *Mutation Res.* **1999**, *437*, 195-203.
5. N. Papadopoulos, and A. Lindblom. *Human Mutation.* **1997**, *10*, 89-99.
6. P. Peltomaki. *Human Mol. Gen.* **2001**, *10*, 735-740.
7. D.A. Lawes, S. SenGupta, and P.B. Boulos. *European J. of Surgical Oncology.* **2003**, *29*, 201-212.
8. J.G. Herman, A. Umar, K. Polyak, J.R. Graff, N. Ahuja, J.J. Issa, S. Markowitz, J.K.V. Willson, S.R. Hamilton, K.W. Kinzler, M.F. Kane, R.D. Kolodner, B. Vogelstein, T.A. Kunkel, and S.B. Baylin. *Proc. Natl. Acad. Sci. USA.* **1998**, *95*, 6870-6875.
9. I.I. Arzimanoglou, F. Gilbert, and H.R.K. Barber. *Cancer.* **1998**, *82*, 1808-1820.
10. K. Pors and L.H. Patterson. *Current Topics in Medicinal Chemistry.* **2005**, *5*, 1133-1149.
11. A.M. Valentini, M. Armentano, M. Pirrelli, and M.L. Caruso. *Cancer Treatment Reviews.* **2006**, *32*, 607-618.
12. J.M. Carethers, M.T. Hawn, D.P. Chauhan, M.C. Luce, G. Marra, M. Koi, and C.R. Boland. *J. of Clinical Investigation.* **1996**, *98*, 199-206.

13. D. Fink, S. Nebel, S. Aebi, H. Zheng, B. Cenni, A. Nehme, R.D. Christen, and S.B. Howell. *Cancer Res.* **1996**, *56*, 4881-4886.
14. J.M. Carethers, D.P. Chauhan, D. Fink, S. Nebel, R.S. Bresalier, S.B. Howell, and C.R. Boland. *Gastroenterology.* **1999**, *117*, 123-31.
15. S. Aebi, D. Fink, R. Gordon, H.K. Kim, H. Zheng, J.L. Fink, and S.B. Howell. *Clinical Cancer Res.* **1997**, *3*, 1763-1767.
16. A. Fedier, V.A. Schwarz, H. Walt, R.D. Carpini, U. Haller, and D. Fink. *International J. of Cancer.* **2001**, *93*, 571-576.
17. D. Fink, S. Aebi, and S.B. Howell. *Clinical Cancer Res.* **1998**, *4*, 1-6.
18. P. Karran, J. Offman, and M. Bignami. *Biochimie.* **2003**, *85*, 1149-1160.
19. B.A. Jackson and J.K. Barton. *J. Am. Chem. Soc.* **1997**, *119*, 12986-12987.
20. B.A. Jackson and J.K. Barton. *Biochemistry.* **2000**, *39*, 6176-6182.
21. H. Junicke, J.R. Hart, J. Kisko, O. Glebov, I. Kirsch, and J.K. Barton. *Proc. Natl. Acad. Sci. USA.* **2003**, *100*, 3737-3742.
22. B.M. Zeglis, V.P. Pierre, and J.K. Barton. *Chem. Commun.* **2007**, *44*, 4565-4579.
23. V.C. Pierre, J.T. Kaiser, and J.K. Barton. *Proc. Natl. Acad. Sci. USA.* **2007**, *104*, 429-434.
24. C.L. Kielkopf, K.E. Erkkila, B.P. Hudson, J.K. Barton, and D.C. Rees. *Nature Structural Biology.* **2000**, *7*, 117-121.
25. C. Cordier, V.C. Pierre, and J.K. Barton. *J. Am. Chem. Soc.* **2007**, *129*, 12287-12295.
26. J.R. Hart, O. Glebov, R.J. Ernst, I.R. Kirsch, and J.K. Barton. *Proc. Natl. Acad. Sci. USA.* **2006**, *103*, 42, 15359-15363.

27. M. Koi, A. Umar, D.P. Chauhan, S.P. Cherian, J.M. Carethers, T.A. Kunkel, and C.R. Boland. *Cancer Res.* **1994**, *54*, 4308-4312.
28. C.A. Puckett and J.K. Barton. *J. Am. Chem. Soc.* **2007**, *129*, 46-47.
29. C.A. Puckett and J.K. Barton. *Biochemistry.* **2008**, *47*, 11711-11716.
30. J. Brunner and J.K. Barton. *Biochemistry.* **2006**, *45*, 12295-12302.
31. B.M. Zeglis and J.K. Barton. *Nature Protocols.* **2007**, *2*, 357-371.
32. N.E. Dixon, G.A. Lawrance, P.A. Lay, and A.M. Sargeson. *Inorg. Chem.* **1983**, *22*, 846-847.
33. N.E. Dixon, G.A. Lawrance, P.A. Lay, and A.M. Sargeson. *Inorg. Chem.* **1984**, *23*, 2940-2947.
34. A.H. Reitmar, R. Risley, R.G. Bristow, T. Wilson, A. Ganesh, A. Jang, J. Peacock, S. Benchimol, and R.P. Hill *et al.* *Cancer Res.* **1997**, *57*, 3765-3771.
35. H.G. Gratzner. *Science* **1982**, *218*, 474-475.
36. A.H. Krotz, L.Y. Kuo, T.P. Shields, and J.K. Barton. *J. Am. Chem. Soc.* **1993**, *115*, 3877-3882.
37. J.K. Barton. *Science.* **1986**, *233*, 727-734.
38. J. SantaLucia Jr. and D. Hicks. *Annu. Rev. Biophys. Biomol. Struct.* **2004**, *33*, 415-440.
39. V. Rajendiran, M. Murali, E. Suresh, M. Palaniandavar, V.S. Periasamy, and M.A. Akbarsha. *Dalton Trans.* **2008**, 2157-2170.
40. S.M. Napolitano and J.R. Aprille. *Advanced Drug Delivery Reviews.* **2001**, *49*, 63-70.

41. M.P. Murphy and R.A.J. Smith. *Advanced Drug Delivery Reviews*. **2000**, *41*, 235-250.

CHAPTER 4: CYTOTOXIC EFFECTS OF RH METALLOINSERTORS WITH DIPYRIDYLAMINE ANCILLARY LIGANDS

4.1. Introduction

The direct correlation between the binding affinity of rhodium metalloinsertors for DNA mismatches and the differential in their activity between the HCT116N and HCT116O cell lines fails to predict the high activity of $[\text{Rh}(\text{HDPA})_2\text{chrysi}]^{3+}$. In light of the shorter incubations required for this complex, it seems likely that accelerated cellular uptake is a contributing factor in the increased cellular response. As $[\text{Rh}(\text{HDPA})_2\text{chrysi}]^{3+}$ is not luminescent, another method is needed to examine its cellular uptake. The high atomic mass and monoisotopic distribution of rhodium make the cellular accumulation of rhodium metalloinsertors well suited to analysis by inductively coupled plasma–mass spectrometry (ICPMS).¹⁻³ The high anti-proliferative activity of $[\text{Rh}(\text{HDPA})_2\text{chrysi}]^{3+}$ also raised questions as to whether additional biological responses to rhodium treatment might appear that were not observed with other complexes.

The preceding work demonstrated the anti-proliferative activity of rhodium metalloinsertors against human cancer cell lines as a function of mismatch repair competency, with a mismatch repair deficient cell line displaying enhanced susceptibility to the agents versus a repair proficient sister cell line. Importantly, the difference in activity observed between the cell lines was positively correlated with the binding affinity for DNA mismatches, supporting the hypothesis that mismatches are the cellular target of rhodium metalloinsertors. In these studies activity was measured with an ELISA for

Acknowledgements: Curtis Schneider synthesized the MeDPA ligand. Alexis Komor assisted with the PARP inhibition assays.

DNA synthesis, which served as a proxy for cellular proliferation. This assay however does not distinguish between senescence and other types of cell death, and therefore is insufficient to demonstrate cytotoxicity. Here, the MTT assay for metabolic activity is used as a true measure of cytotoxicity, and rhodium metalloinsertors are shown to preferentially kill the MMR-deficient HCT116O cell line versus its MMR-proficient sister cell line, HCT116N. Caspase inhibition and dye exclusion assays are used to show that this cell death occurs through a necrotic rather than apoptotic mechanism. Furthermore, propidium iodide staining and flow cytometric analysis are used to show that cell death is preceded by cell cycle arrest at the G1/S phase boundary. This observation is consistent with activation of the DNA damage response by rhodium metalloinsertors.

4.2. Experimental Protocols

4.2.1 Materials

RhCl_3 was purchased from Pressure Chemical, Inc. (Pittsburgh, PA). $[\text{Rh}(\text{NH}_3)_5\text{Cl}]\text{Cl}_2$ was obtained from Strem Chemical, Inc. (Newburyport, MA). 2,2'-dipyridylamine (HDPA) and Sephadex ion exchange resin were obtained from Sigma Aldrich (St. Louis, MO). Sep-Pak C_{18} solid phase extraction cartridges were purchased from Waters Chemical Co. (Milford, MA). Media and supplements were purchased from Invitrogen (Carlsbad, CA). The 3-[4,5-dimethylthiazol-2-yl]-2,5-diphenyl tetrazolium bromide (MTT) labeling reagent and acidified lysis buffer (10% SDS in 10 mM HCl) were purchased in kit format from Roche Molecular Biochemicals (Mannheim, Germany). Z-VAD-FMK caspase inhibitor was purchased from Promega. The PARP inhibitor 3,4-dihydro-5-[4-(1-piperidinyl)butoxyl]-1(2H)-isoquinolinone (DPQ) was purchased from Sigma Aldrich. All commercial materials were used as received.

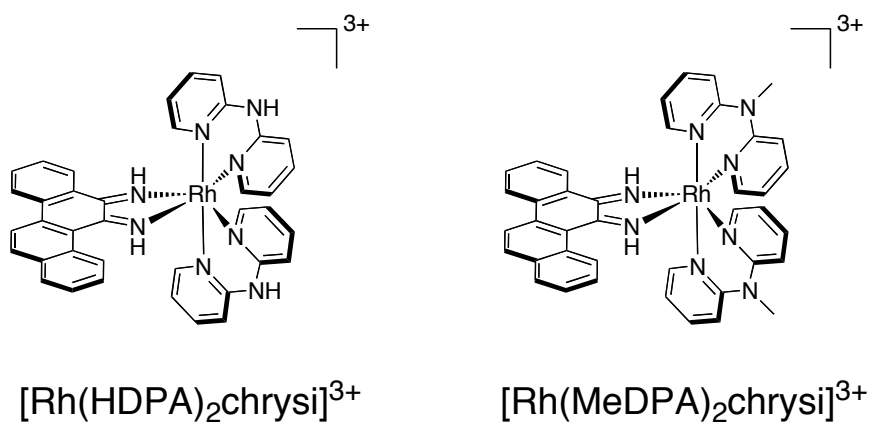


Figure 4.1. Rhodium metalloinsertors bearing dipyriddyamine ancillary ligands.

4.2.2 Synthesis of MeDPA Ligand

N-methyl-2,2'-dipyridylamine (MeDPA). An oven-dried 50 mL round bottom flask equipped with a stirbar and septa was charged with sodium hydride (0.24 g, 10 mmol) and anhydrous THF under a constant purge of argon. The suspension was cooled in an ice bath. 2,2'-dipyridylamine (1.71 mg, 10 mmol) in 2 mL anhydrous THF was added dropwise at 0 °C to the hydride suspension. Iodomethane (1.85 g, 13 mmol) was added dropwise as the reaction warmed slowly to room temperature and brought to a reflux for 17 hours. The reaction was concentrated *in vacuo* and extracted with dichloromethane and dilute sodium bicarbonate. The organic layer was dried over sodium sulfate and concentrated to a light yellow oil. The desired product can be purified by silica gel chromatography with 1:9 ethyl acetate:hexane mobile phase. Yield: 0.47 g (2.5 mmol, 25 %) ¹H-NMR (CDCl₃): 8.35 (d of d, 2H); 7.54 (t, 2H); 7.17 (d, 2H); 6.86 (t, 2H), 3.62 (s, 3H). ESI-MS: 186 m/z [M+H]⁺ (observed).

4.2.3 Synthesis of Metal Complexes

[Rh(HDPA)₂chrysi]Cl₃ was prepared according to previously described procedures (Chapter 3). [Rh(MeDPA)₂chrysi]Cl₃ was synthesized by refluxing [Rh(NH₃)₄chrysi]TFA₃ with 2 equivalents of MeDPA in 1:1 ethanol:water overnight (figure 4.2.). The reaction mixture was cooled to room temperature, and the solvent was removed *in vacuo*. The desired product was isolated by cation exchange chromatography with Sephadex CM-25 resin, eluting with 0.03 M MgCl₂ (aq). Excess magnesium was removed by solid phase extraction with a Sep-pak C₁₈ cartridge and the TFA counterion was exchanged for the chloride by anion exchange chromatography with Sephadex QAE-125 resin.

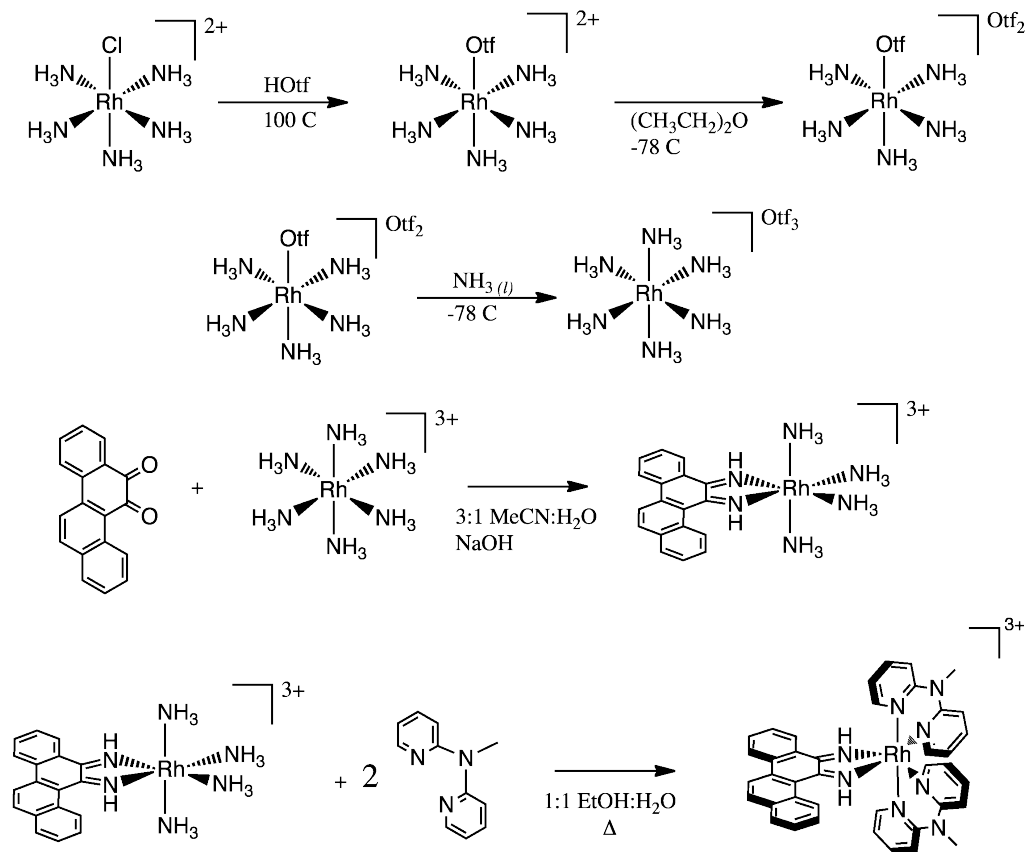


Figure 4.2. Synthesis of $[\text{Rh}(\text{MeDPA})_2\text{chrysi}]\text{Cl}_3$.

Formation of the desired product was confirmed by UV/vis (H₂O, pH 5): 295 nm (55,000 M⁻¹cm⁻¹), 320 nm (39,700 M⁻¹cm⁻¹), 390 nm (14,000 M⁻¹cm⁻¹) and ESI-MS (cation): 727.1 m/z ([M-2H]⁺), 364.3 m/z ([M-H]²⁺) obs., 727.2 m/z ([M-2H]⁺) calc. Purity was confirmed by analytical HPLC ($t_{\text{retention}} = 13.5$ minutes, 10:90:0.1 MeCN:H₂O:TFA to 40:60:0.1 MeCN:H₂O:TFA over 45 minutes).

4.2.4 Inductively-Coupled Plasma Mass Spectrometry (ICP-MS)

Analysis of exogenous transition metal complexes by ICP-MS is greatly enabled by the fact that no background exists within the cell. While ICP-MS and AAS represent very sensitive methods to assay for metal content, these assays cannot be accomplished with monitoring in real time. Cell lysates are instead prepared from cells that have been incubated with metal complex, prior to assay for metal uptake. When adherent cells are used, they are either detached from the culture dish and then lysed, or lysed directly in the dish. Alternatively, the cells can be detached and treated with complex in suspension. This cell lysate is analytically diluted, and the amount of metal in the solution is quantified. Rhodium counts measured in the samples are a highly linear measure of concentration, as shown by the calibration standard shown in figure 4.4. The normalized counts from the samples are shown with standard error bars for three trials.

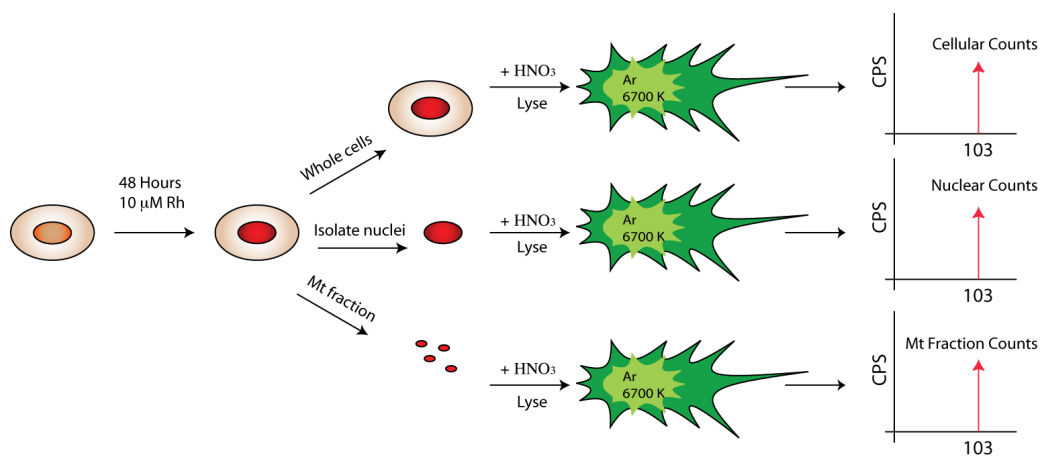


Figure 4.3. Cellular ICP-MS. Methodology for analysis of rhodium accumulation and localization in HCT116 cell lines by ICP-MS. After incubation with rhodium complexes, cells are counted and separated into three samples. Cell lysates, nuclear fractions, and mitochondrial fractions are then prepared and analyzed for rhodium content by ICP-MS.

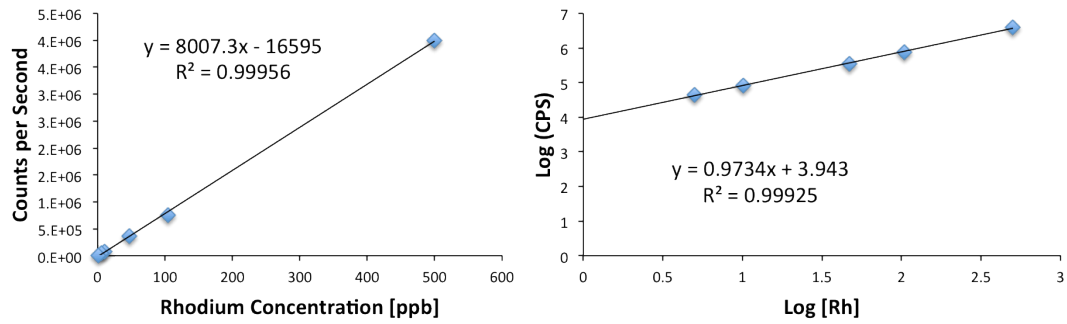


Figure 4.4. ICP-MS Calibration. Regression fit for rhodium counts as a function of concentration for serial dilutions of a rhodium standard solution. Rhodium counts are a linear function of concentration.

4.2.5 Cell Culture

HCT116N and HCT116O cells were grown in RPMI medium 1640 supplemented with: 10% FBS; 2 mM L-glutamine; 0.1 mM non-essential amino acids; 1 mM sodium pyruvate; 100 units/mL penicillin; 100 µg/mL streptomycin; and 400 µg/mL geneticin (G418). Cells were grown in tissue culture flasks and dishes (Corning Costar, Acton, MA) at 37°C under 5% CO₂ and humidified atmosphere.

4.2.6 Preparation of whole cell lysate

The whole cell pellet was resuspended in 1% HNO₃ (v/v), lysed by repeated freeze/thaw cycles in liquid nitrogen, and analyzed for rhodium content on an HP-4500 ICP-MS unit.

4.2.7 Preparation of nuclei

The cell pellet was suspended in extraction buffer (320 mM sucrose, 5 mM MgCl₂, 10 mM HEPES, 1% Triton X-100, pH 7.4), briefly vortexed, and incubated on ice for 10 minutes. The nuclei were collected by centrifugation at 2000 x g for 3-4 minutes. The pellet was rinsed with wash buffer (320 mM sucrose, 5 mM MgCl₂, 10 mM HEPES) twice. Nuclei were then counted with 1:1 dilution in Trypan blue (0.4% in PBS) and resuspended in 1% HNO₃ (v/v), homogenized by three freeze/thaw cycles in liquid nitrogen, and analyzed for rhodium content on an HP-4500 ICP-MS unit.

4.2.8 Preparation of mitochondrial fraction

The cell pellet was suspended in extraction buffer (isotonic solution, 10 mM HEPES, pH 7.5, 200 mM mannitol, 70 mM sucrose, and 1 mM EGTA) and Dounce homogenized or lysed with detergent for 5 minutes on ice. The homogenate or lysate was then centrifuged at 600 x g for 5 minutes. The supernatant was carefully collected and transferred to a fresh microcentrifuge tube. After centrifugation at 11,000 x g, the pellet

was collected and resuspended in 1% HNO₃ (v/v), homogenized by three freeze/thaw cycles in liquid nitrogen, and analyzed for rhodium content on an HP-4500 ICP-MS unit.

4.2.9 Cellular Proliferation ELISA

HCT116N and HCT116O cells were plated in 96-well plates at 2,000 cells/well and allowed 24 hours to adhere. The cells were then incubated with rhodium for the durations specified. For incubation less than 72 hours, the Rh-containing media were replaced with fresh media, and the cells were grown for the remainder of the 72 hour period. Cells were labeled with BrdU 24 hours before analysis. The BrdU incorporation was quantified by antibody assay according to established procedures.^{4,5} Cellular proliferation was expressed as the ratio of the amount of BrdU incorporated by the treated cells to that of the untreated cells.

4.2.10 MTT Cytotoxicity Assay

HCT116N and HCT116O cells were plated in 96-well plates at 50,000 cells/well and incubated with rhodium for the durations specified. After rhodium incubation cells were labeled with MTT for 4 hours at 37°C under 5% CO₂ and humidified atmosphere. The resulting formazan crystals were dissolved with 10% SDS acidified with 10 mM HCl purchased from Roche in kit format according to the manufacturer's instructions. The dissolved formazan was quantified as the absorbance at 570 nm minus the background absorbance at 690 nm. Percent viability was determined as the ratio of the amount of formazan in the treated cells to that of the untreated cells. For caspase inhibition assays, Z-VAD-FMK was added from a 20 mM stock solution in DMSO to a final concentration of 20–40 μM. For PARP inhibition assays, DPQ was added from a 5 mg/mL stock in DMSO to a final concentration of 25–50 μM.

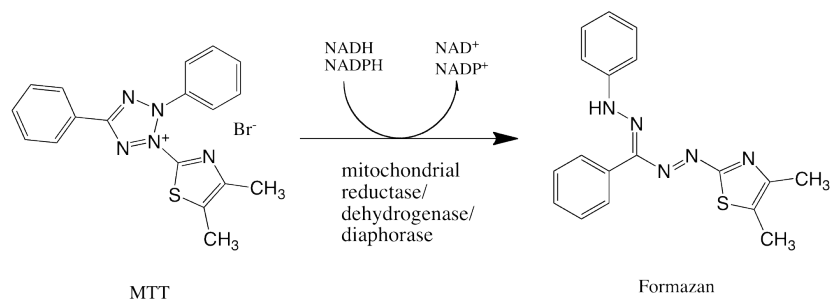


Figure 4.5. MTT cytotoxicity assay. The tetrazolium salt (MTT) is reductively cleaved by various mitochondrial enzymes to yield formazan crystals, leading to an absorbance band centered around 570 nm. The crystals can be dissolved by addition of 10% SDS acidified with 10 mM HCl to give a purple solution. The absorbance of this solution directly reflects the number of metabolically viable cells in the sample.

4.2.11 Cell Cycle Distribution Flow Cytometry Assay

Cells were harvested from adherent culture by trypsinization and washed with cold PBS. The resultant pellet was resuspended in PBS (chilled to 4 °C), and ice-cold ethanol was added dropwise to a final concentration of 70% (v/v), with continuous gentle agitation. Cells were fixed at 4°C for 30 minutes and stored for up to one week. Prior to analysis, the fixed cells in 70% ethanol were diluted 1:3 in cold PBS and centrifuged at 1,400 x g for 5 minutes. The resultant pellet was washed twice and resuspended in ice-cold PBS. Ribonuclease was added to a final concentration of 30 µg/mL and the cells were incubated overnight at 4 °C. The next day propidium iodide was added to a final concentration of 20 µg/mL and cells were analyzed by flow cytometry. Data analysis was performed using the FloJo software package (version 8.7.1).

4.2.12 Cell Death Mode Flow Cytometry Assay

After 24–72 hour incubation with rhodium, cells were harvested from adherent culture by trypsinization and washed with ice cold PBS. The resultant pellet was resuspended in ice-cold PBS and stained with propidium iodide and with YO-PRO-1 to a final concentration of 200 nM for 30 minutes on ice prior to analysis by flow cytometry.

4.3. Results

4.3.1 ICP-MS for Cellular Accumulation

Each cell line was treated with 10 µM of $[\text{Rh}(\text{bpy})_2\text{chrysi}]^{3+}$, $[\text{Rh}(\text{HDPA})_2\text{chrysi}]^{3+}$, or $[\text{Rh}(\text{NH}_3)_4\text{chrysi}]^{3+}$ for 48 hours. After rhodium incubation, the cells were harvested from adherent culture by trypsinization, washed with cold PBS, counted on a hemacytometer, and separated into three equal groups. Whole cell lysate was prepared from the first group, nuclei were isolated from the second, and a cellular fraction enriched in mitochondrial was isolated from the third.

The fractions were analyzed for rhodium levels by ICP-MS, and the data are shown in figure 4.6. Two notable observations can be made. As expected, the HDPA complex exhibits a higher degree of cellular uptake than the other complexes. This supports the notion that the early activity displayed by the complex in the ELISA assay (Chapter 3) results from accelerated uptake. It should be noted that these treatment conditions directly reflect those used in the ELISA. Secondly, the ammine complex exhibits a higher degree of nuclear localization, as determined by the ratio of nuclear counts to whole cell counts. This is not surprising; since the ammine ligands lack the lipophilic nature of the bpy and HDPA ligands, they are not as likely to be concentrated in the mitochondria, where lipophilic cations are known to accumulate.⁶⁻¹¹ There is also no real difference in the rhodium levels in mitochondria between HCT116N and HCT116O cells.

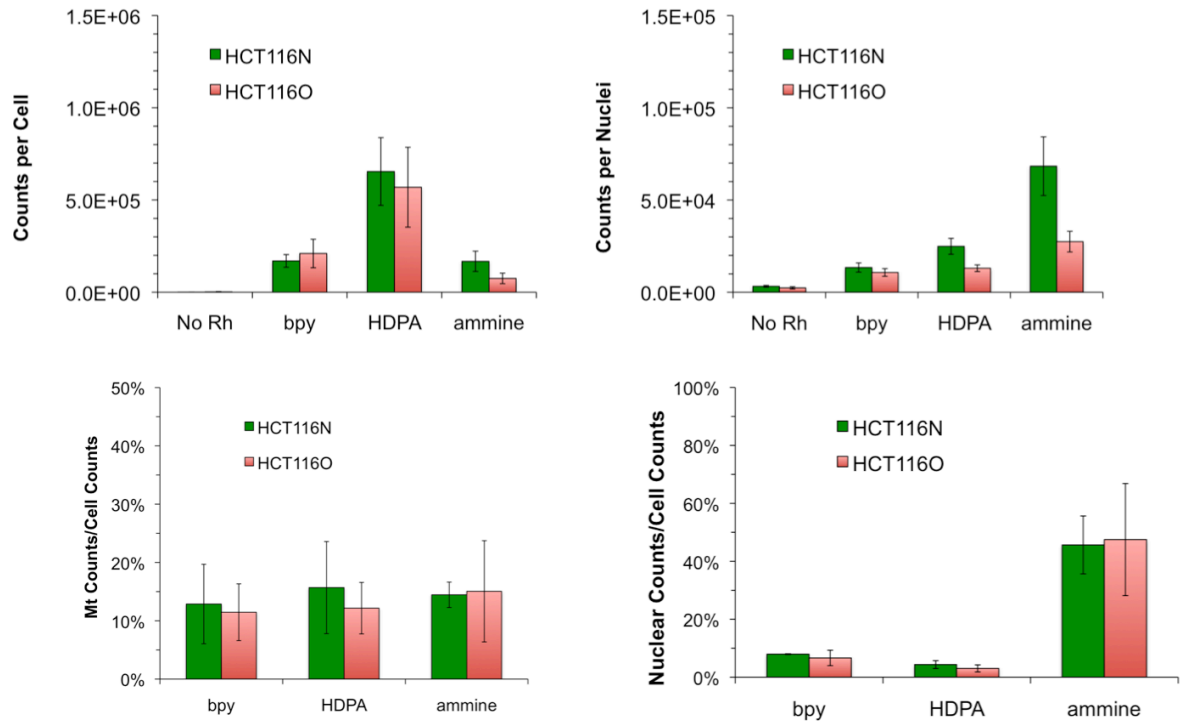


Figure 4.6. ICP-MS Assay for Rhodium Accumulation. Normalized rhodium counts for whole cell lysates (top left), isolated nuclei (top right), along with the ratio of mitochondrial counts to whole cell counts (bottom left), and the ratio of nuclear counts to whole cell counts (bottom right). Standard error bars for three trials are shown.

4.3.2 MTT Cytotoxicity Assay

The cytotoxicities of $[\text{Rh}(\text{HDPA})_2\text{chrysi}]^{3+}$ and $[\text{Rh}(\text{MeDPA})_2\text{chrysi}]^{3+}$ were determined by MTT assay. Briefly, reduction of the MTT reagent by mitochondrial enzymes leads to the production of formazan, which can then be dissolved in acidified SDS and produces a characteristic absorbance at 570 nm. This absorbance reflects the relative metabolic activity, which in turn reflects the percentage of viable cells in each sample.

HCT116N and HCT116O cells were plated and treated with 0-25 μM of $[\text{Rh}(\text{HDPA})_2\text{chrysi}]^{3+}$ or $[\text{Rh}(\text{bpy})_2\text{chrysi}]^{3+}$ for 24, 48, or 72 hours. The results are shown in figure 4.7. At 24 hours, no differential cytotoxicity is observed for either complex, but at 48 to 72 hours $[\text{Rh}(\text{HDPA})_2\text{chrysi}]^{3+}$ clearly displays an enhanced toxicity in the MMR-deficient HCT116O cell line versus the HCT116N cell line. For example, 72 hours after treatment with 20 μM $[\text{Rh}(\text{HDPA})_2\text{chrysi}]^{3+}$, the number of viable HCT116N cells is 80 ± 5.2 % of untreated controls, whereas the number of viable HCT116O cells is 37 ± 4.4 % of untreated controls.

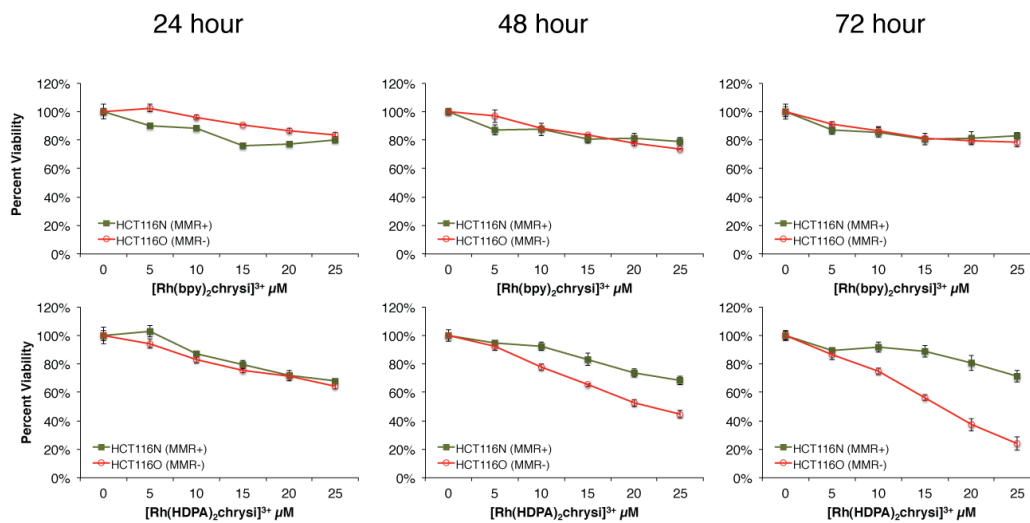


Figure 4.7. $[\text{Rh}(\text{HDPA})_2\text{chrysi}]^{3+}$ is selectively toxic in MMR-deficient cells.

HCT116N and HCT116O cells were plated in 96-well format at densities of 5×10^4 cells/well and treated with 0–25 μM of $[\text{Rh}(\text{bpy})_2\text{chrysi}]^{3+}$ or $[\text{Rh}(\text{HDPA})_2\text{chrysi}]^{3+}$.

After 24–72 hours, the cells were labeled with MTT for 4 hours. The resulting formazan crystals were dissolved by addition of 10% SDS acidified with 10 mM HCl, and absorbance was measured at 570 nm. While the first generation complex $[\text{Rh}(\text{bpy})_2\text{chrysi}]^{3+}$ is non-toxic, the dipyrindylamine derivative $[\text{Rh}(\text{HDPA})_2\text{chrysi}]^{3+}$ exhibits toxicity specifically in the MMR-deficient HCT116O cell line.

Before testing $[\text{Rh}(\text{MeDPA})_2\text{chrysi}]^{3+}$ in the MTT assay, the complex was tested in the ELISA (figure 4.8.) HCT116N and HCT116O cells were plated and treated with 0-25 μM of $[\text{Rh}(\text{MeDPA})_2\text{chrysi}]^{3+}$ for 12–72 hours. The appearance of differential activity against the HCT116O cell line after a 12 hour incubation suggested that the MeDPA complex showed the same accelerated uptake as $[\text{Rh}(\text{HDPA})_2\text{chrysi}]^{3+}$. As expected then, $[\text{Rh}(\text{MeDPA})_2\text{chrysi}]^{3+}$ also shows differential toxicity against the HCT116O cell line in the MTT assay comparable to that of $[\text{Rh}(\text{HDPA})_2\text{chrysi}]^{3+}$ from 0–50 μM over 48–72 hours (figure 4.9).

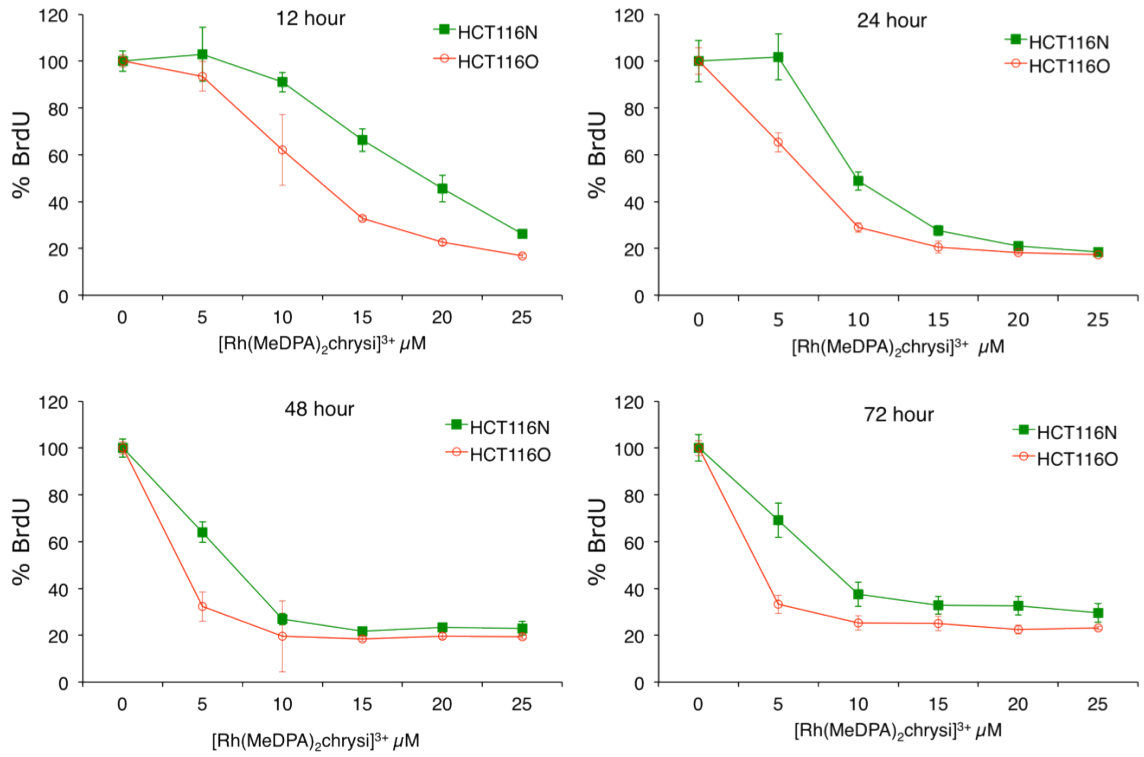


Figure 4.8. [Rh(MeDPA)₂chrysi]³⁺ selectively inhibits MMR-deficient cells in ELISA. HCT116N and HCT116O cells were plated in 96-well format at densities of 2×10^3 cells/well and treated with 0–25 μM of [Rh(MeDPA)₂chrysi]³⁺. After 12–72 hours, the media was removed and replaced with fresh media containing no rhodium. Cells were labeled with BrdU for 24 hours prior to analysis.

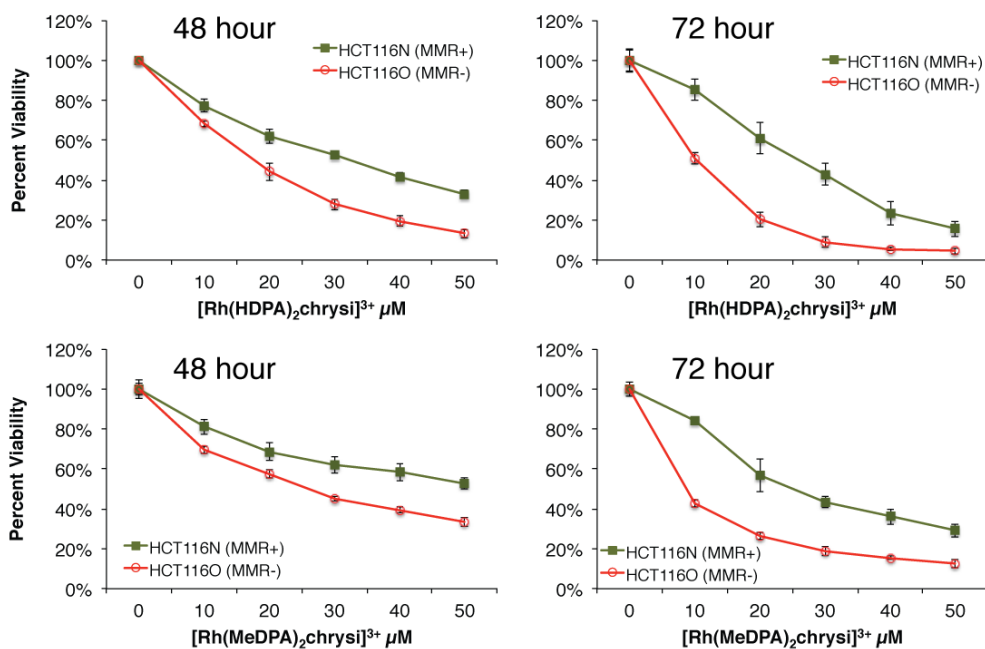


Figure 4.9. $[\text{Rh}(\text{MeDPA})_2\text{chrysi}]^{3+}$ is selectively toxic in MMR-deficient cells.

HCT116N and HCT116O cells were plated in 96-well format at densities of 5×10^4 cells/well and treated with 0–50 μM of $[\text{Rh}(\text{HDPA})_2\text{chrysi}]^{3+}$ or $[\text{Rh}(\text{MeDPA})_2\text{chrysi}]^{3+}$. After 24–72 hours, the cells were labeled with MTT for 4 hours. The resulting formazan crystals were dissolved by addition of 10% SDS acidified with 10 mM HCl, and absorbance was measured at 570 nm.

4.3.3 Effects on the Cell Cycle.

Given the previous observation that the complexes inhibit DNA synthesis, a flow cytometry assay was performed to determine if the cytotoxicity of $[\text{Rh}(\text{HDPa})_2\text{chrysi}]^{3+}$ is accompanied by disruption of the cell cycle. MMR-proficient HCT116N and MMR-deficient HCT116O cells were treated with 20 μM $[\text{Rh}(\text{HDPa})_2\text{chrysi}]^{3+}$ for 24 or 48 hours. After treatment, cells were stained with propidium iodide (PI) and analyzed by flow cytometry. The PI fluorescence reports the amount of DNA in each cell and follows a bimodal distribution, where the first peak contains cells with one copy of the genome, i.e., cells in G0/G1 phase, and the second peak contains cells with two copies of the genome, i.e., cells in G2 or M phase. Cells in S-phase occupy the region between the two peaks. Figure 4.10 shows these distributions for both cell lines, with or without rhodium treatment. In both cases, a decrease in the area under the curve between the peaks can be seen, indicating a depletion of the S-phase populations. Figure 4.11 fits the raw distributions to G1, S, or G2/M phases, and confirms the depletion of the S-phase population, concomitant with an increase in the G1 population. Notably, at this concentration of $[\text{Rh}(\text{HDPa})_2\text{chrysi}]^{3+}$ large differentials in both the ELISA and MTT assay were observed. The changes to the cell cycle are more pronounced in the MMR-deficient HCT116O cell line, which continues to grow aggressively at 48 hours (> 50% S-phase) in the absence of rhodium treatment, whereas growth of the HCT116N cell line slows slightly as the density of the culture increases. Furthermore, the HCT116O cell line also shows a significant increase in the G2/M population as well as the G1 population.

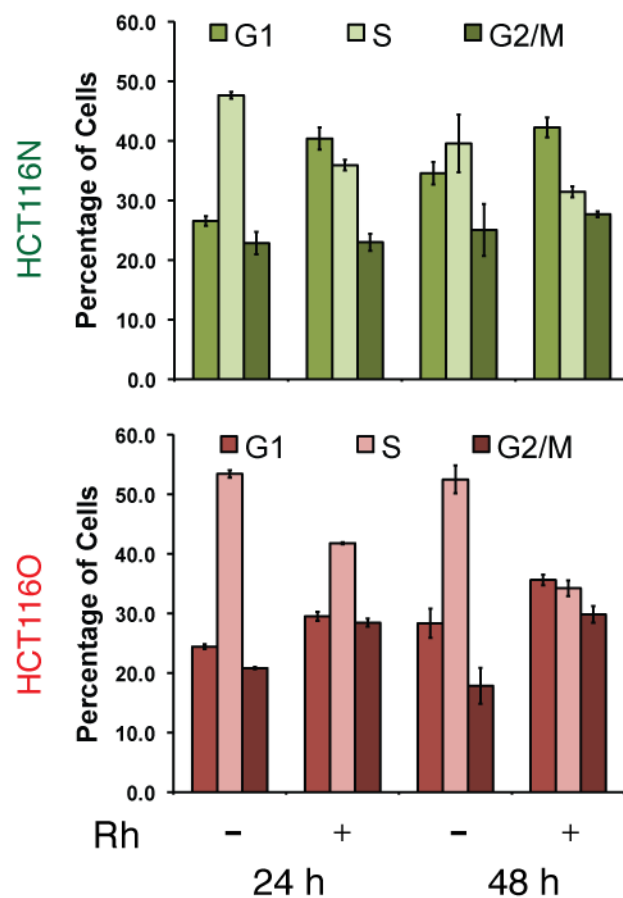


Figure 4.11. Cell cycle distribution assay. HCT116N (top) and HCT116O (bottom) cells were treated with 20 μM $[\text{Rh}(\text{HDP A})_2\text{chrysi}]^{3+}$ for 24 or 48 hours. After fixation and staining with PI, cells were analyzed by flow cytometry. The raw distributions were analyzed for cell cycle phase using commercially available software. Upon rhodium treatment, the S-phase population is depleted, with a concomitant increase in the G1-phase population.

4.3.4 Cell Death Pathway by Flow Cytometry

To characterize the cell death occurring in response to rhodium treatment, a dye exclusion flow cytometry assay, depicted schematically in figure 4.12, was employed. The assay differentiates between live cells, dead cells, and cells undergoing apoptosis or necrosis through concurrent staining with propidium iodide (a dead cell permeable dye) and YO-PRO-1 (an apoptotic cell permeable dye). By plotting the fluorescence of the YO-PRO-1 channel against the PI channel, a pattern emerges. Healthy cells are seen in the lower lefthand corner of the plot. Apoptotic cells exhibit higher YO-PRO-1 fluorescence, but still exclude propidium iodide, placing them in the upper lefthand quadrant of the pattern. Dead cells admit both dyes and are therefore seen in the upper righthand quadrant of the image. Upon flow cytometry analysis, cells can be classified as live, apoptotic, necrotic, or dead after gating, or defining regions in the fluorescence plane corresponding to each category.

The HCT116N and HCT116O cell lines were incubated with 0–30 μM of $[\text{Rh}(\text{HDPA})_2\text{chrysi}]^{3+}$ for 24–72 hours. After harvesting the cells and staining with both PI and YO-PRO-1, the cells were analyzed by flow cytometry to obtain raw fluorescence data. Representative data for 20 μM rhodium treatment for 72 hours are shown in figure 4.13. YO-PRO-1 fluorescence is shown on the y -axis, and PI fluorescence is shown on the x -axis. The color scale represents the number of cells, with blue indicating fewer cells at a given pair of fluorescence levels, and orange representing a greater number of cells at a given pair of fluorescence levels.

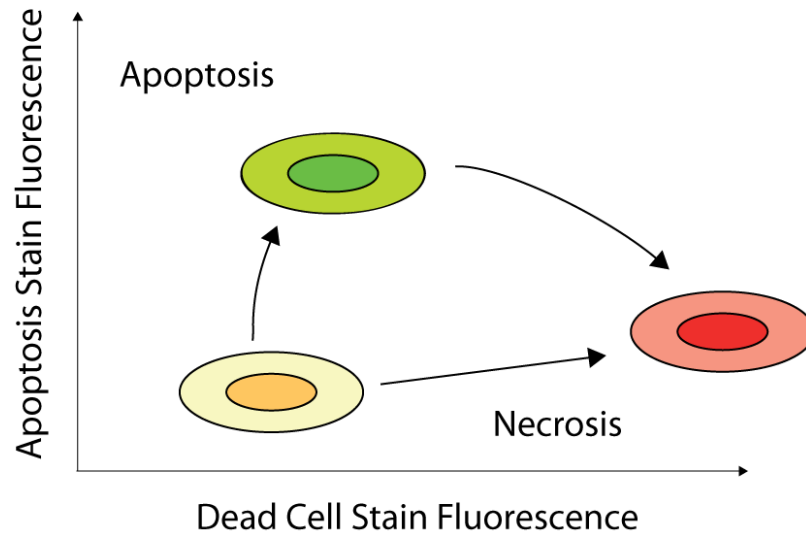


Figure 4.12. Cell death mode dye exclusion assay. HCT116N and HCT116O cells were treated with rhodium, harvested, resuspended in PBS, and stained with PI (dead cell permeable dye) and YO-PRO1 (apoptotic cell permeable dye). The cells were gated by position in the fluorescence plane and classified as live, apoptotic, necrotic, or dead.

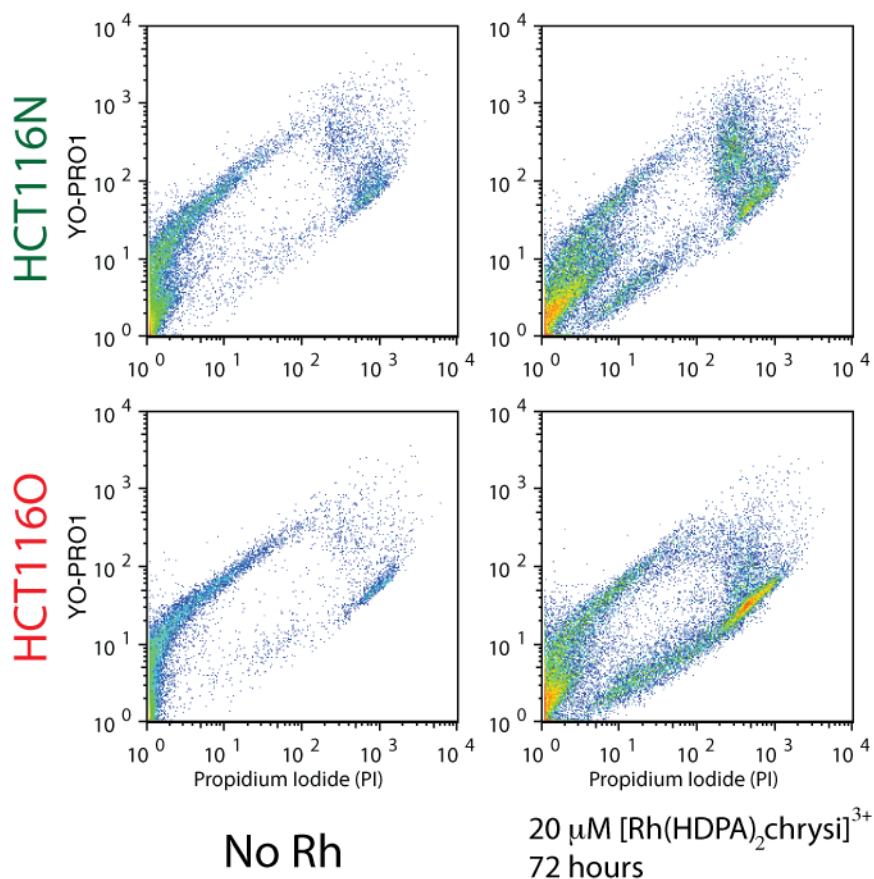


Figure 4.13. $[\text{Rh}(\text{HDPA})_2\text{chrysi}]^{3+}$ induces necrosis in HCT116O cells. HCT116N and HCT116O cells were treated with $20 \mu\text{M}$ $[\text{Rh}(\text{HDPA})_2\text{chrysi}]^{3+}$ for 72 hours. Cells were harvested, resuspended in PBS, and stained with PI (dead cell permeable) and YO-PRO1 (apoptotic cell permeable). The cells were gated by regions in the fluorescence plane and classified as live, apoptotic, necrotic, or dead. Rhodium treatment causes cells to move away from the origin, along the necrotic pathway (lower branch of pattern). The effect is more pronounced in the HCT116O cell line.

Raw fluorescence data was analyzed by gating the fluorescence events into one of four categories, depending on the fluorescence levels of the two dyes. Figure 4.14 shows the resulting histograms of live, apoptotic, necrotic, and dead cells for HCT116N and HCT116O cells treated with 0–30 μM $[\text{Rh}(\text{HDP A})_2\text{chrysi}]^{3+}$ for 72 hours. The percentage of cells in the live region decreases, while the percentages of cells in the necrotic and dead regions increase in a concentration-dependent fashion. The effect is more pronounced in the MMR-deficient HCT116O cell line, which drops from 77 ± 7.4 % to 27 ± 4.8 % of cells in the live region versus the MMR-proficient HCT116N cell line, which shows a smaller drop from 59 ± 4.4 % to 30 ± 0.8 % after treatment with 30 μM $[\text{Rh}(\text{HDP A})_2\text{chrysi}]^{3+}$.

Figure 4.15 shows histograms of live, apoptotic, necrotic, and dead cells for HCT116N and HCT116O cells treated with 20 or 25 μM $[\text{Rh}(\text{HDP A})_2\text{chrysi}]^{3+}$ for 24 – 72 hours. As before, rhodium treatment induces necrosis preferentially in the MMR-deficient HCT116O cell line; here the toxicity increases steadily with time. A slight, but appreciable toxicity is seen at 24 hours, and the largest increase in the percentage of necrotic and dead cells is seen to occur between 24 and 48 hours after treatment. After 72 hours, the highest percentages of necrotic and dead cells are seen. Again, the HCT116O cell line, where live cells drop from 73 ± 2.2 % to 37 ± 2.5 %, is more sensitive to rhodium than the HCT116N cell line, where live cells drop from 58 ± 5.2 % to 47 ± 5.5 % after treatment with 20 μM $[\text{Rh}(\text{HDP A})_2\text{chrysi}]^{3+}$ for 72 hours.

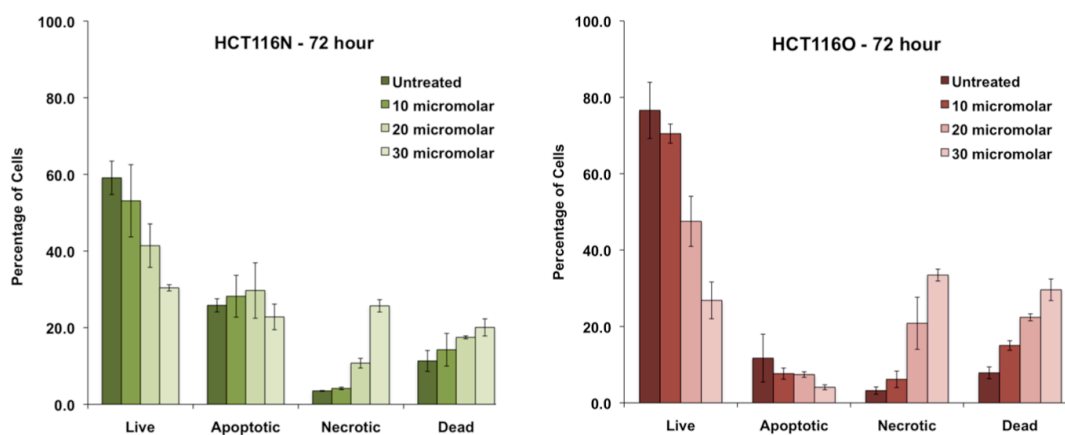


Figure 4.14. $[\text{Rh}(\text{HDPA})_2\text{chrysi}]^{3+}$ induced necrosis is concentration dependent.

HCT116N and HCT116O cells were treated with 0–30 μM $[\text{Rh}(\text{HDPA})_2\text{chrysi}]^{3+}$ for 72 hours. Cells were harvested, resuspended in PBS, and stained with PI (dead cell permeable) and YO-PRO1 (apoptotic cell permeable). The cells were gated by regions in the fluorescence plane and classified as live, apoptotic, necrotic, or dead. Rhodium treatment causes a sharp decrease in the live population of the HCT116O cell line with a corresponding increase in the necrotic and dead cell populations. Minimal effect is seen in the HCT116N cell line.

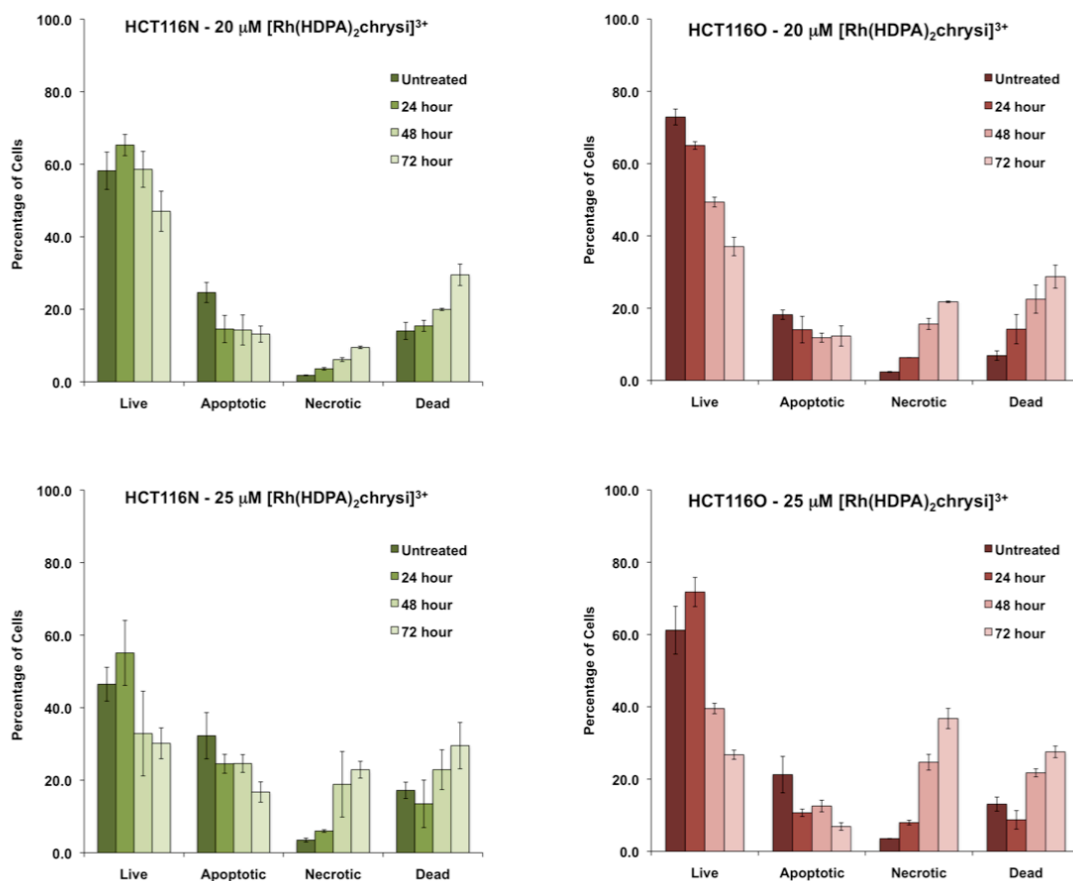


Figure 4.15. $[\text{Rh}(\text{HDPA})_2\text{chrysi}]^{3+}$ induced necrosis increases over 24 to 72 hours.

HCT116N and HCT116O cells were treated with 20 μM or 25 μM $[\text{Rh}(\text{HDPA})_2\text{chrysi}]^{3+}$ for 24–72 hours. Cells were harvested, resuspended in PBS, and stained with PI (dead cell permeable) and YO-PRO1 (apoptotic cell permeable). The cells were gated by regions in the fluorescence plane and classified as live, apoptotic, necrotic, or dead. Rhodium treatment causes a sharp decrease in the live population of the HCT116O cell line with a corresponding increase in the necrotic and dead cell populations. Minimal effect is seen in the HCT116N cell line.

Finally, figure 4.16 shows histograms of live, apoptotic, necrotic, and dead cells for the HCT116N and HCT116O cell lines treated with a combination of rhodium and the dihydrofolate reductase (DHFR) inhibitor methotrexate. Rhodium treatment was either 20 or 25 μM $[\text{Rh}(\text{HDPa})_2\text{chrysi}]^{3+}$ for 72 hours, and methotrexate treatment was 500 nM for 72 hours. As before, rhodium treatment alone induces necrosis preferentially in the MMR-deficient HCT116O cell line; there is no significant change in the percentage of cells in the apoptotic region in either cell line. The effect is more pronounced in the MMR-deficient HCT116O cell line, which drops from $79 \pm 3.8\%$ to $37 \pm 5.3\%$ after treatment with 20 μM $[\text{Rh}(\text{HDPa})_2\text{chrysi}]^{3+}$ and to $27 \pm 8.9\%$ after treatment with 20 μM $[\text{Rh}(\text{HDPa})_2\text{chrysi}]^{3+}$ and 500 nM methotrexate, versus the MMR-proficient HCT116N cell line, which shows a minimal decrease in live cells from $62 \pm 0.6\%$ to $54 \pm 5.1\%$ after treatment with 20 μM $[\text{Rh}(\text{HDPa})_2\text{chrysi}]^{3+}$ and to $53 \pm 1.0\%$ after treatment with 20 μM $[\text{Rh}(\text{HDPa})_2\text{chrysi}]^{3+}$ and 500 nM methotrexate.

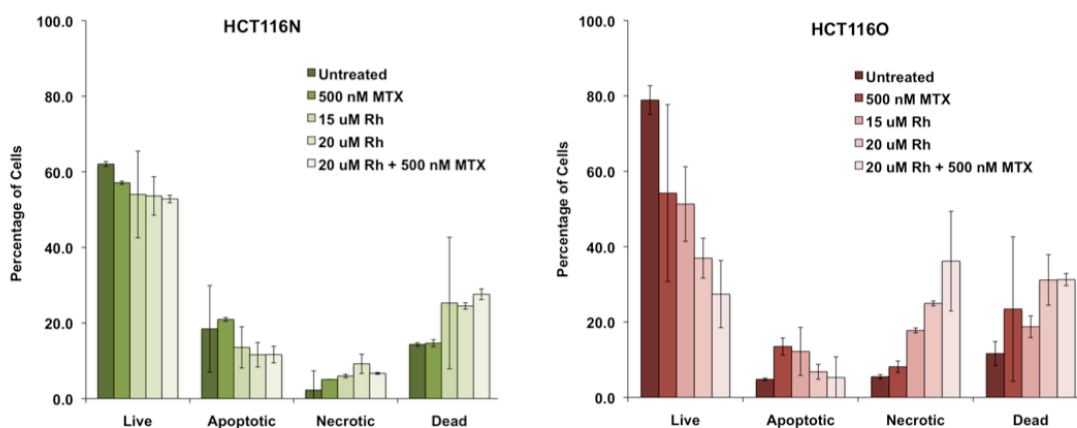


Figure 4.16. $[\text{Rh}(\text{HDPA})_2\text{chrysi}]^{3+}$ induces necrosis in combination with methotrexate (MTX). HCT116N and HCT116O cells were treated with 20 μM $[\text{Rh}(\text{HDPA})_2\text{chrysi}]^{3+}$ for 24–72 hours. Cells were harvested, resuspended in PBS, and stained with PI (dead cell permeable) and YO-PRO1 (apoptotic cell permeable). The cells were gated by regions in the fluorescence plane and classified as live, apoptotic, necrotic, or dead. Rhodium treatment causes a sharp decrease in the live population of the HCT116O cell line with a corresponding increase in the necrotic and dead cell populations. Minimal effect is seen in the HCT116N cell line.

4.3.5 Caspase Inhibitor MTT

As a complement to the dye exclusion flow cytometry assay, the MTT cytotoxicity assay was repeated in the absence and presence of the pan-caspase inhibitor Z-VAD-FMK (figure 4.17).¹² This inhibitor works by irreversibly binding to the active site of caspases. As before, the HCT116N and HCT116O cell lines were treated with 0–30 μM of the $[\text{Rh}(\text{HDPA})_2\text{chrysi}]^{3+}$ complex for 24–72 hours. In addition, each treatment was also combined with the inhibitor at a final concentration of 20 μM (figure 4.18) or 40 μM (figure 4.19). As before, the rhodium complex exhibited selective toxicity in the repair-deficient HCT116O cell line, with cell viability dropping to $9.7 \pm 4.4\%$ after treatment with 30 μM metal complex for 72 hours, versus $63 \pm 5.7\%$ viability in the repair-proficient HCT116N cell line. Addition of the caspase inhibitor at 20 μM offered no protection from rhodium to the HCT116N cell line ($63 \pm 5.7\%$ without inhibitor, $52 \pm 9.8\%$ with inhibitor) or to the HCT116O cell line ($9.7 \pm 4.4\%$ without inhibitor, $9.8 \pm 7.8\%$ with inhibitor). At a final concentration of 40 μM , the caspase inhibitor provided some protection from rhodium to the HCT116O cell line ($16 \pm 10\%$ without inhibitor, $28 \pm 3.7\%$ with inhibitor), but this difference was small in relation to the differential between the HCT116N and HCT116O cell lines and roughly within error.

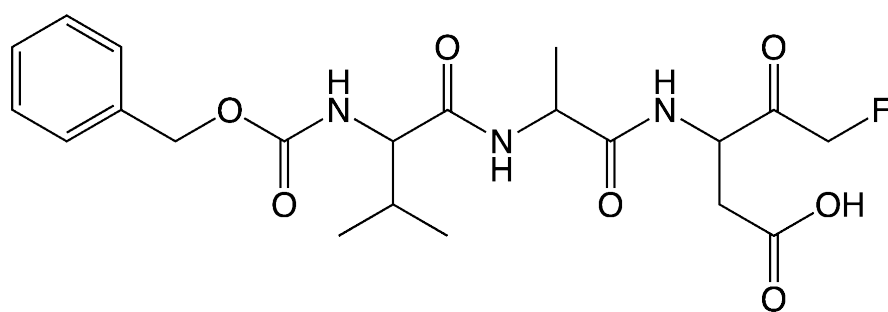


Figure 4.17. Z-VAD-fmk caspase inhibitor.

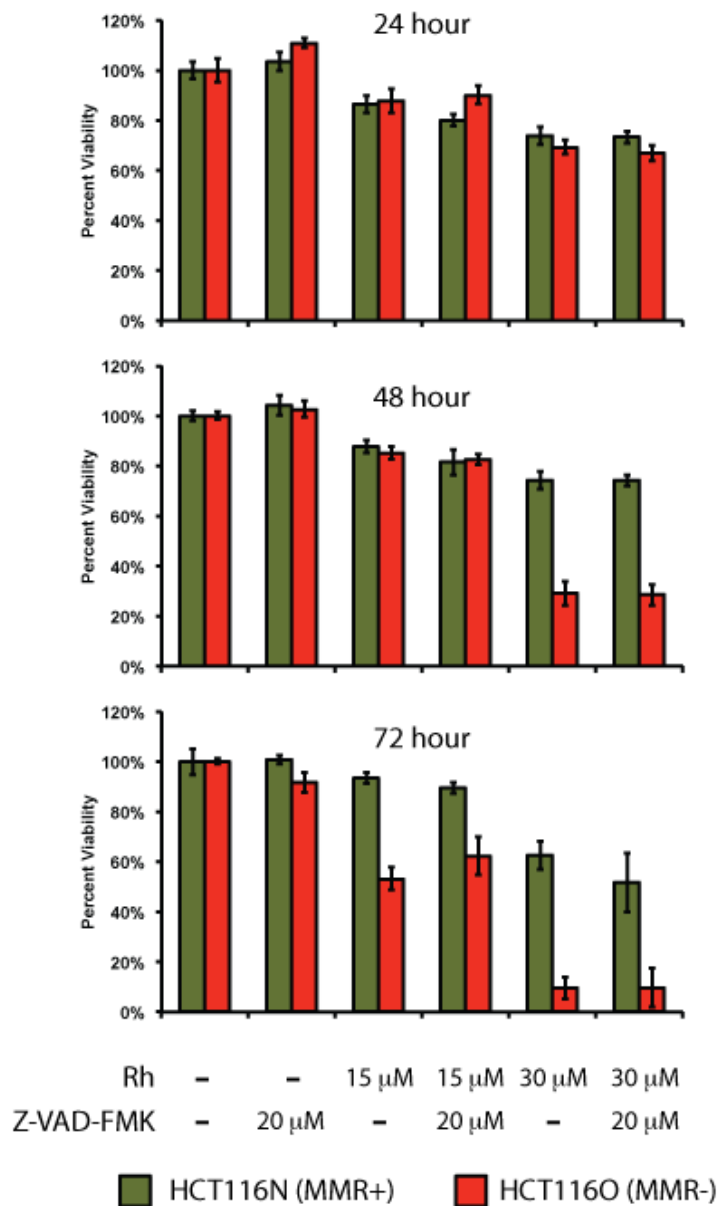


Figure 4.18. 20 μ M Caspase inhibition assay. HCT116N and HCT116O cells were plated in 96-well format at densities of 5×10^4 cells/well and treated with 0–30 μ M of $[\text{Rh}(\text{HDP A})_2\text{chrysi}]^{3+}$ with or without 20 μ M of the pan-caspase inhibitor Z-VAD-FMK. After 24–72 hours, the cells were labeled with MTT for 4 hours. The resulting formazan crystals were dissolved by addition of 10% SDS acidified with 10 mM HCl, and absorbance was measured at 570 nm. The caspase inhibitor confers no protection from rhodium-induced toxicity in either cell line.

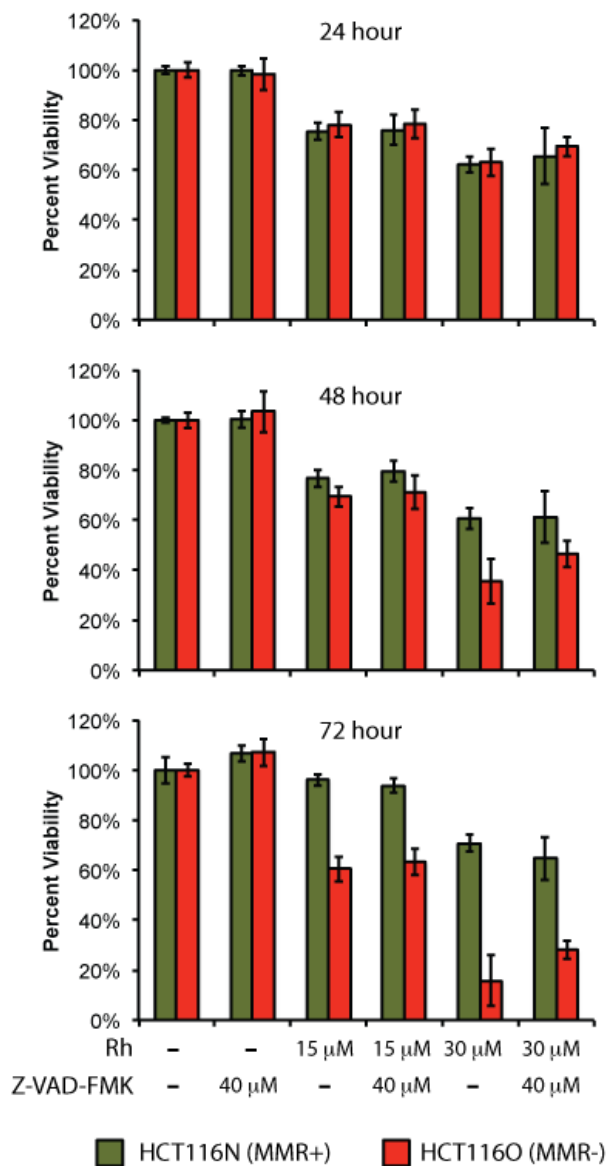


Figure 4.19. 40 μ M Caspase inhibition assay. HCT116N and HCT116O cells were plated in 96-well format at densities of 5×10^4 cells/well and treated with 0–30 μ M of $[\text{Rh}(\text{HDP A})_2\text{chrysi}]^{3+}$ with or without 40 μ M of the pan-caspase inhibitor Z-VAD-FMK. After 24–72 hours, the cells were labeled with MTT for 4 hours. The resulting formazan crystals were dissolved by addition of 10% SDS acidified with 10 mM HCl, and absorbance was measured at 570 nm. The caspase inhibitor confers no protection from rhodium-induced toxicity in either cell line.

4.3.6 PARP Inhibitor MTT

The MTT cytotoxicity assay was also repeated in the conjunction with the PARP inhibitor DPQ (figure 4.20). As before, the HCT116N and HCT116O cell lines were treated with 0 or 20 μM of the $[\text{Rh}(\text{HDPA})_2\text{chrysi}]^{3+}$ complex for 72 hours, with 0–50 μM of DPQ. The rhodium complex alone exhibited selective toxicity in the repair-deficient HCT116O cell line, with cell viability dropping to $9.7 \pm 4.4\%$ versus $63 \pm 5.7\%$ viability in the repair-proficient HCT116N cell line. Addition of the caspase inhibitor at 50 μM offered protection from rhodium to both cell lines (HCT116N: $39 \pm 3.6\%$ without inhibitor, $47 \pm 2.1\%$ with inhibitor, HCT116O: $14 \pm 1.7\%$ without inhibitor, $41 \pm 2.0\%$ with inhibitor). Importantly, this inhibition significantly decreased the differential in toxicity ($25 \pm 4.0\%$ without inhibitor, $6.4 \pm 2.9\%$ with inhibitor) between the cell lines, suggesting that PARP is involved in the MMR-dependent response to $[\text{Rh}(\text{HDPA})_2\text{chrysi}]^{3+}$.

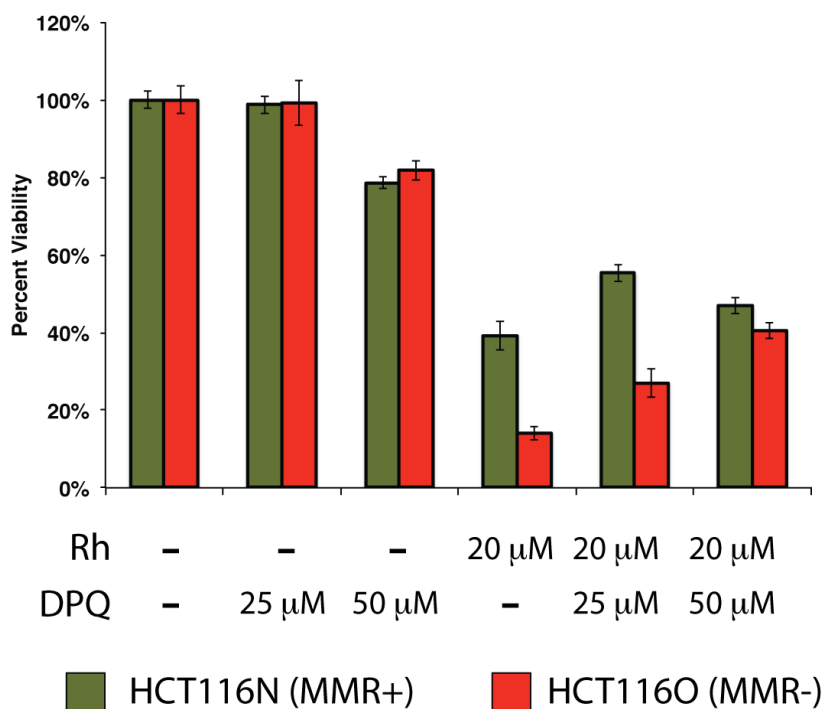


Figure 4.20. PARP inhibition assay. HCT116N and HCT116O cells were plated in 96-well format at densities of 5×10^4 cells/well and treated with 0 or 20 μM of $[\text{Rh}(\text{HDPA})_2\text{chrysi}]^{3+}$ with or without 25 or 50 μM of the PARP inhibitor DPQ. After 72 hours, the cells were labeled with MTT for 4 hours. The resulting formazan crystals were dissolved by addition of 10% SDS acidified with 10 mM HCl, and absorbance was measured at 570 nm. The PARP inhibitor confers protection from rhodium-induced toxicity in both cell lines, reducing the differential activity significantly.

4.4. Discussion

ICP-MS affords a relative comparison of the cellular accumulation of a series of rhodium metalloinsertors after treatments similar to those applied in ELISA assays for activity.

The highest levels of cellular accumulation are clearly seen for the complex bearing the HDPA ligand, which was expected in light of the previous observation that $[\text{Rh}(\text{HDPA})_2\text{chrysi}]^{3+}$ exhibits increased activity against the HCT116 cell lines at shorter incubation times than other rhodium metalloinsertors. Significant activity is seen with $[\text{Rh}(\text{HDPA})_2\text{chrysi}]^{3+}$ in as little as 12 hours, while $[\text{Rh}(\text{bpy})_2\text{chrysi}]^{3+}$ and $[\text{Rh}(\text{NH}_3)_4\text{chrysi}]^{3+}$ display no activity at this incubation time. There are several possible explanations for the increased rate of uptake. The central amine may make the HDPA ligands more flexible than bpy ligands, allowing the complex to deform more easily and increasing its ability to diffuse through the plasma membrane. Alternatively, the hydrogen bonding capability may facilitate active uptake by fostering interaction with some unknown transport protein.

Rhodium metalloinsertors have shown differential anti-proliferative activity in an ELISA assay for DNA synthesis. This assay directly reports on the amount of BrdU label incorporated during DNA replication, and as such, does not distinguish between cells that are viable but not replicating, e.g., G0 cells that have exited the cell cycle, and cells that are inviable, or dead. Therefore, this assay can be used to determine *inhibitory*, but not *cytotoxic* activity. In contrast, the MTT assay reports directly on cell viability as measured by metabolic activity, with the action of mitochondrial reductases catalyzing the cleavage of the labeling agent MTT. Here cells that are viable still produce signal, i.e., formazan absorbance, whether or not they are actively dividing. Thus, this assay can distinguish between senescence and true cell death, and the effects observed in response

to rhodium treatment are truly cytotoxic. Importantly, the concentration ranges and incubation times of the treatments applied in the MTT assays for $[\text{Rh}(\text{HDPA})_2\text{chrysi}]^{3+}$ and the closely related complex $[\text{Rh}(\text{MeDPA})_2\text{chrysi}]^{3+}$ (0–50 μM , 24–72 hours) are similar, if not identical, to those that inhibit DNA synthesis as seen by ELISA (0–25 μM , 24–72 hours).

Accordingly, the result that $[\text{Rh}(\text{HDPA})_2\text{chrysi}]^{3+}$ and $[\text{Rh}(\text{MeDPA})_2\text{chrysi}]^{3+}$ trigger cell death selectively in the MMR-deficient HCT116O cell line versus the MMR-proficient HCT116N cell line as measured by MTT assay represents a significant advance in the development of these complexes as anti-cancer agents; clearly, these agents are more potent than previously understood. Although $[\text{Rh}(\text{bpy})_2\text{chrysi}]^{3+}$ does not appear to be selectively toxic at these concentrations, it is likely that this is due to differences in the kinetics of cellular uptake, rather than fundamental differences in its mode of action as compared to $[\text{Rh}(\text{HDPA})_2\text{chrysi}]^{3+}$, since both bind DNA mismatches with equal affinity (Chapter 3). For either activity assay, the complex must first accumulate within the cell, and then cellular response must be triggered. While $[\text{Rh}(\text{HDPA})_2\text{chrysi}]^{3+}$ displays activity in ELISA after 12 hour incubations, $[\text{Rh}(\text{bpy})_2\text{chrysi}]^{3+}$ requires 48 hours or more to show significant differential activity. In light of the higher levels of rhodium accumulation seen by ICP-MS after treatment with the HDPA complex *versus* the bpy complex, it seems likely that accumulation of the bpy complex is delayed by ~36 hours relative to the HDPA complex. Cellular responses that occur quickly after accumulation, such as the inhibition of DNA synthesis, can still be observed within the 72 hour timeframe of the ELISA assay, and both complexes display activity. However, a lag time will exist between the inhibition of DNA synthesis and the onset of cell death, and when

combined with the slow uptake of $[\text{Rh}(\text{bpy})_2\text{chrysi}]^{3+}$, ($t > 48$ hours), cell death is delayed accordingly and cannot be observed within the timeframe of the MTT assay (also 72 hours).

The fact that the $[\text{Rh}(\text{MeDPA})_2\text{chrysi}]^{3+}$ complex displays differential toxicity against the HCT116O cell lines comparable to that of the $[\text{Rh}(\text{HDPA})_2\text{chrysi}]^{3+}$ complex suggests that it shares the accelerated uptake of the HDPA complex. This was certainly expected, as the complexes are almost identical, but does address the question of uptake mechanism, and clearly refutes the hypothesis that accelerated uptake requires a hydrogen bonding interaction with the bridging secondary amine of the HDPA ligand. More importantly, this suggests that selective toxicity as a function of MMR-competency is a general property of rhodium metalloinsertors with dipyridylamine ancillary ligands, and establishes these ligands as the basis for the development of the next generation of complexes.

Flow cytometry analysis reveals that cell death is preceded by disruption of the cell cycle. Treatment with 20 μM $[\text{Rh}(\text{HDPA})_2\text{chrysi}]^{3+}$ for 24 hours leads to a marked depletion of the S-phase population with a concomitant increase in the G1 population. These data suggest that the G1/S-phase DNA damage checkpoint may be activated in response to rhodium treatment, and call for biochemical assays to probe for phosphorylation of checkpoint kinases such as Chk1 and Chk2 that arrest the cell cycle in response to DNA damage. In the case of the HCT116O line, the G2/M-phase population also increases in response to rhodium treatment. This could represent a secondary checkpoint activation occurring at the G2/M-phase transition, and might signal a “two-alarm fire” that accompanies the enhanced activity against this cell line. Again,

additional biochemical assays are needed to probe the regulatory network controlling this checkpoint.

The two main modes of cell death are apoptosis and necrosis. The biochemical events associated with apoptosis have been extensively studied since Kerr and Wylie's seminal paper¹³ in 1972. An extensive network of regulatory proteins controls the initiation of this process in response to both internal and external signals.¹⁴ Upon activation, the cascade of initiator and effector caspases cleaves a variety of substrates to bring about the morphological changes associated with this mode of cell death, including nuclear condensation and fragmentation, plasma membrane blebbing, decomposition of the cell into apoptotic bodies, and ultimately, the engulfment of these bodies by neighboring cells through phagocytosis.¹⁵ Importantly, apoptotic cells retain their membrane integrity until the very last stages of this process, preventing release of cytokines and thus avoiding inflammation. By comparison, both the causes and the progression of necrosis are much less defined at the molecular level, and this mode of cell death is most frequently characterized by morphological criteria.¹⁵⁻¹⁷ Perhaps the most reliable marker of necrosis then, is the early rupture of the plasma membrane, in direct contrast to apoptosis. These differences in membrane integrity enable the facile characterization of cell death by flow cytometry assay. The admission of the dead cell stain propidium iodide by the HCT116 cell lines upon rhodium treatment reveals that cell death proceeds through a necrotic, rather than apoptotic, pathway. This conclusion is supported by the observation that the caspase inhibitor Z-VAD-fmk is unable to block rhodium-induced toxicity in the MTT assay, indicating that death occurs in a caspase-independent fashion.

It is interesting to consider that rhodium metalloinsertors selectively induce necrosis in MMR-deficient cells. Traditionally, necrotic cell death has been considered to be “accidental,” occurring mainly in response to non-physiological insults.^{18,19} More recently however, the notion that necrosis may in fact be an ancestral mode of programmed cell death has gained attention in the literature and community of cell death research.^{15,16} Hitomi *et al.* screened an siRNA library covering the mouse genome and identified 432 gene knockdowns that blocked the induction of necrosis.²¹ Chan *et al.* found anti-necrotic proteins encoded in the genomes of several viruses.²² While these studies present some of the most compelling evidence for the notion that necrosis is in fact a regulated process, several other groups are also working to provide a molecular definition for the process as has been done for apoptosis.^{19,20}

Thompson and co-workers have reported that the DNA repair protein poly ADP-ribose polymerase-1 (PARP-1) mediates the induction of necrosis in response to DNA damage by the alkylator MNNG.²³ Upon activation at sites of DNA damage, PARP-1 covalently modifies itself with long chains of ADP-ribose polymers in order to recruit downstream components of the repair machinery.²⁴ As a result, PARP-1 along with PARP-2 has attracted much attention as a therapeutic target recently, and several specific and potent inhibitors of the enzyme are currently in clinical trials.²⁵ Here, treatment with the PARP inhibitor DPQ rescues cells from rhodium-induced toxicity. This suggests that PARP is involved in the induction of necrosis by rhodium metalloinsertors, and may represent the first molecular insight into the events underlying rhodium toxicity. Although the role of PARP in regulating necrosis is still emerging, confirmation that these rhodium complexes activate PARP as a component of a broader DNA damage

response would support the notion that rhodium metalloinsertors target mismatches in genomic DNA.

As necrosis triggers a proinflammatory response by releasing cytokines, selective induction of necrosis in cancerous tissues may be a way to activate the immune system against cancer cells and ultimately improve efficacy of a therapeutic agent.²⁶ One accepted trigger of necrosis is bioenergetic catastrophe, i.e., severe ATP depletion.^{18,19} Rhodium metalloinsertors might trigger such a catastrophe by targeting mitochondrial DNA. Previously, it was thought that damaged mitochondrial genomes simply would be degraded and replaced by the replication of undamaged DNA.²⁷ However, emerging research has uncovered DNA repair processes in mitochondria, including mismatch repair capability.^{27,28} As lipophilic cations, rhodium metalloinsertors likely accumulate in mitochondria,⁶⁻¹¹ as we have seen with analogous ruthenium complexes in our laboratory.²⁹ If mitochondrial DNA mismatches are in fact a target for rhodium metalloinsertors, then the resultant disruption of mitochondrial function would lead to energy depletion and necrosis. Future mechanistic work must explore the biochemical consequences of mismatch binding in nuclear DNA *versus* mitochondrial DNA. It should be noted that these mechanisms are not mutually exclusive; as such, both might contribute to the biological response to rhodium metalloinsertors.

4.5. Conclusions

These studies support the notion that rhodium metalloinsertors bearing HDPA ligands benefit from increased cellular accumulation, and thus provide an explanation for the observation that $[\text{Rh}(\text{HDPA})_2\text{chrysi}]^{3+}$ exceeds the activity predicted by its binding affinity for DNA mismatches.

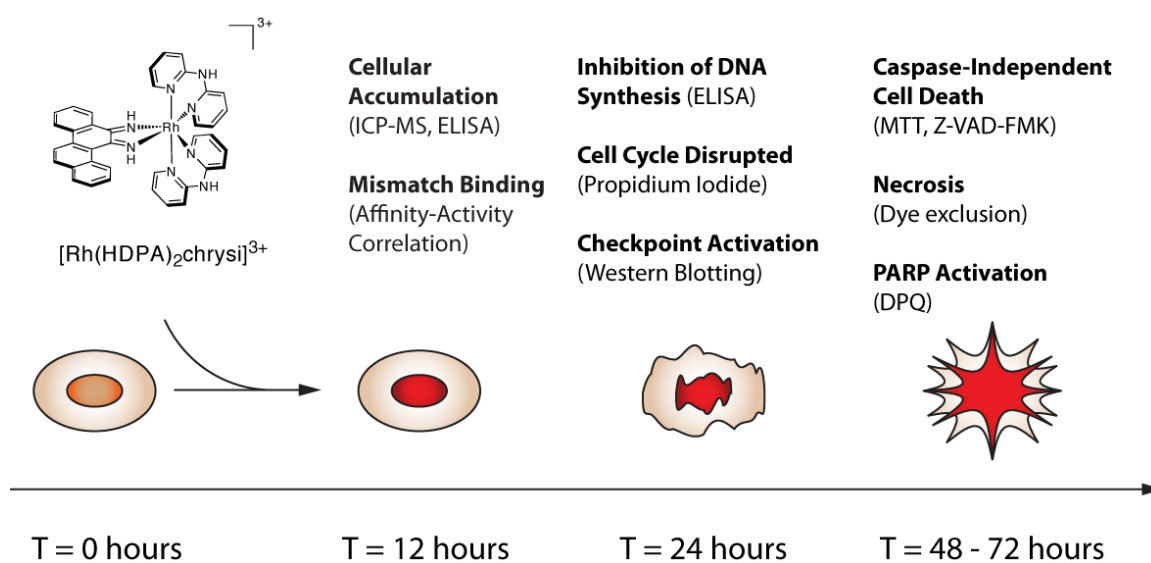


Figure 4.21. Model of the cellular response to rhodium metalloinsertors.

This increased uptake allows us to observe additional cellular responses to these agents, and, as a whole, a picture of the biological response to rhodium metalloinsertors, exemplified by $[\text{Rh}(\text{HDPA})_2\text{chrysi}]^{3+}$ in particular, is beginning to emerge (figure 4.21). Over the course of the first 12 hours, the rhodium complex accumulates in cells, binding to either mitochondrial or genomic DNA mismatches. Within 24 hours, DNA synthesis is inhibited, and cells accumulate in G1 phase. Over the next 24–48 hours, the DNA damage response is likely activated, and ultimately leads to cell death by a caspase-independent, necrotic mechanism. These biological effects are more pronounced at each stage of the response in the MMR-deficient HCT116O cell line relative to the MMR-proficient HCT116N cell line, strongly suggesting that DNA mismatches are in fact the cellular target of rhodium metalloinsertors. Furthermore, these cellular responses are consistent with the idea that repair proteins are activated in response to DNA mismatch binding.

The structural analogue $[\text{Rh}(\text{MeDPA})_2\text{chrysi}]^{3+}$ is also shown to be toxic, suggesting that dipyriddyamine ancillary ligands in general can serve to accelerate uptake, and form the foundation for the next generation of complex development. This new class of agents is significantly more potent than previously understood, and the work begun here on understanding their mechanism of action advances their development as novel anti-cancer agents.

4.6. References

1. E. Egger, C. Rappel, M. A. Jakupec, C. G. Hartinger, P. Heffeter, and B. K. Keppler. *J. Anal. At. Spectrom.* **2009** 24, 51–61.

2. M. Ghezzi, C. Aceto, E. Cassino, D. Gabano and J. Osella. *J. Inorg. Biochem.* **2004** *98*, 73–78.
3. S.I. Kirin, I. Ott, R. Gust, W. Mier, T. Weyhermüller and N. Metzler-Nolte, *Angew. Chem. Int. Ed.* **2008** *47*, 955–959.
4. A.H. Reitmar, R. Risley, R.G. Bristow, T. Wilson, A. Ganesh, A. Jang, J. Peacock, S. Benchimol, and R.P. Hill. *et al. Cancer Res.* **1997**, *57*, 3765–3771.
5. H.G. Gratzner. *Science* **1982**, *218*, 474–475.
6. S.M. Napolitano and J.R. Aprille. *Adv. Drug Delivery Rev.* **2001** *49*, 63–70.
7. M.P. Murphy and R.A.J. Smith. *Adv. Drug Delivery Rev.* **2000** *41*, 235–250.
8. O. Rackham, S.J. Nichols, P. J. Leedman, S.J. Berners-Price, and A. Filipovska. *Biochem. Pharmacol.* **2007** *74*, 992–1002.
9. J.J. Liu, P. Galettis, A. Farr, L. Maharaj, H. Samarasinha, A.C. McGechan, B.C. Baguley, R.J. Bowen, S.J. Berners-Price, and M.J. McKeage. *J. Inorg. Biochem.* **2008** *102*, 303–310.
10. E.A. Liberman, V.P. Topali, L.M. Tsofina, A.A. Jasaitis and V.P. Skulachev. *Nature* **1969** *222*, 1076–1078.
11. L.V. Johnson, M.L. Walsh, and L.B. Chen. *Proc. Natl. Acad. Sci. U.S.A.* **1980** *77*, 990–994.
12. P. Vandenabeele, T. Vanden Berghe, and N. Festjens. *Science STKE.* **2006** *358*, pe44.
13. J.F.R. Kerr, A.H. Wyllie, and A.R. Currie. *Br. J. Cancer* **1972** *26*, 239–257.
14. N.N. Danial and S.J. Korsmeyer. *Cell* **2004** *116*, 205–219.

15. A.L. Edinger and C.B. Thompson. *Current Opinion in Cell Biology* **2004** *16*, 663–669.
16. G. Kroemer, W.S. El-Deiry, P. Golstein, M.E. Peter, D. Vaux, P. Vandenabeele, B. Zhivotovsky, M.V. Blagosklonny, W. Malorni, R.A. Knight, M. Piacentini, S. Nagata, and G. Melino. *Cell Death and Differentiation* **2005** *12*, 1463–1467.
17. G. Kroemer, L. Galluzzi, P. Vandenabeele, J. Abrams, E.S. Alnemri, E.H. Baehrecke, M.V. Blagosklonny, W.S. El-Deiry, P. Golstein, D.R. Green, M. Hengartner, R.A. Knight, S. Kumar, S.A. Lipton, W. Malorni, G. Nunez, M.E. Peter, J. Tschopp, J. Yuan, M. Piacentini, B. Zhivotovsky, and G. Melino. *Cell Death and Differentiation* **2009** *16*, 3–11.
18. P. Golstein and G. Kroemer. *Trends in Biochemical Sciences* **2007** *32*, 37–43.
19. K. McCall. *Current Opinion in Cell Biology* **2010** *22*, 882–888.
20. L. Galluzzi and G. Kroemer. *Cell* **2008** *135*, 1161–1163.
21. J. Hitomi, D.E. Christofferson, A. Ng, J. Yao, A. Degterev, R.J. Xavier, and J. Yuan. *Cell* **2008** *135*, 1311–1323.
22. F.K. Chan, J. Shisler, J.G. Bixby, M. Felices, L. Zheng, M. Appel, J. Orenstein, B. Moss, and M.J. Lenardo. *Journal of Biol. Chem.* **2003** *278*, 51613–51621.
23. W.X. Zong, D. Ditsworth, D.E. Bauer, Z.-Q. Wang, and C.B. Thompson. *Genes and Development* **2004** *18*, 1272–1282.
24. M. Malanga and F.R. Althaus. *Biochemistry and Cell Biology*, **2005** *83*, 354–364.
25. Annunziata CM, O'Shaughnessy J. *Clin. Cancer Res.* **2010** *16*, 4517–4526.
26. M.S. Ricci and W.X. Zong. *The Oncologist* **2006** *11*, 342–357.

27. P. Boesch, F. Weber-Lotfi, N. Ibrahim, V. Tarasenko, A. Cosset, F. Paulus, R.N. Lightowlers, and A. Dietrich. *Biochimica et Biophysica Acta*. **2011** *1813*, 186–200.
28. N.C. de Souze-Pinto, P.A. Mason, K. Hashiguchi, L. Weissman, J. Tian, D. Guay, M. Lebel, T.V. Stevnsner, L.J. Rasmussen, and V.A. Bohr. *DNA Repair (Amst)*. **2009** *8*, 704–719.
29. C.A. Puckett and J.K. Barton. *J. Am. Chem. Soc.* **2007** *129*, 46–47.

CONCLUSION

Modern drug development harnesses the power of screening-based approaches to identify many natural products and lead compounds with great promise as therapeutic agents. Yet these efforts come at great cost, and only a small fraction of compounds tested are ultimately successful. This work argues that the rational design of new agents can play an important role in contributing to the development pipeline, especially when the design effort is founded on thoughtful chemical insight and meaningful experimental validation.

Rhodium metalloinsertors are well-defined chemical agents whose ability to target mismatches has been extensively characterized *in vitro*. This thesis was the first step in exploring their functionality in a biological system, with all its inherent complexity. It should be noted that the activity of rhodium metalloinsertors against human cancer cell lines was, like so many other scientific discoveries, somewhat fortuitous. The *in vitro* development of these complexes suggested that as non-covalent DNA binders, they might require photoactivation to exert a biological effect. The strong and selective activity against MMR-deficient cells in the absence of irradiation was first observed then as the unexpected result of a necessary control.

Our work has sought to capitalize on this good fortune and to realize all the promise of these unique agents. The characterization of the cellular responses to rhodium metalloinsertors not only demonstrates their potential, but also provides critical insights that will direct future explorations at the molecular level.

While the discoveries we have made are exciting in themselves, the story does not end here by any means. The ultimate goal of this work is not simply success in an

academic setting. It is our hope and deepest desire that as ongoing research continues to elucidate further the basis of activity and to inform the design of new complexes, the development of these agents will graduate from the bench to the clinic, and someday provide a class of targeted and useful weapons in the fight against cancer.